

University of Southern Queensland

Faculty of Engineering and Surveying

**Properties of Nickel as a Magnetostrictive
Material for Ultrasonic Conditions**

A dissertation submitted by

Mr William McHugh

in fulfilment of the requirements of

Courses ENG4111 and 4112 Research Project

towards the degree of

Bachelor of Engineering (Electrical/Electronic)

Submitted: October 2011

Abstract

Joule, in 1842, discovered the magnetostrictive effect, also referred as the Joule effect, where a material will change its physical length when subjected to an induced magnetic field. Magnetostrictive transducers convert magnetic energy into mechanical energy. That is, nickel can use an oscillating magnetic field to produce oscillating mechanical energy or sound energy. The magnetostrictive effect was used extensively in World War 2 for sonar transducers. More recent uses include dentistry, ultrasonic cleaning, plastic welding and improved metal refining.

This project involves the implementation of procedures by IEC 60782 and Petošić, Svilar and Ivančević to examine magnetostrictive transducers. Results were variable, mainly due to the function generators inability to supply the relative high currents. But with persistence some useable data was obtained.

Results include the confirmation of the resonant frequency of the transducer via mechanical vibration analysis and related to the physical design of the transducer.

The transducers respond as an almost pure inductor, resulting in a measured power factor in the vicinity of 0.09. Under ultrasonic conditions an electroacoustic efficient was calculated around 30 per cent.

Limited investigation were then performed on cavitation which provided some interesting results such as the electrocavitation efficiency being around 3.82 per cent with a cavitation resonant frequency differing from the ultrasonic resonant frequency.

University of Southern Queensland
Faculty of Engineering and Surveying

ENG4111 Research Project Part 1 & ENG4112 Research Project Part 2
--

Limitations of Use

The Council of the University of Southern Queensland, its Faculty of Engineering and Surveying, and the staff of the University of Southern Queensland, do not accept any responsibility for the truth, accuracy or completeness of material contained within or associated with this dissertation.

Persons using all or any part of this material do so at their own risk, and not at the risk of the Council of the University of Southern Queensland, its Faculty of Engineering and Surveying or the staff of the University of Southern Queensland.

This dissertation reports an educational exercise and has no purpose or validity beyond this exercise. The sole purpose of the course pair entitled “Research Project” is to contribute to the overall education within the student's chosen degree program. This document, the associated hardware, software, drawings, and other material set out in the associated appendices should not be used for any other purpose: if they are so used, it is entirely at the risk of the user.



Professor Frank Bullen
Dean
Faculty of Engineering and Surveying

Certification

I certify that the ideas, designs and experimental work, results, analyses and conclusions set out in this dissertation are entirely my own effort, except where otherwise indicated and acknowledged.

I further certify that the work is original and has not been previously submitted for assessment in any other course or institution, except where specifically stated.

Student Name: William McHugh
Student Number: Q95226720

Signature

Date

Acknowledgements

This research was carried out under the patient, persistent and practical supervision of Dr. Leslie Bowtell.

Appreciation is also due to

Miss Melanie Tecarr

My Family

Dr Tony Ahfock (USQ)

Mr Erin Heaton (Top Bloke)

Miss Anita Frederiks

Dr Harry Butler

The staff at the University of Southern Queensland

New Wave Leather Pty Ltd

Table of Contents

<i>Abstract</i>	<i>i</i>
<i>Certification</i>	<i>iii</i>
<i>Acknowledgements</i>	<i>iv</i>
<i>List of Figures</i>	<i>xi</i>
<i>List of Tables</i>	<i>xiii</i>
<i>List of Appendices</i>	<i>xiv</i>
<i>Nomenclature and Acronyms (Abbreviations)</i>	<i>xv</i>
<i>Chapter 1 – Introduction</i>	<i>1</i>
1.1 Introduction	1
1.2 Project Aim	1
1.3 Outline of Study	1
1.4 The Problem	2
1.5 Research Objectives	2
<i>Chapter 2 – Literature Review</i>	<i>4</i>
2.1 Nickel	4
2.2 Magnetostriction	4
2.2.1 Inverse Magnetostriction	5
2.3 Theories on Magnetostriction	5
2.3.1 Atomic Magnetostriction	7
2.3.2 Thermal Magnetostriction	8
2.3.3 Classical Magnetostriction	9
2.4 Ultrasonic Energy	10
2.5 Transducer Design	10
2.6 Uses for Magnetostrictive Transducers	11
<i>Chapter 3 – Properties of Nickel</i>	<i>12</i>
3.1 Electromagnetic Properties of Nickel	12

3.1.1 Permittivity	12
3.1.2 Permeability	12
3.2 Magnetic Materials	13
3.2.1 Diamagnetic Material	13
3.2.2 Paramagnetic Material	14
3.2.3 Ferromagnetic Material	14
3.2.4 Anti-ferromagnetic Material	14
3.2.5 Ferrimagnetic Material	15
3.2.6 Curie Temperature	15
3.3 Mechanical Properties of Nickel.....	15
3.3.1 Modulus of Elasticity.....	16
3.3.2 Young's Modulus	16
3.3.4 Poisson's Ratio	17
3.3.5 Creep.....	18
3.3.6 Nickel Mechanical Properties.....	18
<i>Chapter 4 – Magnetism.....</i>	<i>20</i>
4.1 Generation of Magnetic Fields	20
4.1.2 Hysteresis.....	21
4.1.3 Inductance.....	22
4.2 Interaction of Magnetic Flux and Mechanical Action.....	23
4.3 Resonant Frequency.....	25
4.3.1 Harmonics.....	26
4.4 Magnetostrictive Transducer Design	26
<i>Chapter 5 – Uses of Ultrasonic Energy.....</i>	<i>27</i>
5.1 Introduction.....	27
5.2 Uses of Ultrasonic Transducers	27
5.3 Detection Ultrasonic Transducers.....	27

5.4 Sonification Ultrasonic Transducer	28
5.5 Destructive Ultrasonic Transducers	28
5.6 Cavitation.....	29
5.6.1 Sono-Chemistry	30
<i>Chapter 6 – Safety</i>	31
<i>Chapter 7 – Methodology</i>	32
7.1 Introduction.....	32
7.2 Supply Voltage Waveforms.....	32
7.2.1 Principle Waveforms	33
7.2.2 DC Biased Waveforms	35
7.2.3 Duty Cycle Biased Waveforms.....	37
7.3 Methodology by IEC 60782	38
7.3.1 Input Electrical Power	38
7.3.2 Resonant Frequency.....	40
7.3.3 Bandwidth (Δf) and mechanical Quality (Q) Factor.....	40
7.3.4 Electrical Impedance at Resonance	41
7.3.5 Electrical Impedance Outside of Resonance	41
7.3.6 Electroacoustic Efficiency	42
7.4 Methodology Improved with Petošić et al[23]	43
7.4.1 Energizing Impedance	44
7.4.2 Transducer Impedance.....	45
7.4.3 Electroacoustic Efficiency	46
7.5 Electromagnetic Simulation.....	47
7.5.1 Calculating the values of the magnetostrictive equivalent RLC electrical circuit.....	49
7.5.2 IEC 60782 – Measurements of Ultrasonic Magnetostrictive Transducers [39].....	49
7.5.3 Petošić et al [23]	50

7.6 Mechanical Vibration Analysis	51
<i>Chapter 8 – Required Resources</i>	53
8.1 Transducer Analysis	53
8.1.1 Nickel Laminations.....	53
8.1.2 Windings.....	56
8.1.3 Transducer Properties	58
8.2 Function Generators.....	60
8.2.1 Tektronic AFG 3022B	60
8.2.2 HAMEG HM 8030–4 Function Generator	61
8.2.3 BWD 160A Function Generator	63
8.2.4 IGBT Semikron AN–8005.....	64
8.3 Recording equipment.....	66
8.3.1 Digital Oscilloscope.....	66
8.3.2 Vibration Meter	66
8.3.3 LCR Meter	67
8.3.4 Gauss Meter	67
<i>Chapter 9 – Results and Discussion</i>	68
9.1 Introduction.....	68
9.2 Input Electrical Power	69
9.3 Electrical Resonance.....	70
9.3.1 Unloaded Electrical Resonance	71
9.3.2 Loaded Electrical Resonance.....	72
9.4 Mechanical Resonance	73
9.4.1 Unloaded Mechanical Resonance.....	73
9.4.2 Loaded Mechanical Resonance	74
9.5 Bandwidth (Δf) and Mechanical Quality (Q) Factor.....	76
9.5.1 Sinusoidal Bandwidth and Mechanical Quality Factor	76

9.5.2 Square Bandwidth and Mechanical Quality Factor	77
9.5.3 Triangular Bandwidth and Mechanical Quality Factor	78
9.6 Electrical Impedance at Resonance	79
9.6.1 Sinusoidal Electrical Impedance at Resonance	79
9.6.2 Square Electrical Impedance at Resonance	80
9.6.3 Triangular Electrical Impedance at Resonance	80
9.7 Electrical Impedance Outside of Resonance	80
9.7.1 Sinusoidal Electrical Impedance Outside of Resonance.....	80
9.7.2 Square Electrical Impedance Outside of Resonance	81
9.7.3 Triangular Electrical Impedance Outside of Resonance.....	81
9.8 Mechanical Output Power (Vibration Analysis)	82
9.8.1 Sinusoidal Voltage Mechanical Output Power.....	82
9.8.2 Square Voltage Mechanical Output Power.....	82
9.8.3 Triangular Voltage Mechanical Output Power.....	83
9.8.4 Comparison of Mechanical Output Power	83
9.9 Electroacoustic Efficiency	83
9.9.1 Sinusoidal Voltage Electroacoustic Efficiency	84
9.9.2 Square Voltage Electroacoustic Efficiency	85
9.9.3 Triangular Voltage Electroacoustic Efficiency	86
9.9.4 Comparison of Electroacoustic Efficiency	87
9.10 Equivalent RLC Electrical Circuit	87
9.10.1 Sinusoidal Voltage Equivalent RLC Electrical Circuit	87
9.10.2 Square Voltage Equivalent RLC Electrical Circuit	89
9.10.3 Triangular Voltage Equivalent RLC Electrical Circuit	90
9.11 Inductance Results	92
9.11.1 Calculated Inductance.....	92
9.11.2 Measured Inductance via LCR Meter.....	92

9.11.3 Calculated Inductance via Measure Peak Current	93
9.11.4 Calculated Inductance via RLC Equivalent Electrical Circuit	93
9.11.5 Comparison of Calculated and Measured Inductance	94
9.12 Variations of the Square Voltage Waveform.....	94
9.12.1 Variations in the DC Offset	95
9.12.2 Variations in Duty Cycle	95
9.12.3 Variations in Polarity	96
9.13 Cavitation.....	97
<i>Chapter 10 – Conclusion</i>	<i>103</i>
10.1 Achievement of Project	103
10.2 Project Limitation	104
10.3 Further Research Recommendations	105
<i>Appendices</i>	<i>106</i>
<i>References</i>	<i>117</i>

List of Figures

Figure 1. Magnetic Domain Structure.....	6
Figure 2. Extension Magnetostriction.....	6
Figure 3. Compression Magnetostriction.....	7
Figure 4. Young’s Modulus.....	16
Figure 5. Poisson’s Ratio.....	17
Figure 6. Magnetic Field Created by a Coil.....	20
Figure 7. Magnetic Hysteresis.....	22
Figure 8. Peizoceraminc Equivalent RLC Electrical Circuit.....	24
Figure 9. Magnetostrictive Equivalent RLC Electrical Circuit.....	25
Figure 10. Process of Creating Cavation.....	29
Figure 11. Microjet Creation from a Vaccum Bubble [32].....	29
Figure 12. Principle Sinusoidal Waveform.....	33
Figure 13. Principle Sqaure Waveform.....	34
Figure 14. Principle Triangular Waveform.....	34
Figure 15. Positive DC Biased Sqaure Waveform.....	35
Figure 16. Negative DC Biased Sqaure Waveform.....	36
Figure 17. Duty Cycle of 5 per cent.....	37
Figure 18. Duty Cycle of 95 per cent.....	38
Figure 19. IEC60782 Basic Impedance Circuit.....	39
Figure 20. IEC60782 Basic Impedance Circuit with Additional Series Resistance.....	40
Figure 21. Electroacoustic Efficiency Diagram.....	42
Figure 22. Electrocavitation Efficiency Diagram.....	43
Figure 23. Peizoceramic Equivalent RLC Electrical Circuit.....	43
Figure 24. Magnetostrictive Equivalent RLC Electrical Circuit.....	44
Figure 25. Petošić et al Electroacoustic Efficiency Diagram.....	47
Figure 26. Gooberman [2] Magnetostrictive Equivalent RLC Electrical Circuit.....	48
Figure 27. Piezoceramic Equivalent RLC Electrical Circuit.....	48
Figure 28. Magnetostrictive Equivalent RLC Electrical Circuit.....	49
Figure 29. Small Transducer Design.....	54
Figure 30. Large Transducer Design.....	55
Figure 31. Supplied Nickel Laminations from New Wave Leather on an A4 Sheet of Paper.....	55

Figure 32. Produced Windings by W.A. McHugh on an A4 Sheet of Paper.....	57
Figure 33. Produced Magnetostrictive Transducer by W.A. McHugh on an A4 Sheet of Paper.	59
Figure 34. Unstable Square Waveform for Tektronic AFG 3022B.	61
Figure 35. Unstable Square Waveform from HAMEG HM8030-4.....	62
Figure 36. Unstable Square Waveform for BWD 160A.	64
Figure 37. Square Waveform from the Semikron AN-8005.....	65
Figure 38. Circuit Diagram for Half Controlled H Bridge.....	65
Figure 39. Unloaded Electrical Input Power.	69
Figure 40. Loaded Electrical Input Power.	70
Figure 41. Unloaded Electrical Resonance.	71
Figure 42. Loaded Electrical Resonance.....	72
Figure 43. Unloaded Mechanical Resonance.	73
Figure 44. Loaded Mechanical Resonance.	75
Figure 45. Bandwidth and Quality Factor for Sinusoidal Waveform (Loaded).	76
Figure 46. Bandwidth and Quality Factor for Square Voltage Waveform (Loaded)....	77
Figure 47. Bandwidth and Quality Factor for Triangular Voltage Waveform (Loaded).....	78
Figure 48. Electroacoustic Efficiency Diagram for Sinusoidal Voltage Waveform....	84
Figure 49. Electroacoustic Efficiency Diagram for Square Voltage Waveform.	85
Figure 50. Electroacoustic Efficiency Diagram for Triangular Voltage Waveform....	86
Figure 51. Sinusoidal Voltage Supply Equivalent RLC Electrical Circuit.....	88
Figure 52. Square Voltage Supply Equivalent RLC Electrical Circuit.....	90
Figure 53. Triangular Voltage Supply Equivalent RLC Electrical Circuit.....	91
Figure 54. Variations of DC Offset for a 20kHz Square Voltage Waveform.....	95
Figure 55. Variations of Duty Cycle for a 20kHz Square Voltage Waveform.	96
Figure 56. Variations of Polarity for a 20kHz Square Voltage Waveform (including DC offset).	97
Figure 57. Creation of Cavitation Cloud.....	98
Figure 58. Frequency Spectrum of 5.255 kHz at Cavitation.....	99
Figure 59. Input Electrical Power Waveforms at 11.013 kHz Producing Cavitation.	100
Figure 60. Frequency Spectrum of 11.013 kHz at Cavitation.	101
Figure 61. Electro-cavitation Efficiency Diagram at 11.013 kHz.	102

List of Tables

Table i. Electromagnetic Properties of Nickel.	13
Table ii. Magnetic Materials [5].....	15
Table iii. Mechanical Properties of Nickel.	19
Table iv. Transducers Optimum Operating Frequencies.	53
Table v. Continuous Current Rating of Produced Windings [41].....	56
Table vi. Continuous Current Rating of Produced Windings [41].	56
Table vii. Adjusted Continuous Current Rating of Produced Windings.	57
Table viii. Maximum Load Current per Transducer Combination.	58
Table ix. Characteristics of Tektronic AFG 3022B.	60
Table x. Characteristics of HAMEG HM 8030–4.	61
Table xi. Characteristics of BWD 160A.	63
Table xii. Approximate Unloaded Resonant Frequencies.....	74
Table xiii. Approximate Loaded Resonant Frequencies.	75
Table xiv. Sinusoidal Bandwidth and Quality Factor (approx).	77
Table xv. Square Bandwidth and Quality Factor (approx).	78
Table xvi. Triangular Bandwidth and Quality Factor (approx).	79
Table xvii. Transducer Impedance and Phase Angle.	81
Table xviii. Mechanical Output Power.	83
Table xix. Comparison of Electroacoustic Efficiency for all Three Voltage Waveforms.....	87
Table xx. Measured Inductance Values of all Transducers.	92
Table xxi. Calculated Inductance via Peak Current Values.	93
Table xxii. Comparison of Calculated Inductance.	94
Table xxiii. Cavitation at 5.525 kHz Electroacoustic Efficiency.....	99
Table xxiv. Cavitation at 11.013 kHz Electroacoustic Efficiency.....	101

List of Appendices

Appendix A. Project Specification.....	106
Appendix B. Transducer Design.....	107
Appendix C. Unloaded UMST. Various Voltage Waveforms.....	109
Appendix D. Loaded UMST. Various Voltage Waveforms.....	111
Appendix E. Vibration Analysis of Unloaded UMST. Various Voltage Waveforms.	113
Appendix F. Vibration Analysis of Loaded UMST. Various Voltage Waveforms.	115

Nomenclature and Acronyms (Abbreviations)

General

USQ	University of Southern Queensland
UMST	Ultrasonic Magnetostrictive Transducer
MST	Magnetostrictive Transducer
AFG	Arbitrary Function Generator
rms	root mean square
DC	Direct Current
AC	Alternating Current
RLC circuit	Electrical circuit containing pure values of Resistance, Inductance and Capacitance
RCD	Residual Current Device
LCR meter	Inductance, Capacitance and Resistance meter
FFT	Fast Fourier Transform
Hz	Hertz - oscillations per second or frequency. 1000 oscillations per second equals 1000 hertz equal 1kHz
Medium	Material where the ultrasonic energy is transmitted into in normal operation, such as water or chemical solutions
PLC	Programmable Logic Controller

V	Volts (unit of electricity)
A	Amps (unit of electrical current)
W	Watts (unit of power)
V_P	Measurement of voltage from 0 volts to maximum (peak) volts
V_{PP}	Measurement of voltage from minimum volts to maximum volts

Electromagnetic

H	Magnetic field intensity ($A.m^{-1}$)
E	Electric flux intensity ($V.m^{-1}$)
B	Magnetic flux density (T)
D	Electric flux density ($C.m^{-2}$)
J	Electric current density ($A.m^{-2}$)
ρ	Electric flux density ($C.m^{-2}$)
μ	Permeability of the medium ($H.m^{-1}$)
ϵ	Permittivity of the medium ($F.m^{-1}$)
σ	Conductivity of the medium ($S.m^{-1}$)

Mechanical

K	Bulk modulus (GPa)
E	Young's Modulus (GPa)
μ	Poisson's Ratio (No units)
σ	Tensile stress (Pa)

ε	Tensile strain (m.m^{-1})
V	Volume of the material (m^3)
p	External pressure of the material (Pa)
F	Force applied (N)
A	Cross sectional area (m^2)
l	Length (m)
ε_y	Transverse strain (m.m^{-1})
ε_x	Longitudinal or axial strain (m.m^{-1})

Chapter 1 – Introduction

1.1 Introduction

One of the properties of nickel is the ability to resist various forms of corrosion. This property allows nickel to be used in harsh and toxic environments, such as the ocean or with industrial chemicals. Another special property of nickel is that it is magnetostrictive. Joule, in 1842 [1], discovered the magnetostrictive effect, also referred to as the Joule effect, where a material will change its physical length when subjected to an induced magnetic field. Magnetostrictive transducers convert magnetic energy into mechanical energy. That is, nickel can use an oscillating magnetic field to produce oscillating mechanical energy. The magnetostrictive effect was used extensively in World War 2 for sonar transducers. More recent uses include dentistry, ultrasonic cleaning, plastic welding and improved metal refining.

1.2 Project Aim

This project aims to investigate the magnetostrictive properties of nickel. The nickel, with its magnetostrictive effect, will be used as an ultrasonic transducer. Including detailed operation of the transducer with the aim of optimising transducer design.

1.3 Outline of Study

The outline of this study is to research the magnetostrictive properties of almost pure nickel (99.5%). Magnetostriction is a complicated effect so some further explanation is required. The details start with the properties of nickel, a definition of magnetostriction leading to a current theory of ‘Classical Magnetostriction’. The study progresses to the primary use of magnetostrictive transducers. The primary use is the generation of acoustic energy and cavitation. A nickel magnetostrictive transducer will then be tested. With the combination of theory and practical results

the nickel magnetostrictive transducer will be optimised to produce the maximum amount of acoustic energy compared to the electrical input power.

1.4 The Problem

This project has many parts that require separate and detailed investigations to get a full understanding on how acoustic energy is created by a nickel magnetostrictive transducer. Magnetostrictive transducers can be defined as the conversion of electrical energy into mechanical energy and the conversion of that mechanical energy into acoustic energy [2]. Niemczewski [3] takes it one step further with the conversion of acoustic energy into cavitation.

1.5 Research Objectives

This project is divided into five primary sections and three secondary sections. The primary sections were designed to get a full appreciation of the research process and an in-depth understanding to magnetostriction.

The primary sections are:

- Research magnetostriction including the interaction of magnetic flux and mechanical action;
- Develop a power electronic system to accurately drive the magnetostrictive effect of the transducer;
- Design an electromagnetic simulation of a known transducer;
- Investigate the electrical method of determining mechanical output; and
- Optimise the power electronic design to suit standard mains supply.

A further three sections will be attempted if time permits. The secondary sections are designed to use advance simulation methods to gain a better understanding of the primary sections.

The secondary sections are:

- Simulate the magnetostrictive effect of different materials.
- Simulate the magnetostrictive effect on different physical transducer designs.
- Investigate the mechanical wave pattern produced by different transducer designs.

Chapter 2 – Literature Review

2.1 Nickel

Nickel is an abundant metallic element found in the earth. Nickel makes up approximately three per cent of the earth's crust and can be found in many large ore deposits around the world. Refined nickel has the appearance of a silvery white metal which can have a high polish. It has been used for tools and coins since 4 000 BC although mistakenly thought of as silver or iron.

The name nickel was from the first recognised ore body in Germany called 'Kupfernickel'. The uses of nickel have increased since the process of refining was developed by A.F. Cronstedt in the mid-18th century [4].

Nickel is used in producing alloys because of its high melting temperature and high resistance to corrosion. The magnetic properties of nickel have been known for some time, but have only been exploited since the 20th century.

2.2 Magnetostriction

Magnetostriction was first investigated by J.P. Joule in 1842 [1], where he was approached by Mr F.D. Arstall to investigate a potentially new form of electromagnet engine. Joule investigated the effects of magnetism on copper and iron and confirmed iron does indeed increase its length when subjected to an external magnetic field. When the magnetic field is removed the iron resumes its original length. This effect was not witnessed in copper. The measured increase in length is in the order of 1/720 000 or approximately a 0.000 139 per cent increase.

Neelakanta [5] p316, best describes magnetostriction.

When a ferromagnetic material is magnetised, changes in the physical dimensions, in general occur. This is known as magnetostriction. The dimensional change occurring along the direction of induced magnetic field is called the Joule effect magnetostriction. The converse of magnetostriction is known as the Villari effect.

Magnetostriction is only in ferromagnetic material. Magnetostriction is where the physical dimension of a ferromagnetic material will change when it is subjected to an external magnetic field.

2.2.1 Inverse Magnetostriction

While this definition is not required for this dissertation it is useful in the understanding of magnetostriction.

Inverse magnetostriction is known as the Villari effect. The Villari effect is where the magnetic flux density (T) and magnetic field intensity ($A.m^{-1}$) of a material change when subjected to a physical force.

2.3 Theories on Magnetostriction

Magnetostriction can be explained by the magnetic domain theory. As the ferromagnetic material is solidified from a molten state, many crystalline structures grow at different rates. Each crystalline structure has its own unique magnetic intensity and direction. By combining the individual crystalline states, an overall magnetic intensity and density can be identified. When an external magnetic field is induced on the ferromagnetic material the internal magnetic domain realign themselves with the external magnetic field as shown in figure 1. In the process of realigning, the physical dimensions of the ferromagnetic material change, thus creating mechanical movement as shown in figure 2 and 3.

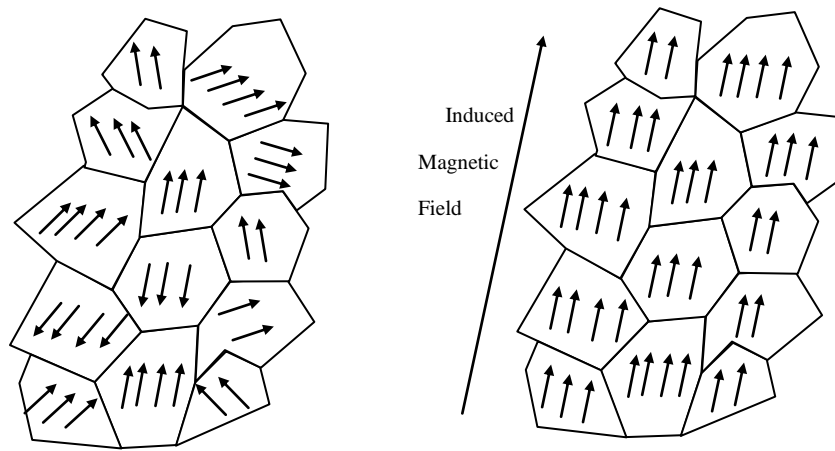


Figure 1. Magnetic Domain Structure.

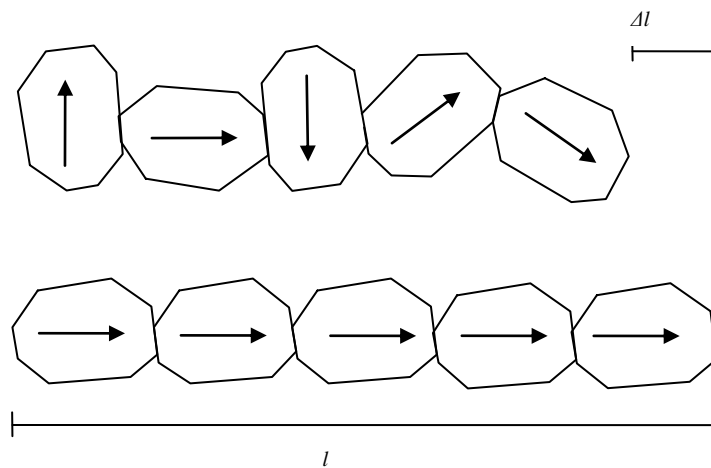


Figure 2. Extension Magnetostriction.

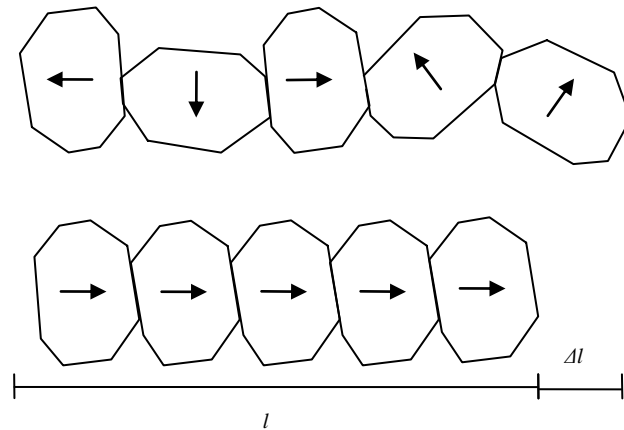


Figure 3. Compression Magnetostriction.

In figures 2 and 3 l represents the length of the material and Δl is the change in the length.

There have been many theories about the relationship between magnetic flux and mechanical action in magnetostrictive materials. With most initial theories limited by technology they focused on the electromagnetic properties of the material [6-9]. It was not until the 20th century that the physical properties of the materials, such as stress, strain, and elastic values, were included in magnetostriction theories [2, 10-13]. It was not until the mid 20th century that Kapitza [14] identified three modern theories of magnetostriction. They are

- Atomic magnetostriction,
- Thermal magnetostriction and
- Classical magnetostriction.

2.3.1 Atomic Magnetostriction

Atomic magnetostriction is beyond the scope of this dissertation, but a brief explanation is provided for the benefit of the reader.

Atomic magnetostriction is based on the disturbance caused by the induced magnetic field upon the atoms in the crystalline structure. The details of the crystalline

structure and the electron shells composition of the elements are required to accurately measure the magnetostrictive effect. Buschow & De Boer [15], Huston et al [16] and Brabers et al [17] have explored the atomic theories on magnetostriction. An example on the complexities of the atomic magnetostrictive theory can be best shown by Buschow and De Boer [15] magnetostrictive equation:

$$\frac{\Delta l}{l} = \frac{3}{2} \lambda_{100} \left(\alpha_x^2 \beta_x^2 + \alpha_y^2 \beta_y^2 + \alpha_z^2 \beta_z^2 - \frac{1}{3} \right) + 3\lambda_{111}(\alpha_x \alpha_y \beta_x \beta_y + \alpha_y \alpha_z \beta_y \beta_z + \alpha_x \alpha_z \beta_x \beta_z) \quad (1)$$

where λ_{100} is crystalline structure in the y direction ($\lambda_{y,xz}$), λ_{111} is crystalline structure in the direction of y, x and z ($\lambda_{y,xz}$), α_x , α_y and α_z are the alpha constants in the x, y and z direction, β_x , β_y and β_z are the beta constants in the x, y and z direction.

2.3.2 Thermal Magnetostriction

It is commonly known that metals expand when their temperature increase. Thermal magnetostriction theory uses thermal expansion to explain the change on length.

When an induced magnetic field is applied to the magnetostrictive material the internal crystalline structures attempt to realign. This realignment or small physical movement within each crystal causes internal heating thereby creating thermal expansion.

Nizhankovskii [18] has been investigating thermal magnetostriction at temperatures of 4 Kelvin where the Hysteresis effect appears to not exist.

2.3.3 Classical Magnetostriction

As science and technology increase their abilities, various formulas attempt to explain classical magnetostriction. Classical magnetostriction broadly relies on the physical properties of the material and the induced magnetic field.

In 1930 Smith [9, 19] attempted to explain magnetostriction by the Villari effect. His proposed formulas are:

$$\tau' = K.H \quad (2)$$

$$M' = K'.\varepsilon \quad (3)$$

where τ' is the alternating driving force, ε is the alternating mechanical strain, H is the magnetic field intensity, M' is the alternating magnetisation produced by the Villari effect and K and K' are Smiths constants (in phase).

Smith theories were improved with the assistance of Butterworth [8, 12] in 1931 with the following theory:

$$\tau' = \lambda.B \quad (4)$$

$$H' = \gamma.\varepsilon \quad (5)$$

where τ' is the alternating driving force, ε is the alternating mechanical strain, H' is the magnetomotive force, B is the alternating magnetic flux density, λ and γ is Butterworth and Smith's constants (in phase).

Kikuchi [12, 20] in 1940 proposed more theories that incorporated Young's modulus of the magnetostrictive material.

$$\tau' = \Gamma.M \quad (6)$$

$$H' = \Gamma'.\varepsilon \quad (7)$$

with

$$\Gamma = E.\left(\frac{\delta\left(\frac{\Delta l}{l}\right)}{\delta M}\right) \quad (8)$$

Where τ' is the alternating driving force, ε is the alternating mechanical strain, H' is the magnetomotive force, E is Young's modulus, M is magnetic flux density, Γ and Γ' is Kikuchi constants (complex).

The magnetomotive force can be determined by

$$H = IN, \quad (9)$$

where I is the peak current and N is the number of turns in the winding.

2.4 Ultrasonic Energy

The human hearing range is approximately between 10 Hz and 20 kHz. This is commonly referred to as the sonic region, where humans are able to hear sound energy. The sonic range, generally, decrease for humans as they age to the extent where frequencies above 15 kHz cannot normally be heard by adults. The ultrasonic region is defined as the frequency above the human hearing range. This can be generalised as frequencies above 20 kHz.

As with all signals, Fourier analysis can be applied to ultrasonic frequencies. Fourier analysis is where the signal is converted from the time domain into the frequency domain.

2.5 Transducer Design

The physical process of creating sonic and ultrasonic energy can be attributed to the design of the transducer where the resonant frequency is determined by the physical dimensions of the transducer. The resonant frequency is where there is a maximum efficiency of output energy as compared to input energy.

The details of many transducer designs are commercially confidential but Kikuchi [12] and Goberman [2] provide some fundamental information. It is widely known that the United States Navy has many designs on magnetostrictive transducers. These designs are based on the manufactured material Terfenol-D. Terfenol-D can provide an order up to $3\ 600 \times 10^{-6}$ [4, 21] when operated at resonance. Another

commercially available material is Nitinol which can have an order of $60\,000 \times 10^{-6}$ [21].

2.6 Uses for Magnetostrictive Transducers

Magnetostrictive transducers can be defined as the conversion of electromagnetic energy into mechanical energy and the conversion of mechanical energy into acoustic energy [2]. Niemczewski [3] takes it one step further with the conversion of acoustic energy into cavitation. Magnetostrictive transducers are used where sonic and ultrasonic energy is required.

Magnetostrictive transducers have two major advantages over its main competitor piezo-electric transducers. They are the ability to operate with more electrical power and reliance on current, not voltage for its electromagnetic source. The physical dimensions of the magnetostrictive material can be large enough to operate at many kilowatts.

Chapter 3 – Properties of Nickel

3.1 Electromagnetic Properties of Nickel

Although the electrical properties are not required for this research it is important to realise that electrical properties and magnetic properties are interrelated as defined by Maxwell's Laws.

3.1.1 Permittivity

Permittivity is the property of the material to attract or repel electric fields as compared to free space (vacuum).

$$\varepsilon = \varepsilon_0 \varepsilon_r \quad (10)$$

Where ε_0 is the permittivity of free space $1/(36\pi) \times 10^{-9}$ Farad per metre (F.m^{-1}) and ε_r is the permittivity ratio of the material. The permittivity of the material is ε .

Nickel is a solid conductive metal thereby having a permittivity ratio of infinite, ∞ . The permittivity of nickel is infinite, ∞ .

3.1.2 Permeability

Permeability is the property of the material to attract or repel magnetic fields. An example of a permeable material can be found in an in the core of an electrical transformer. A magnetic field is produced by the primary winding and is conducted through the core to the secondary windings. The core material can attract or repel the magnetic field. In the case of an electrical transformer it is desired to attract the magnetic field.

The value of attraction or repulsion of a magnetic field is known as permeability. Permeability is referenced to the magnetic field in free space (vacuum) by the following equation

$$\mu = \mu_0 \mu_r \quad (11)$$

where μ_0 is the permeability of free space $4\pi \times 10^{-7}$ Henry per metre (H.m^{-1}) and μ_r is the permeability ratio of the material. The permeability of the material is μ .

The electromagnetic values of nickel are displayed in table i.

Table i. Electromagnetic Properties of Nickel.

Electromagnetic Properties of Nickel		
Property	Symbol	Value
Permittivity	ϵ	$\infty \text{ F.m}^{-1}$
Permeability	μ	$753.98 \times 10^{-6} \text{ H.m}^{-1}$

3.2 Magnetic Materials

The ability of the material to attract or resist an induced magnetic field is the primary method that classifies the magnetic properties of the material. This is referred to as the permeability ratio of the material. The permeability ratio of the material is attributed to the spin and orbital spin of electrons around the nucleus of the atom and incomplete inner electron shells [22].

3.2.1 Diamagnetic Material

A diamagnetic material exhibits negative magnetism [5]. A diamagnetic material repels an external magnetic field by producing a smaller internal magnetic field in opposite polarity. The external magnetic field will conduct around the diamagnetic material, rather than through the diamagnetic material. The permeability of diamagnetic material is less than one and negative.

3.2.2 Paramagnetic Material

A paramagnetic material has the permeability of less than one. That is the magnetic field can conduct through the paramagnetic material although the magnetic field will experience less resistance by conducting around the paramagnetic material. An external magnetic field may tend to polarize the random moments by creating thermal agitations causing only a very small (partial) magnetism [5].

3.2.3 Ferromagnetic Material

Ferromagnetic materials are a refined material that has the ability to conduct higher magnetic flux compared to free space. Ferromagnetic materials have a permeability greater than one and therefore attract magnetic flux compared to free space. The three ferromagnetic elements are iron, cobalt and nickel.

Soft ferromagnetic material have high permeability and will return to its natural state when the induced magnetic field is removed. Soft ferromagnetic materials are used in transformers where the magnetic flux changes direction every cycle.

Nickel is classed as a soft ferromagnetic material.

Hard ferromagnetic materials have high permeability and will attempt to retain its induced magnetised state. Hard ferromagnetic materials are ideal permanent magnets.

3.2.4 Anti-ferromagnetic Material

Antiferromagnetic material relies on temperature to become permeable. The temperature that allows maximum permeability is known as the Neel Temperature. The permeability of antiferromagnetic material is usually less than 1.

3.2.5 Ferrimagnetic Material

Naturally found materials, such as iron ore and nickel ore, that have an overall magnetic flux are known as ferrimagnetic.

3.2.6 Curie Temperature

The curie temperature is the temperature where the stable magnetic properties of the material change due to the extra energy provided by heat. Ferromagnetic materials become paramagnetic when the temperature is above the curie temperature [5]. When the magnetic properties of the material change, this also changes the permeability of the material.

A description of all magnetic materials is provided in table ii.

Table ii. Magnetic Materials [5].

Magnetic Material	Susceptibility to induced Magnetic Field	Permeability	Example
Diamagnetic	Negative and Small	< -1	Cu, Ag, Au
Paramagnetic	Positive and Small	> 1	Mg, Li
Ferromagnetic	Positive and very large	$\gg 1$	Fe, Ni
Anti-ferromagnetic	Positive and small	< 1	NiO
Ferrimagnetic	Positive and Large	$\gg 1$	Fe ₂ O ₃

3.3 Mechanical Properties of Nickel

Original theories of magnetostriction relied upon the mechanical properties of the ferromagnetic material. The following provides a description of the some of the physical properties.

3.3.1 Modulus of Elasticity

The modulus of elasticity can be any type of force acting on a material that causes temporary deformation. In the case of a transducer, repetitive temporary deformation is ideal. Permanent deformation will lead to a broken transducer.

3.3.2 Young's Modulus

The initial linear section of the ratio of stress and strain of the material is referred to as Young's Modulus. Young's Modulus is used as the basis for the amount of elastic deformation. Elastic deformation can be repetitive and will not provide permanent deformation to the material. The definition of Young's Modulus is provided in figure 4.

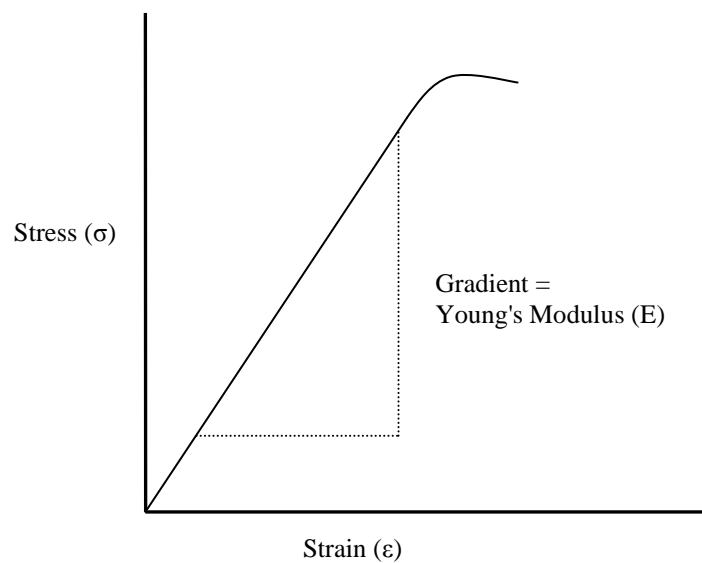


Figure 4. Young's Modulus.

Young's Modulus is

$$E = \frac{\sigma}{\epsilon} \quad (12)$$

where σ is the tensile stress and ϵ is the tensile strain.

Tensile stress can be further explained by

$$\sigma = \frac{F}{A} \quad (13)$$

where F is the force applied and A is the cross sectional area.

Tensile strain can be further explained by

$$\varepsilon = \frac{\Delta l}{l} \quad (14)$$

where Δl is the change in length and l is the original length.

This results in Young's Modulus being

$$E = \frac{\frac{F}{A}}{\frac{\Delta l}{l}} = \frac{Fl}{\Delta l A}. \quad (15)$$

3.3.4 Poisson's Ratio

Poisson's ratio is the ratio of force inflicted on the material to the resulting perpendicular force displayed by the material.

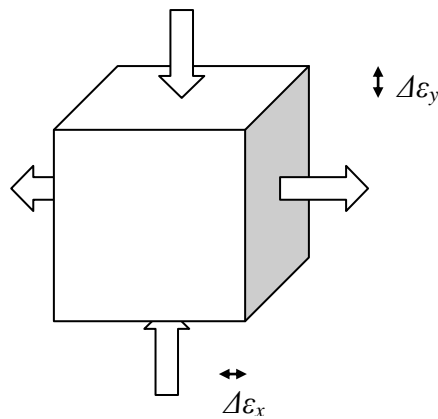


Figure 5. Poisson's Ratio.

Poisson's Ratio is

$$\mu = -(\Delta\varepsilon_y/\Delta\varepsilon_x) \quad (16)$$

where $\Delta\varepsilon_y$ is the transverse strain and $\Delta\varepsilon_x$ is the longitudinal or axial strain.

While Poisson's ratio can be used to explain magnetostriction, it is also important for the design of the transducer face. Most MSTs are designed with the nickel transferring the acoustic (mechanical) energy to the transducer face plate by direct connection. The face plate should be highly resistant to corrosion and have a low Poisson's ratio as the face plate should transfer the acoustic energy in the desired direction.

3.3.5 Creep

Creep is the process where permanent deformation occurs due to repetitive stress [4, 21]. The susceptibility of creep increases as the operating temperature increases. A method to reduce the effects of creep deformation is to operate the material below the homologous temperature. The homologous temperature is usually half the absolute melting temperature of the material [4].

3.3.6 Nickel Mechanical Properties

The mechanical properties of nickel are listed in table iii. The transducer will be designed to operate below 100°C. Due to this temperature limitation the melting and homologous temperature (creep) will not be a factor.

As the output of the transducer is sound energy, the speed of sound in nickel is also provided in table iii.

Table iii. Mechanical Properties of Nickel.

Mechanical Properties of Nickel		
Mechanical Properties	Symbol	
Bulk Modulus	K	180GPa
Young's Modulus	E	206GPa
Poisson's Ratio	μ	0.30
Melting Temp	T_m	1455 K (1182°C)
Curie Temp	T_c	626K (353°C)
Homologous Temp (Creep)	T_h	727.5K (454.5°C)
Speed of Sound	v_s	4 900 m.s ⁻¹

Chapter 4 – Magnetism

4.1 Generation of Magnetic Fields

A magnetic field is created by the flow of current. If the current is flowing in a coil the magnetic field is concentrated in the centre of the coil. If the centre of the coil is a ferromagnetic material, that attracts the magnetic field, then the magnetic field intensity and density can be increased. Figure 6 shows the concentration of the magnetic field in a coil of wire. The generation of the magnetic field in a MST is created by a wire coil or winding.

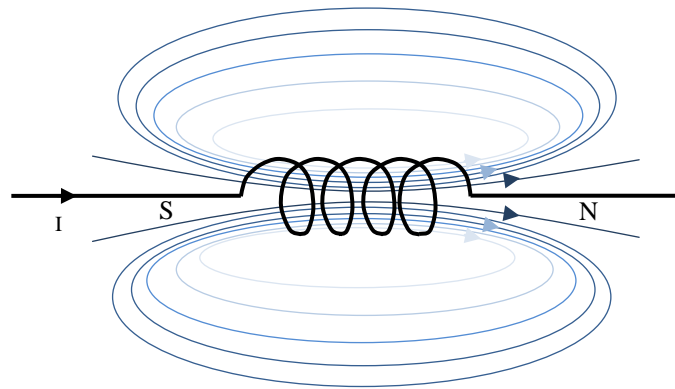


Figure 6. Magnetic Field Created by a Coil.

A magnetic field is defined by two parameters, being magnetic field intensity (H) and magnetic flux density (B). The following equation state the relationship of magnetic field intensity and magnetic flux density,

$$B = \mu H = \frac{\phi}{A} \quad (17)$$

where H is the magnetic field intensity ($A.m^{-1}$) and B is the magnetic flux density (T),.

The magnetic flux can be determined by,

$$\phi = BA \quad (18)$$

where ϕ is the magnetic flux (Wb) and A is the cross sectional area (m^2) with the cross sectional area being the area inside the windings.

Due to the high intensity and density of magnetic flux in the centre of the windings miniscule currents are produced. These currents are known as eddy currents. To reduce the effect of eddy currents the centre core is usually made up of laminations of the ferromagnetic material. As the core is made of many laminations a stacking factor is usually incorporated in the cross sectional area of the core material. A stacking factor takes into account the space between the laminations in the centre core material.

4.1.2 Hysteresis

There are limits to the amount of magnetic flux density (B) that the material can withstand. If the magnetic field intensity (H) is increased beyond the saturation level (H_{sat}) the magnetic flux density will not increase beyond the saturation level for magnetic flux density. As the magnetic field intensity is determined by the current and the number of turns, there is a maximum current and a maximum number of turns in achieving the saturation level of magnetic flux density.

These limits can be shown as a hysteresis curve as shown in figure *7*. Hysteresis also shows the different generation and degeneration of the magnetic flux as experienced in an alternating current source.

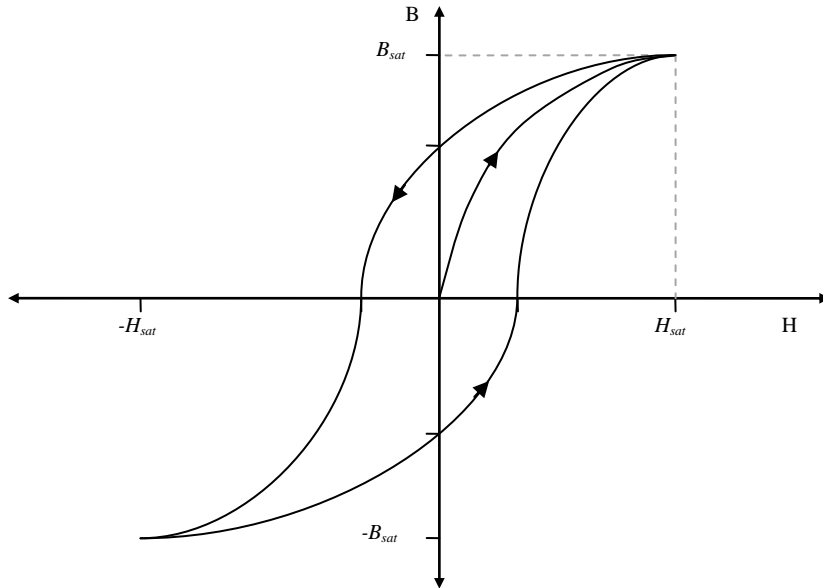


Figure 7. Magnetic Hysteresis.

Nickel has a saturation magnetic flux density (B_{sat}) of 0.617 T [4] and a permeability of $7.54 \times 10^{-7} \text{ H.m}^{-1}$ leading to a saturation magnetic field intensity (H_{sat}) of 818.3 A.m^{-1} .

4.1.3 Inductance

Faraday's Law states

$$E = -N \times \frac{d\phi}{dt} \quad (19)$$

where E is volts, N is the number of turns, ϕ is magnetic flux (Wb) and t is time. Inductance and current can be extracted from Faradays Law as Webers are equivalent to henry.amps. Equation (20) is Faraday's law converted to henrys and amps.

$$V = L \frac{di}{dt} \quad (20)$$

with V being volts L being inductance and i and t being current and time respectively.

As the transducer relies on the generation of a magnetic field i.e. an inductor, the electrical response of the transducer should be similar to the electrical response of an inductor. Equation (20) can be rearrange for inductance,

Inductance in a long solenoid can also be calculated by

$$L = \frac{\mu N^2 A}{l} \quad (21)$$

where L is the calculated inductance, l is the length of the linductor, μ is the permeability, N is the number of turns in the winding and A is the cross sectional area.

4.2 Interaction of Magnetic Flux and Mechanical Action.

As magnetic flux density and intensity is determined by the number of turns, cross sectional area and the current through the coil, the output power (mechanical action) of the magnetostrictive effect can be simulated via an electrical equivalent circuit. Petošić et al [23] has provided a method on the electromechanical properties of the transducer to determine the mechanical output of a piezoceramic transducer. By using Petošić et al as a basis for circuit design a conversion between the electric properties of the piezoceramic with the magnetic properties of a magnetostrictive transducer will produce an equivalent RLC electrical circuit for magnetostrictive transducers.

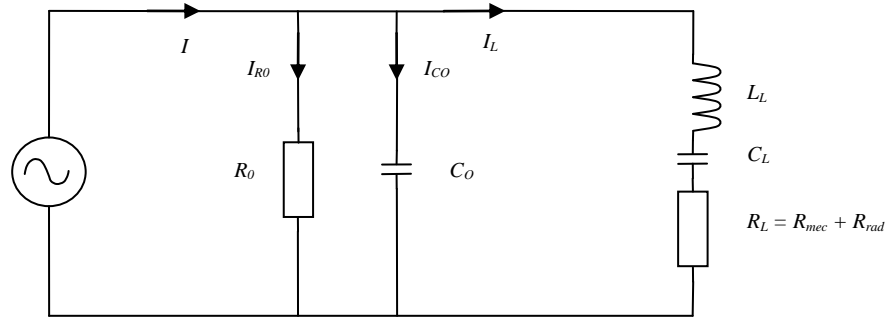


Figure 8. Peizoceraminc Equivalent RLC Electrical Circuit.

Petošić et al piezoceramic power formulas are given by,

$$P_{mec} = \frac{V^2 R_{mec}}{(R_{mec} + R_{rad})^2}, \quad (22)$$

$$P_{rad} = \frac{V^2 R_{rad}}{(R_{mec} + R_{rad})^2}, \quad (23)$$

where R_{mec} and R_{rad} are the mechanical and radiation resistance, V is the input voltage and P_{mec} and P_{rad} are the mechanical and radiated power.

The input to a magnetostrictive device is electrical with the produced output being mechanical action. By this description a magnetostrictive transducer is similar to an electric motor where the input is also electrical and the output is mechanical action, although a motor provides rotating mechanical action. Figure 9 shows the magnetostrictive equivalent RLC electrical circuit, which has similarities to an equivalent RLC circuit to an electrical motor.

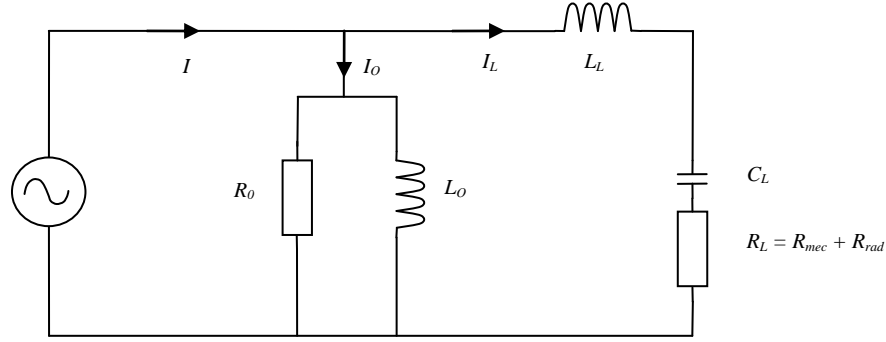


Figure 9. Magnetostrictive Equivalent RLC Electrical Circuit.

Magnetostrictive power formulas are given by

$$P_{rad} = I_L^2 (R_{rad} + R_{mec}) \times \frac{R_{rad}}{R_{rad} + R_{mec}}, \quad (24)$$

$$P_{rad} = I_L^2 R_{rad}, \quad (25)$$

$$P_{mec} = I_L^2 (R_{rad} + R_{mec}) \times \frac{R_{mec}}{R_{rad} + R_{mec}}, \quad (26)$$

$$P_{mec} = I_L^2 R_{mec}. \quad (27)$$

where R_{mec} and R_{rad} are the mechanical and radiation resistance, I_L is the load current voltage and P_{mec} and P_{rad} are the mechanical and radiated power.

The current passing through the load (I_L) will be in terms of rms, as the current will be in various waveforms. Where I_L is derived by

$$I_L = I_S - I_o \quad (28)$$

4.3 Resonant Frequency

The resonant frequency of the transducer is the frequency of operation where the transducer has maximum output power as compared to the input power. The resonant frequency for the UMST will differ when the transducer is vibrating in air as compared to vibrating in a medium as the medium provides more physical resistance to the vibrating transducer.

4.3.1 Harmonics

The transducer is primarily designed around the average magnetic conducting path. If the average magnetic conduction path is one wavelength of 20 kHz, then the transducer will also be efficient in the full harmonics of 20 kHz, being 40 kHz, 60 kHz, 80 kHz, etc.

4.4 Magnetostrictive Transducer Design

It is desirable to design a transducer to operate in the ultrasonic region. This will allow testing without an audible tone being heard. 20 kHz is the chosen frequency which also aligns with some industry standards. For ease of manufacturing a lamination design will be used for the transducer.

Kikuchi [12] recommends the average conducting path needs to be in terms of whole wave length of the desired operating frequency. Goobeman [2] also supports this theory but describes the transducer length being one half-wavelength long. With the desired frequency being 20 kHz and the speed of sound in nickel being $4\,900\text{ m}\cdot\text{s}^{-1}$ will produce a wavelength of 0.245 m and the length of the transducer to be approximately 0.122 5 m.

Chapter 5 – Uses of Ultrasonic Energy

5.1 Introduction

A transducer is any device that converts an input power of one form into an output power of a different form [24]. In the case of magnetostrictive transducers the input energy is in the form of a magnetic field and the output is mechanical energy. The mechanical energy can be used to produce acoustic energy.

5.2 Uses of Ultrasonic Transducers

Ultrasonic transducers operate in the range of sound above human hearing (>20 kHz). Acoustic energy has the ability to pass through a medium and/or reflect back from a medium [2, 25-28], and if the concentration of acoustic energy is enough it can penetrate and disrupt the cells or crystalline structure of the medium[2, 3, 29]. Therefore acoustic transducers can be separated into four distinct fields being detection, sonification, destruction and cavitation.

5.3 Detection Ultrasonic Transducers

Detection ultrasonic transducers are used to provide information without damaging the subject such as medical ultrasound imaging or surveying the world oceans with sonar. Detection involves a known ultrasonic frequency to be transmitted into a medium. Some of the transmitted energy is reflected when the energy meets the boundary of two different densities. An example would be bone and organs in the human body or sand and water in the ocean. The reflected energy is then received. The time difference between the transmitted signal and the return signal determines the distance where the speed of sound of the medium is known. Several receiving transducers can be used to triangulate the direction of the return signal thereby producing direction and distance of the reflecting target.

Another increasing field is non-destructive testing of materials. This is where sound energy is used to test materials for quality of production without destroying them. Detection ultrasonic transducers can identify hairline fractures in solid materials that cannot be seen by the human eye.

5.4 Sonification Ultrasonic Transducer

Sonification is the process of using sound energy as the method of transporting information over distance. This is commonly known in humans as speaking. It is well known that whales and dolphins use sonic and ultrasonic energy transmitted through water to communicate. The sound energy contains the signal in sonification as compared to the distance and direction of the reflected signal in detection ultrasonic transducers.

5.5 Destructive Ultrasonic Transducers

Destructive ultrasonic transducers are used in the cleaning of equipment, sterilisation or de-gassing of liquids. With the use of cavitation, ultrasonic transducers are able to pit or damage solid metals. Powerful ultrasonic energy can be used in the continuous washing of textiles [30] and create and improve materials [31].

Gooberman [2] provides other uses for ultrasonically induced cavitation

- Produce dispersions of normally indispersable materials such as mercury in nitrobenzene.
- Shatter high molecular weight molecules such as polymers, proteins and viruses.
- Remove grease and dirt from surfaces.
- Degas liquids.
- Pit the surface of metals.
- Increase the rate of chemical reactions.

5.6 Cavitation

Cavitation is caused by the rapid physical movement by the transducer face creating very small vacuum bubbles. Due to the pressure surrounding the vacuum bubble it is forced to implode or collapse. The imploding bubble results in a micro-jet of the medium. The micro-jet is the energy that encourages chemical reactions, cleaning and pitting of metallic surfaces. The micro-jet is not frequency dependant as the size of the vacuum bubble can differ in the medium.

Figure 10 shows the creation process of cavitation and figure 11 shows a magnified image of a bubble imploding resulting in a micro-jet.

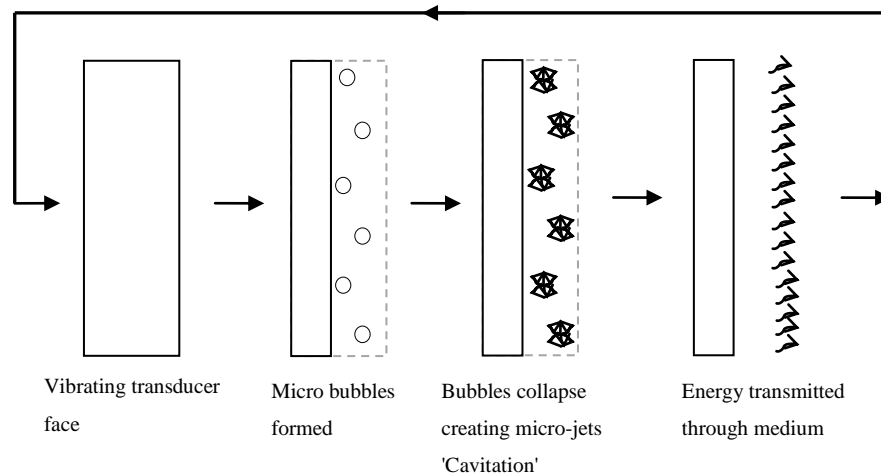


Figure 10. Process of Creating Cavation.

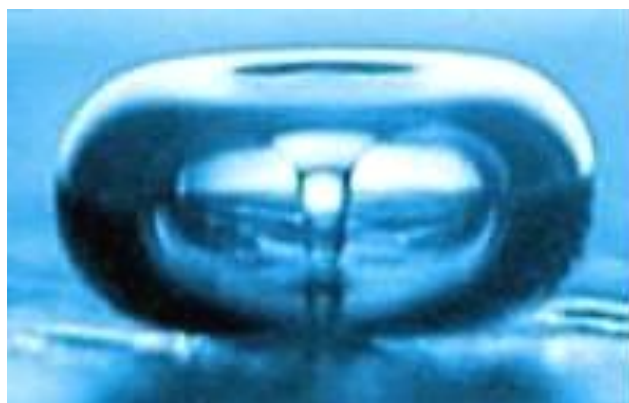


Figure 11. Microjet Creation from a Vacuum Bubble [32].

Gooberman [2] informs when the acoustic pressure is increased causing cavitation the physical and chemical effect of ultrasonics becomes apparent. Cavitation creates sound by the harmonic and sub harmonics of the operating frequency [33], encourages degradation of macroscopic molecules [13] and can result in the pitting of metallic surfaces [34].

Niemczewski [3] has found the temperature, air content of water and the depth of the transducer from the surface affects the intensity of cavitation when produced from the same source.

5.6.1 Sono-Chemistry

Another increasing field of ultrasonics is the sono-chemistry. Similar to the definition of destructive ultrasonic transducers, sono-chemistry focuses on encouraging chemical reactions. This is performed by the decrease in pressure of the vacuum where gaseous states of the medium are present and the high pressure caused by the imploding vacuum bubble. Sono-chemistry improves the ratios of chemicals need for the chemical reaction and decreases the time required for the chemical reaction.

Chapter 6 – Safety

Chapter 7 outlines various procedures in determining the operating conditions of a magnetostrictive transducer. Some UMST can require up to 1000 Volts and 100 Amps for normal operation. The combination of high power and a medium, usually water, can cause a potentially dangerous and life threatening environment. The following precautions were enforced, but not limited to:

- The use of over current circuit breakers and RCDs.
 - Extra care should be taken to avoid electrical shocks as RCDs have a trip time around 5–20 ms equating to 100–400 cycles of a 20 kHz, 100 V_{PP} waveform.
- The use of hearing protection. Especially when the transducer is operating the human hearing range (approximately 10 Hz to 20 kHz).
- No unsupervised experiments should be performed due to dangerous voltages and frequencies involved.
- When cavitation is present, no part of the human body is to come in contact with the transducer or the medium.
- Environmental effects should be considered. As mentioned earlier marine animals use sonic and ultrasonic energy in communicating (sonification). It is also well known that sound energy can travel for many kilometres through the world oceans.

Chapter 7 – Methodology

7.1 Introduction

IEC 60782 [35] provides a comprehensive procedure in identifying the properties of an ultrasonic magnetostrictive transducer (UMST), Petosic et al [23, 36] provides an increase in the analysis of UMST.

Although Petosic et al was primarily researching piezoceramic ultrasonic transducers, their knowledge can be combined with of IEC 61847 [37] and IEC 61088 [38]. This combination will increase the analysis of UMST.

IEC 60782 and Petosic et al use a pure sinusoidal voltage waveform as the supply for the ultrasonic transducer. The research conducted will use the sinusoidal as a primary voltage supply but also investigate alternate voltage waveform supplies as outlined in section 7.2.

The reader should also be reminded that an UMST relies on the induced magnetic field produced by current. The selection of the voltage waveform produces a differing current waveform. Both the voltage and current waveform will be analysed in relation to the UMST.

7.2 Supply Voltage Waveforms

The voltage supply will be no more than ± 50 V, with a maximum peak to peak range of 100 V. Three different voltage waveforms will be investigated. They are the sinusoidal, triangular and square waveform. The following sections provide more details on the properties of the waveforms.

7.2.1 Principle Waveforms

The principle waveforms are the sinusoidal, triangular and square. Initial testing of the UMST had a peak to peak voltage of 15 V and a DC offset of 0 V. Figures 12, 13 and 14 displays the principle waveform, all approximately 20 kHz with a 15V peak to peak and a DC offset of 0V.

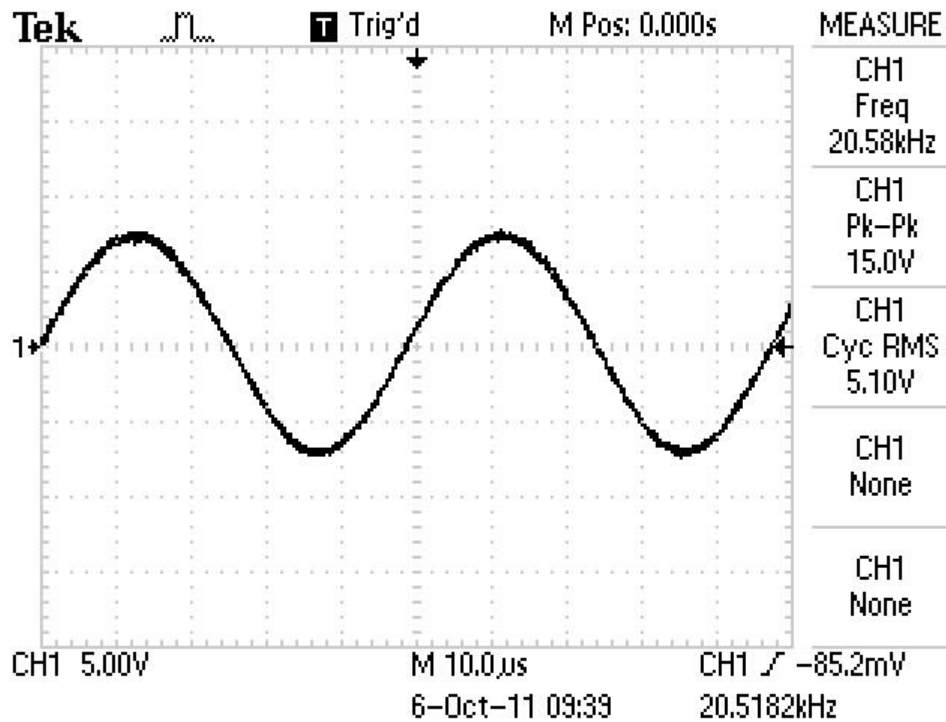


Figure 12. Principle Sinusoidal Waveform.

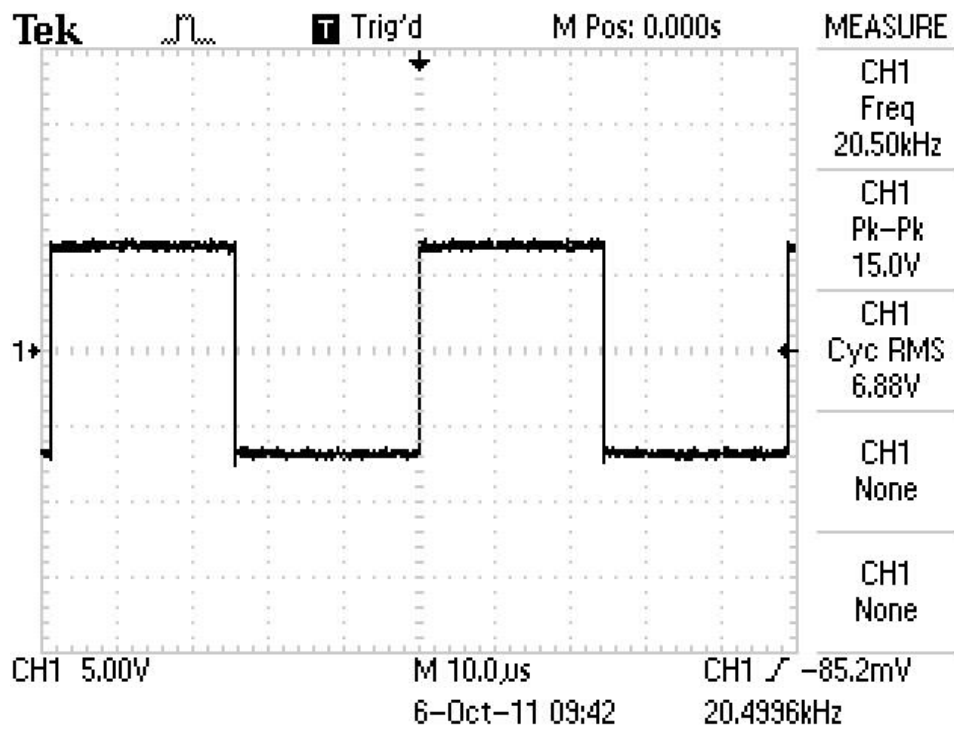


Figure 13. Principle Square Waveform.

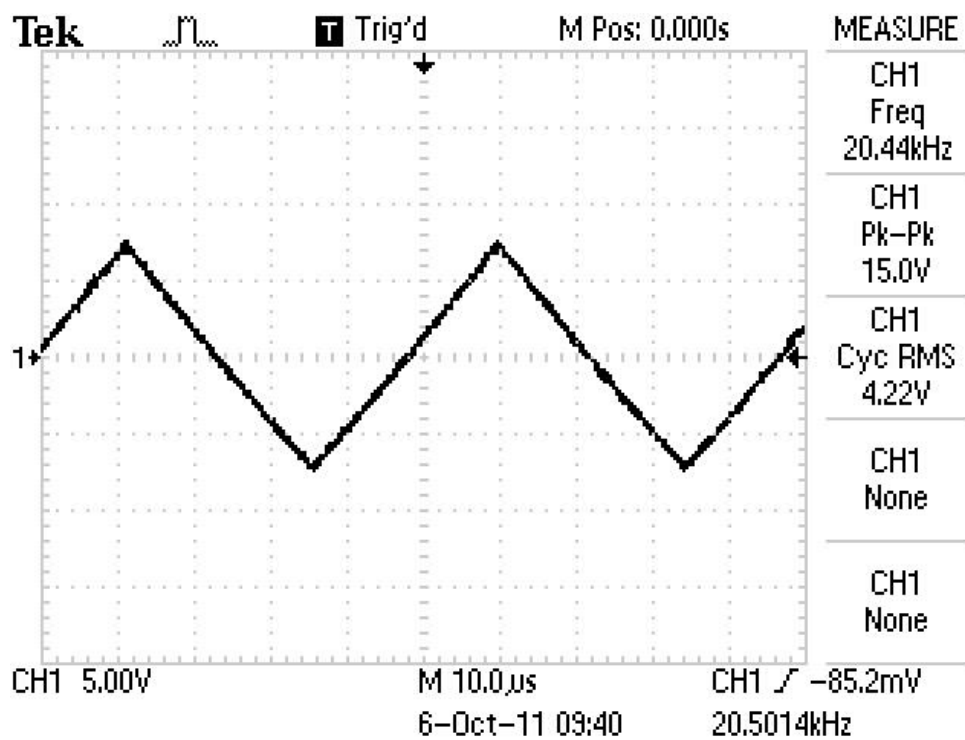


Figure 14. Principle Triangular Waveform.

7.2.2 DC Biased Waveforms

A pure square waveform has an average voltage of 0 V. When a constant voltage is added to a pure square waveform the average voltage is increased to equal the bias voltage. The DC bias can be increased till the whole square waveform is in the positive or negative volts. Figures 15 and 16 display a positive and a negative DC biased square waveforms. DC Biasing can be applied to all waveform including sinusoidal and triangular.

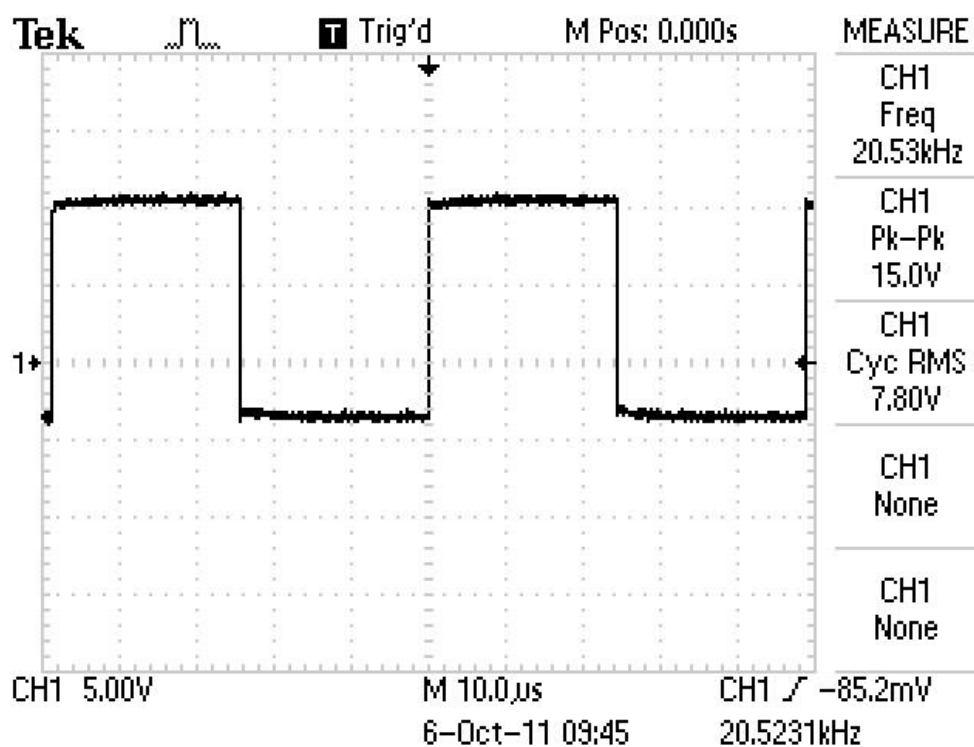


Figure 15. Positive DC Biased Square Waveform.

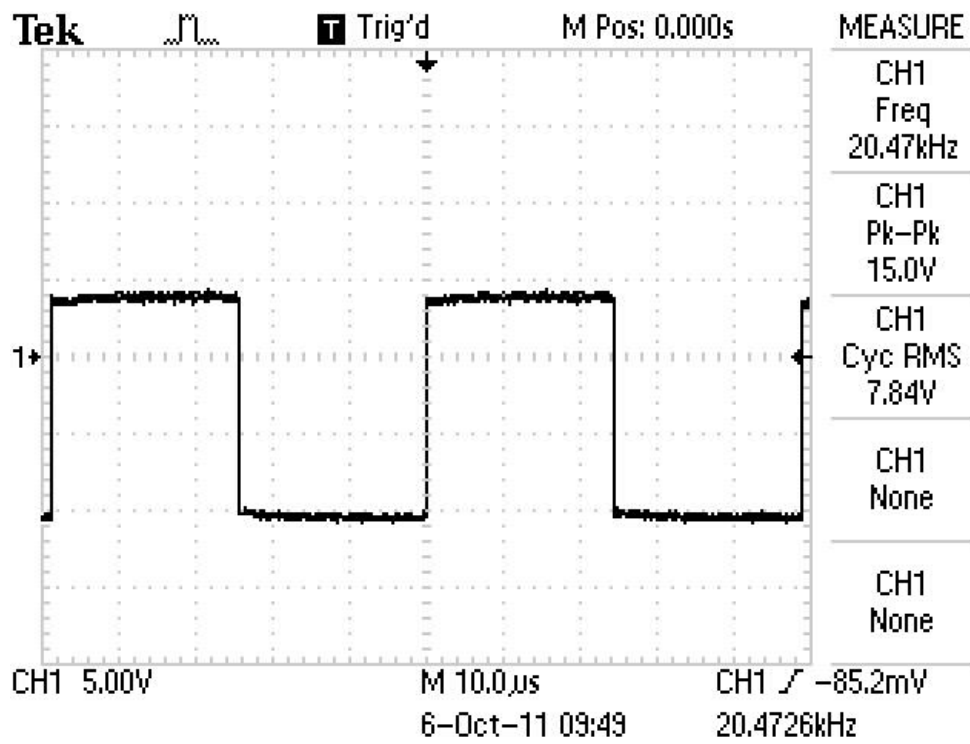


Figure 16. Negative DC Biased Square Waveform.

7.2.3 Duty Cycle Biased Waveforms

The duty cycle of a waveform is the ratio of time of high in the one period of the waveform to the time of one complete cycle. Figure 17 display a five per cent duty cycle of a square waveform. Waveforms like figure 17 are also known a pulse waveforms. Figure 18 display the 95 per cent duty cycle of a square waveform.

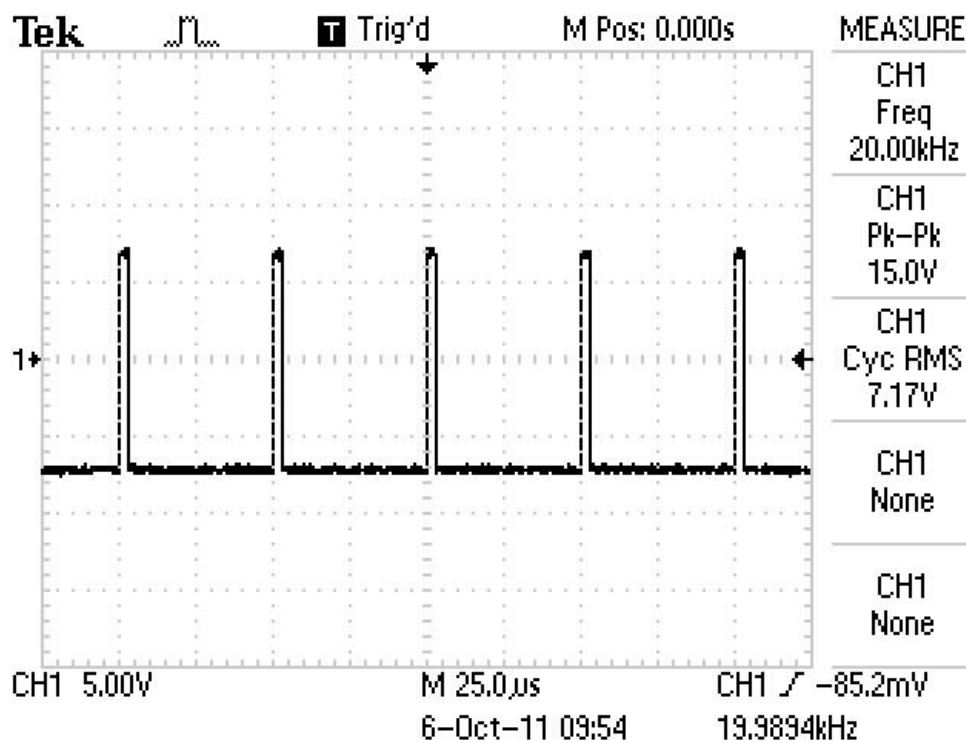


Figure 17. Duty Cycle of 5 per cent.

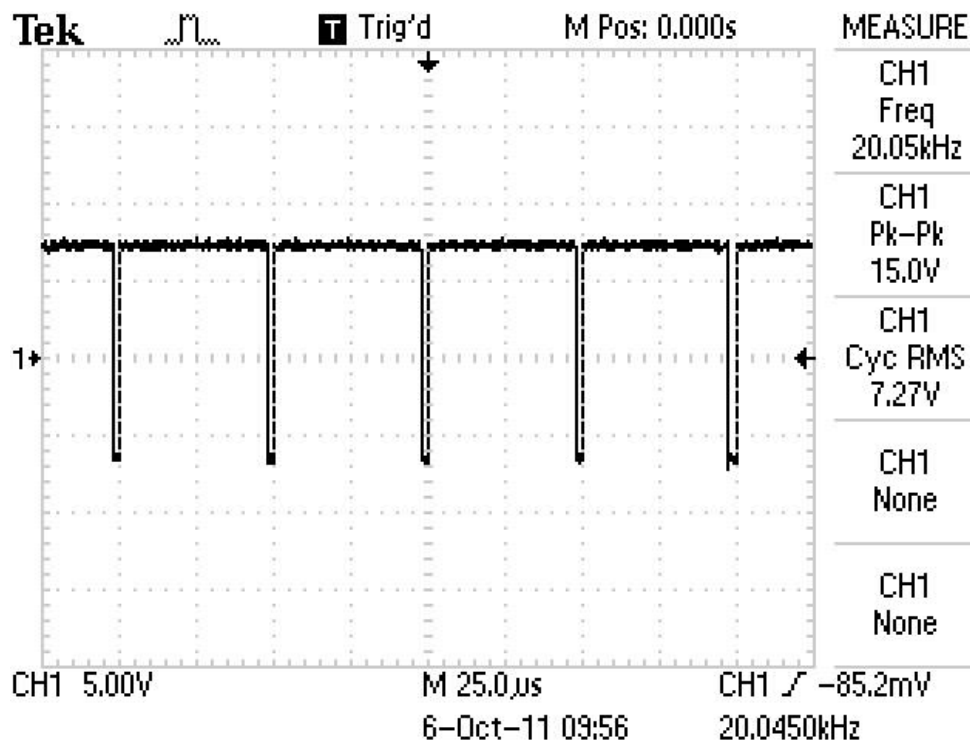


Figure 18. Duty Cycle of 95 per cent.

7.3 Methodology by IEC 60782

IEC 60782 provides a detailed procedure in the obtaining the classical properties of an UMST. The UMST is classed as a category P magnetostrictive transducer. All procedures will be determined by the availability of electrical test equipment.

Some procedures state the UMST should operate in the linear region. The linear region is defined as the sinusoidal voltage and sinusoidal current waveforms should be regular during the operation of the UMST. The medium for the UMST is recommended to be tap water unless otherwise stated.

7.3.1 Input Electrical Power

The input electrical power will be determined by impedance method. The impedance method will initially use a sinusoidal voltage supply, then with the square and triangular voltage waveforms. All three voltage supply waveforms will be used to compare results as well as assist further procedures.

The impedance method requires the voltage across the transducer (V_T) and the current passing through the transducer (I_T). Precautions are taken to ensure the volt meter and amp meter satisfies the frequency, voltage and current demands required for the transducer. If V_T , I_T and P_{in} are known then the phase angle can be calculated by using

$$P_{in} = V_T I_T \cos \delta \quad (29)$$

converting to

$$\cos \delta = \frac{P_{in}}{V_T I_T} \quad (30)$$

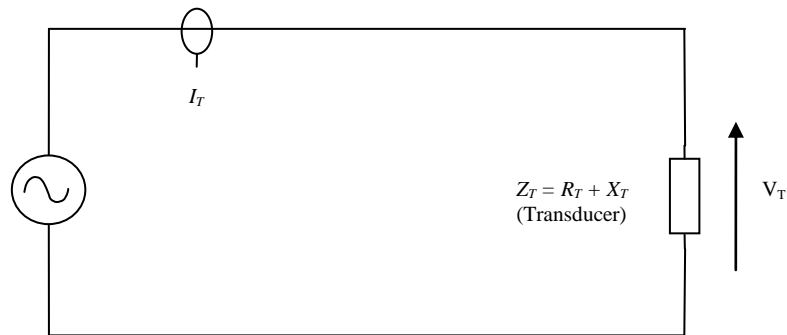


Figure 19. IEC60782 Basic Impedance Circuit.

If a current meter is not available then a known series resistor can be included in the circuit where the current can be calculated by

$$I_T = R_S V_R \quad (31)$$

allowing

$$P_{in} = V_T R_S V_R \cos \delta. \quad (32)$$

A circuit with an introduce known resistance is shown in figure 20.

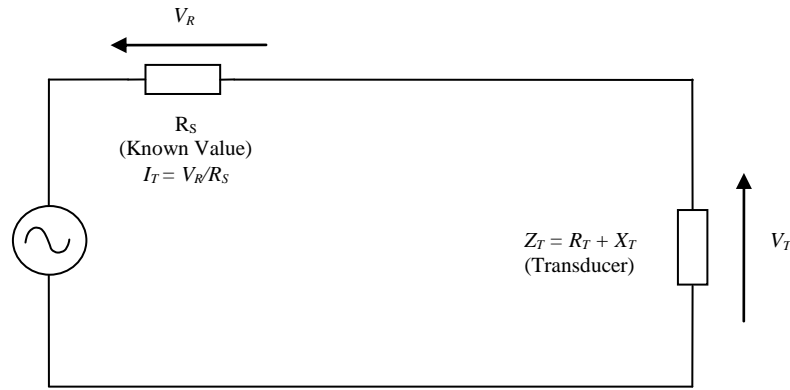


Figure 20. IEC60782 Basic Impedance Circuit with Additional Series Resistance.

7.3.2 Resonant Frequency

The resonant frequency of the transducer is the frequency of operation where the transducer has maximum output power as compared to the input power. The resonant frequency for the UMST will differ when the transducer is vibrating in air as compared to vibrating in a medium as the medium provides more physical resistance to the vibrating transducer.

The maximum power method will be used in determining the resonant frequency of the UMST submerged in the medium (loaded) and in air (unloaded). The maximum power method uses the impedance method as described in section 7.3.1 with the frequency of operation changing.

7.3.3 Bandwidth (Δf) and mechanical Quality (Q) Factor

The bandwidth and quality factor of the UMST are determined by the resonant frequency whilst transmitting into the medium. Using the plot generated by section 7.3.1, a range of frequencies can be selected where the output power is greater than half the maximum output power. This range of frequencies will be symmetrical around the resonant frequency with the bandwidth being half the range of these frequencies.

The quality factor is calculated by the following formulae

$$Q = \frac{f_{res}}{\Delta f} \quad (33)$$

where f_{res} is the resonant frequency and Δf is the bandwidth.

7.3.4 Electrical Impedance at Resonance

The electrical impedance at resonance is determined by impedance method described in section 7.3.1. The electrical impedance values are calculated by determining total supplied power (P_{in}), supplied current (I_T) and voltage across the transducer (V_T). These values are calculated with the operating frequency at the resonant frequency. The electrical impedance (Z_T) can be calculated by

$$Z_T = \frac{V_T}{I_T}. \quad (34)$$

The phase angle (φ) can be calculated by the following formula

$$\cos \varphi = \frac{P_{in}}{V_T I_T}. \quad (35)$$

7.3.5 Electrical Impedance Outside of Resonance

The electrical impedance outside of resonance are similar to the impedance method detailed on section 7.3.1. The frequencies between the resonant frequency minus the bandwidth, and the resonant frequency plus the bandwidth should not be used.

The electrical impedance values outside of resonance are calculated by determining total supplied power (P_{in}), supplied current (I_T) and voltage across the transducer (V_T). These values are calculated with the operating frequency at the resonant frequency. The electrical impedance (Z_T) can be calculated by

$$Z_T = \frac{V_T}{I_T}. \quad (36)$$

The phase angle (φ) can be calculated by the following formula

$$\cos \varphi = \frac{P_{in}}{V_T I_T}. \quad (37)$$

7.3.6 Electroacoustic Efficiency

The method for electroacoustic efficiency is the ratio of output power over the input power. The losses associated with the transducer can be explained by figure 21. The input power to the transducer is the electrical input power. The electrical losses are the losses associated by stray and magnetisation loss of the winding. The mechanical loss is the losses caused by the magnetic field interacting with the nickel. The acoustic losses are caused by the interaction of the transducer face and the transmitting medium. Figure 22 goes one step further with the losses caused by the transfer of acoustics energy into cavitation.

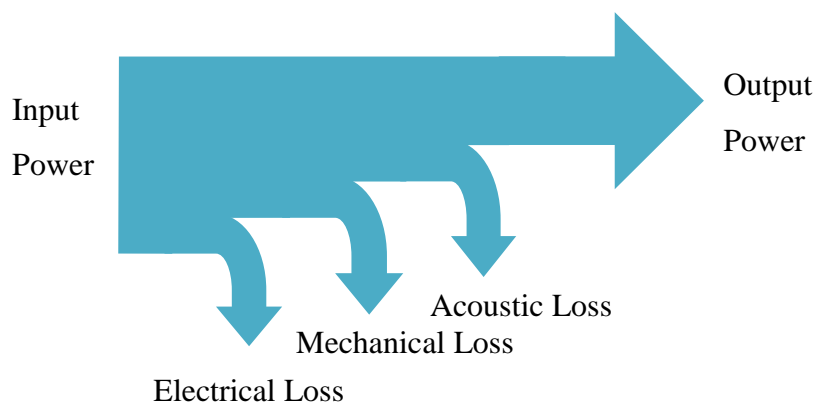


Figure 21. Electroacoustic Efficiency Diagram.

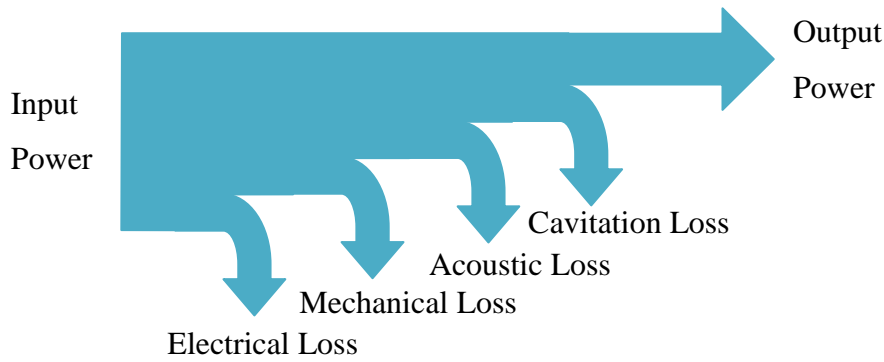


Figure 22. Electrocavitation Efficiency Diagram.

7.4 Methodology Improved with Petošić et al[23]

IEC60782 provides a basic electrical circuit for the UMST but a detailed electrical circuit would be more beneficial in simulating an UMST. Petosic et al, although based on piezoceramic transducers, provides an improved method on obtaining a more realistic electrical circuit where impedances are separated into resistance, inductance and capacitance.

Petošić et al, equivalent RLC electrical circuit of a piezoceramic transducer is provided in figure 23.

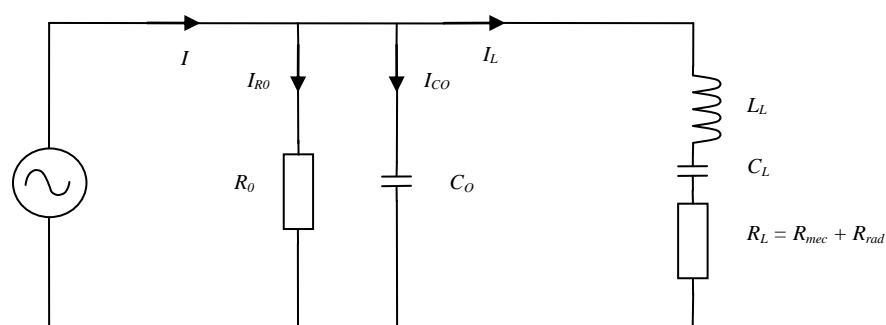


Figure 23. Piezoceramic Equivalent RLC Electrical Circuit.

A piezoceramic transducer produces physical vibrations caused by an oscillating electric field, where magnetostrictive transducers produce physical vibrations caused by an oscillating magnetic field.

Figure 24 is the equivalent RLC electrical circuit of a magnetostrictive transducer.

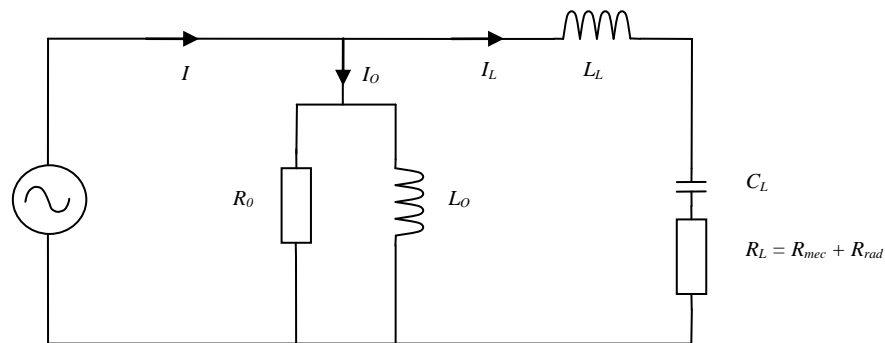


Figure 24. Magnetostrictive Equivalent RLC Electrical Circuit.

By combining the methods provided in IEC60782 and Petošić et al the values of the magnetostrictive RLC components can be defined.

7.4.1 Energizing Impedance

R_0 and L_0 are the real and imaginary components from Z_T as provided by section 7.3 with a phase angle φ , as provided by section 7.3. R_0 and L_0 can be define by

$$R_0 = |Z_T| \cos \varphi \quad (38)$$

$$X_0 = |Z_T| \sin \varphi \quad (39)$$

and

$$L_0 = \frac{X_0}{2\pi f_{res}} \quad (40)$$

where f_{res} is the resonant frequency of the unloaded transducer.

7.4.2 Transducer Impedance

If the transducer is operated unloaded at the unloaded resonant frequency it is assumed that the acoustic energy is poorly radiated there by $R_{rad} \approx 0$ and $R_L \approx R_{mec}$. A generalised formula can be deduced with L_L and C_L for the unloaded resonant frequency. Petošić et al assumed L_0 and R_0 have negligible effect on the unloaded resonant frequency therefore the unloaded resonant frequency can be found by

$$f_{res(unload)} = \frac{1}{2\pi\sqrt{L_L C_L}}. \quad (41)$$

Unloaded resonant frequency ($f_{res(unload)}$) can be identified by section 7.3.2.

L_L and C_L are the load inductance and load capacitance which are unknown at this stage.

Using

$$R_L \approx \frac{R_0 R_{mec}}{R_0 + R_{mec}}, \quad (42)$$

R_{mec} can be deduced to

$$R_{mec} \approx \frac{R_L R_0}{R_L - R_0}. \quad (43)$$

The transducer is loaded with the medium and operated at the loaded resonant frequency. R_L can be defined by

$$R_L \approx \frac{R_0 (R_{mec} + R_{rad})}{R_0 + R_{mec} + R_{rad}} \quad (44)$$

resulting in

$$R_{rad} \approx R_L - R_{mec}. \quad (45)$$

A generalised formula can be deduced with L_L , L_0 and C_L for the loaded resonant frequency is

$$f_{res(load)} = \frac{1}{2\pi} \sqrt{\frac{L_L + L_0}{L_L L_0 C_L}} \quad (46)$$

where L_L and C_L can found by solving simultaneously (41) and (46) as $f_{res(load)}$ and L_0 are previously determined.

7.4.3 Electroacoustic Efficiency

Electroacoustic efficiency can be defined as acoustic power output divided by the electrical power input. This is represented as

$$\eta_{ea} = \frac{P_{out}}{P_{in}}. \quad (47)$$

Petosic et al use the equivalent RLC circuit analysis to defined acoustic power output as

$$P_{rad} = \frac{V^2 R_{rad}}{(R_{mec} + R_{rad})^2 + \left(\omega L_L - \frac{1}{\omega C_L}\right)^2} \quad (48)$$

and since the transducer is operating at resonance then (47) can be simplified to

$$P_{rad} = \frac{V^2 R_{rad}}{(R_{mec} + R_{rad})^2}. \quad (49)$$

Electrical power input is $P_{rad} + P_{mec} + P_{R_0}$ where,

$$P_{mec} = \frac{V^2 R_{mec}}{(R_{mec} + R_{rad})^2 + \left(\omega L_L - \frac{1}{\omega C_L}\right)^2}, \quad (50)$$

is simplified to

$$P_{mec} = \frac{V^2 R_{mec}}{(R_{mec} + R_{rad})^2}, \quad (51)$$

and

$$P_{R_0} = \frac{V^2}{R_0}, \quad (52)$$

leading to the electroacoustic efficiency of

$$\eta_{ea} = \frac{P_{rad}}{P_{rad} + P_{mec} + P_{R_0}}. \quad (53)$$

Relating to the acoustic efficiency diagram (figure 21) P_{rad} is the output power, P_{mec} is the mechanical and acoustic loss and P_{R_0} is the electrical loss. A modified electroacoustic efficiency diagram is shown in figure 25.

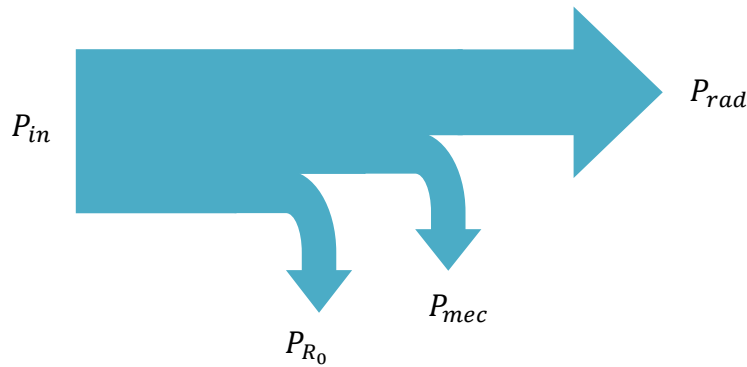


Figure 25. Petošić et al Electroacoustic Efficiency Diagram.

Since the supply voltage squared (V^2) is common to (48), (50) and (51), the electroacoustic efficiency can be refined to (53) as the values of R_0 , R_{mec} and R_{rad} are calculated in sections 7.4.1 and 7.4.2.

$$\eta_{ea} = \frac{R_{rad}}{R_{rad} + R_{mec} + \frac{(R_{mec} + R_{rad})^2}{R_0}} \quad (54)$$

7.5 Electromagnetic Simulation

Goberman [2] provides a detailed design of an equivalent electrical circuit based on an ideal transformer which is shown in figure 26. Goberman uses the complex impedance to show the resonance of the transducer.

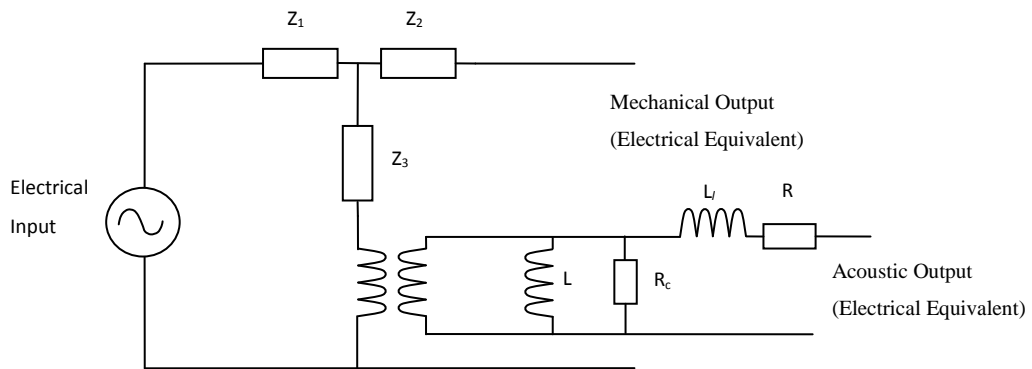


Figure 26. Goberman [2] Magnetostrictive Equivalent RLC Electrical Circuit.

Petošić et al [23] provides a more agreeable equivalent RLC electrical circuit. Although this circuit is based on a piezoceramic transducer, it allows the identification of the transducers natural resonance frequency with L_L and C_L . Figure 27 has the electrical losses by R_0 and C_0 .

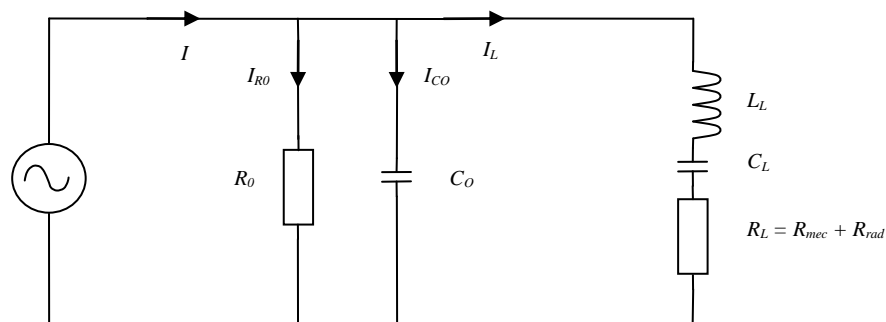


Figure 27. Piezoceramic Equivalent RLC Electrical Circuit.

An equivalent RLC electrical circuit for a magnetostrictive transducer can be designed by combining an electrical motor circuit and Petošić et al circuit. Figure 28 is the resultant magnetostrictive equivalent RLC electrical circuit.

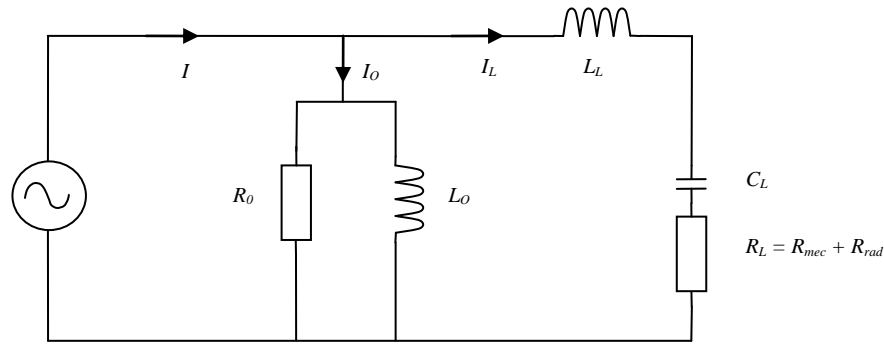


Figure 28. Magnetostrictive Equivalent RLC Electrical Circuit.

7.5.1 Calculating the values of the magnetostrictive equivalent RLC electrical circuit

Values of the RLC components in the equivalent electrical circuit will be calculated by two different methods. A critical piece of information to a transducer is its resonant frequency. The resonant frequency is the optimum frequency for energy transfer. The resonant frequency can be measured by obtaining an input power and frequency plot. Where the input power is at maximum the corresponding frequency is called its resonant frequency (IEC 60782:1984).

7.5.2 IEC 60782 – Measurements of Ultrasonic Magnetostrictive Transducers [39]

The electrical impedance of the transducer at resonance will be calculated by the wattmeter method.

R_0 and L_0 can be calculated when the transducer is operating outside of its resonant frequency thereby the load, represented by L_L , C_L and R_L , will provide an almost open circuit. R_0 and L_0 were calculated when the transducer was operating at 10 kHz. The value of I_0 was also calculated by

$$I_0 = I_{R_0} + I_{L_0}, \quad (55)$$

where

$$I_{R_0} = \frac{V}{R_0}, \text{ and} \quad (56)$$

$$I_{L_0} = \frac{V}{L_0}. \quad (57)$$

The overall supply current can be calculated by

$$I_s = I_L + I_0 \quad (58)$$

where the supply current (I_s) will be found by the impedance method when the transducer is operating at its resonant frequency.

Rearranging equation 58 for I_L gives

$$I_L = I_s - I_0. \quad (59)$$

7.5.3 Petošić et al [23]

R_0 and L_0 can be calculated when the transducer is operating outside of its resonant frequency there by the load represented by L_L , C_L and R_L will provide and almost open circuit. R_0 and L_0 were calculated when the transducer was operating at 10 kHz.

Petošić et al [23] identifies L_L as the effective mass of the vibrating transducer, C_L represents the effective elasticity of the vibrating transducer with R_L being a combination of mechanical resistance (R_{mec}) and radiated resistance (R_{rad}).

R_{mec} is calculated by assuming there is no radiated power when the transducer is operating at resonant frequency in air. R_L is calculated when the transducer is loaded at resonant frequency. It is assumed

$$R_L = R_{mec} + R_{rad}, \quad (60)$$

with R_L and R_{mec} known

$$R_{rad} = R_L - R_{mec}. \quad (61)$$

7.6 Mechanical Vibration Analysis

To reinforce the results of the electrical testing of the UMST, mechanical vibration analysis will be conducted. An accelerometer is secured to the transducer face. The acceleration of the transducer face will be recorded with the three different voltage waveforms at the various operating frequencies. The transducer will also operate in the loaded and unloaded states.

Vibration analysis will be used to calculate the mechanical output power of the transducer.

Using an accelerometer the force emitted by the transducer can be calculated by

$$F = m \times a \quad (62)$$

where F is force (newtons), m is mass (kg) and a is acceleration (m.s^{-2}).

The mass will not be the mass of the transducer lamination but the mass of the medium (water) the transducer face vibrates into. The mass of the water is calculated by the following assumptions

- the overall pressure of medium is constant;
- the mass of the medium is constant;
- the pressure in the direction of the gravity is the same as the pressure in any direction within the medium; and
- thereby the mass of medium pressing transducer face is equivalent to the area of the transducer face multiplied by the average depth.

The transducer has a face area of $75 \times 10^{-6} \text{ m}^2$ ($0.075 \text{ m} \times 0.0001 \text{ m}$) with an average depth of 0.01 m producing a volume of $750 \times 10^{-9} \text{ m}^3$. When the medium is water with a density of $1 \text{ kg per } 0.001 \text{ m}^3$, the mass of water pressing on the transducer face is $75 \times 10^{-6} \text{ kg}$.

The power of the transducer is calculated by

$$P_{out} = F \times v, \quad (63)$$

or

$$P_{out} = m \times a \times v, \quad (64)$$

where P_{out} is the mechanical output power of the transducer and v is the velocity of the transducer face.

Chapter 8 – Required Resources

8.1 Transducer Analysis

Two different nickel laminations were provided by New Wave Leather Pty. Ltd. Four different windings were produced to examine the effect of magnetostriction.

8.1.1 Nickel Laminations

To conduct the testing as outlined in chapter seven one requires magnetostrictive material that is nickel. Appendix B contains the dimensions of the nickel transducers. Both laminations are made of nickel 201 which is made of 99.5% nickel and 0.01% Carbon with the other 0.49% consisting of other impurities [40]. Both transducers were operated in an 'open' state, where magnetic field did not have a closed path. This was chosen to allow for the easy exchange of different windings.

As outlined in section 4.4 the average conducting magnetic path for the transducer should be 0.245 m for a 20 kHz operating frequency. Table iv outline the average magnetic path for the small and large transducer.

Table iv. Transducers Optimum Operating Frequencies.

Lamination	Average Magnetic Path (m)	Optimum Frequency (kHz)
Ideal	0.245	20.000
Small (append B.1)	0.230675	18.831
Large (append B.2)	0.26135	21.335

The dimensions of the small and large transducers are provided in figures 29 and 30. Both transducers should have a resonant frequency at approximately 20 kHz.

The average magnetic path assumes the whole path being within the nickel lamination. For ease of manufacturing the whole magnetic path is not within the nickel so the optimum frequencies will differ slightly. Calculation of the average magnetic path of the small and large transducers with the open end of the transducer would require three dimensional modelling. Due to time restraints and financial cost three dimensional modelling was not performed.

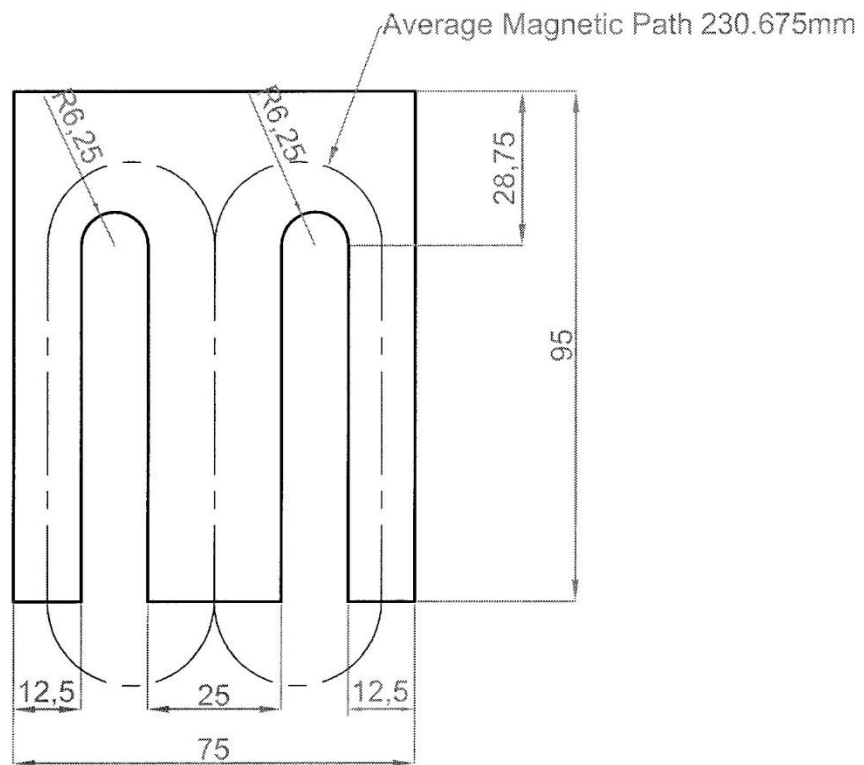


Figure 29. Small Transducer Design.

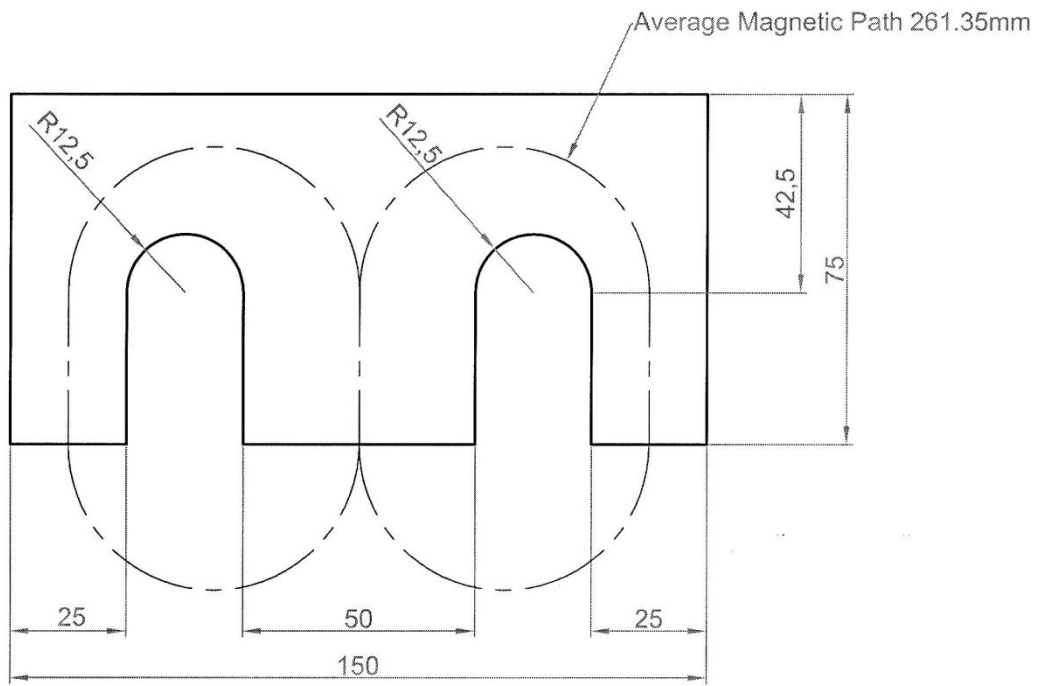


Figure 30. Large Transducer Design.

Figure 31 is the actual nickel lamination used.

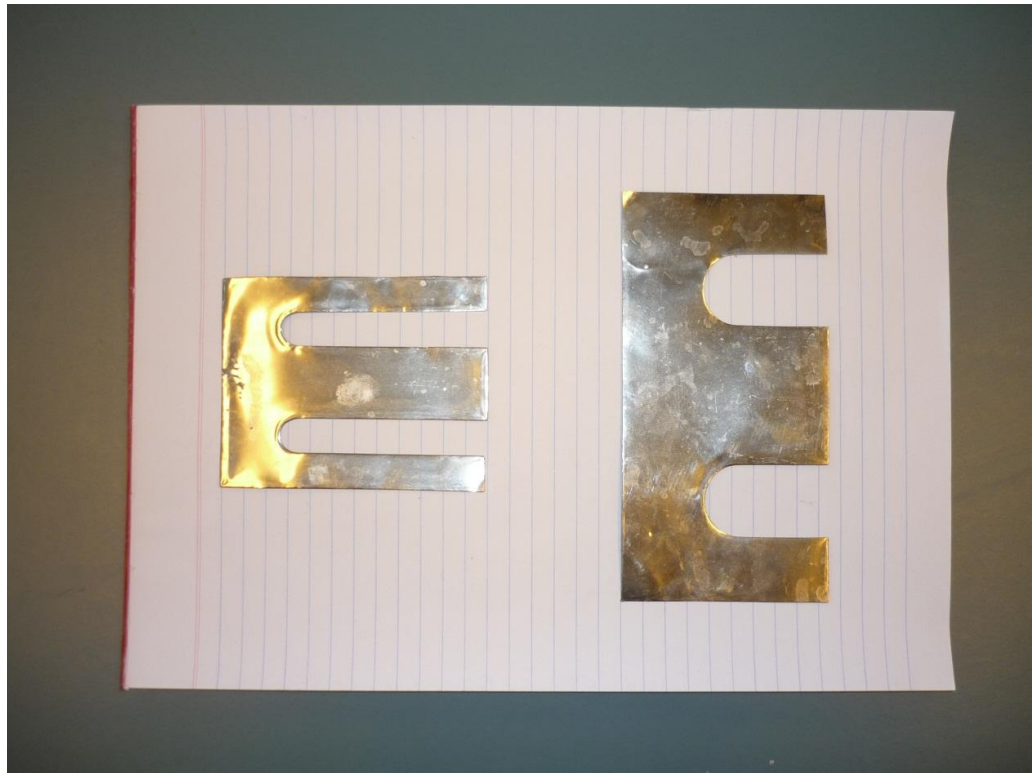


Figure 31. Supplied Nickel Laminations from New Wave Leather on an A4 Sheet of Paper.

8.1.2 Windings

Two different windings were produced manually for both the small and large lamination. The windings comprise of various diameter copper conductor with an enamelled coating for electrical insulation. Details of the windings are listed in table v followed by the current capacity of each windings in table vi.

Table v. Continuous Current Rating of Produced Windings [41].

Lamination	Small		Large	
No. of Turns	249	643	96	115
Wire Diameter (mm)	0.8	0.3	1	0.8
Conductor Size (mm ²)	0.503	0.071	0.784	0.503
Length of Winding (mm)	45	45	45	45
Cross Sectional Area (mm ²)	301.5	30.15	605	605
Average Radius Distance (mm)	9.796	9.796	13.877	13.877

Table vi. Continuous Current Rating of Produced Windings [41].

Lamination	Small		Large	
No. of Turns	249	643	96	115
Wire Diameter (mm)	0.8	0.3	1	0.8
Conductor Size (mm ²)	0.503	0.071	0.784	0.503
Number of Layers	4	4	4	4
Current Capacity (A)	0.5	0.5	7.5	0.5
De-rating Factor	0.4	0.4	0.4	0.4
Continuous Current Rating (A)	0.2	0.2	3	0.2

The continuous current rating provided in table vi does not take into account the added benefit of the transducer being in water. A water de-rating factor is included in table vii adjusting the continuous current rating only when the transducer is submerged in the medium.

Table vii. Adjusted Continuous Current Rating of Produced Windings.

Lamination	Small		Large	
No. of Turns	249	643	96	115
Old Continuous Current (A)	0.2	0.2	3	0.2
Water De-rating Factor	10	10	10	10
Submerged Continuous Current Rating (A)	2	2	30	2

Figure 32 is the actual produced windings used under testing.



Figure 32. Produced Windings by W.A. McHugh on an A4 Sheet of Paper.

8.1.3 Transducer Properties

As described in section 4.1, nickel has a saturation magnetic flux density (B_{sat}) of 0.617Wb.m^{-2} [5], a permeability of $7.54 \times 10^{-7} \text{ H.m}^{-1}$ and a saturation magnetic field intensity (H_{sat}) of 818.3 A.m^{-1} .

Using the H_{sat} value of 818.3A.m^{-1} the maximum current can be determined for each winding of the transducer by the solenoid equation,

$$H_{sat} = \frac{I \times n \times l}{2 \times \sqrt{\left(a^2 + \frac{l^2}{4}\right)}}, \quad (65)$$

rearranged to

$$I_{max} = 2 \times H_{sat} \times \frac{\sqrt{\left(a^2 + \frac{l^2}{4}\right)}}{n \times l}, \quad (66)$$

where I_{max} is the maximum current, a is the average radius distance inside the winding, n is the number of turns and l is the length of the winding.

Table viii shows the maximum current for each winding.

Table viii. Maximum Load Current per Transducer Combination.

	Small		Large	
No. of Turns	249	643	96	115
Maximum Current (A)	3.584	1.388	11.28	9.419

By combining

$$L = \frac{\mu \times n^2 \times A}{l} \quad (67)$$

where L is inductance, μ is material permeability, n is the number of turns, A is the core cross sectional area and l is the length of the winding with (65) an equation for magnetic field intensity can be deduced to,

$$H = (I \times n) \times \left[\frac{\mu \times A}{\sqrt{\left(\frac{2aL}{n^2}\right)^2 + (\mu \times A)^2}} \right] \quad (68)$$

but

$$\left(\frac{2aL}{n^2}\right)^2 \ll 1$$

therefore

$$H \approx (I \times n) \quad (69)$$

or

$$H \approx \left(\frac{V}{X_L} \times n\right) \quad (70)$$

where V is the supply peak voltage and X_L is the characteristic impedance of the winding at the resonant frequency.

Figure 33 shows the Ultrasonic Magnetostrictive Transducer as the combination of the nickel lamination and the winding.



Figure 33. Produced Magnetostrictive Transducer by W.A. McHugh on an A4 Sheet of Paper.

8.2 Function Generators

Certified calibration was not provided on all function generators.

Three different function generators were used during the testing on the UMST. An IGBT was then used as the power source for the creation of cavitation.

8.2.1 Tektronic AFG 3022B

The Tektronic 3022B Arbitrary Function Generator was able to satisfy all requirements for testing of the UMST. Table ix provide a basic characteristics of the Tektronic 3022B.

Table ix. Characteristics of Tektronic AFG 3022B.

Property		Value
Output Voltage	Volts (peak to peak)	10 V
	DC offset	± 2.5 V
Sinusoidal Waveform	Min	1×10^{-6} Hz
	Max	25 MHz
Square Waveform	Min	1×10^{-6} Hz
	Max	12.5 MHz
Triangular Waveform	Min	1×10^{-6} Hz
	Max	250 kHz

A Tektronic AFG 3022B was initially used to create the various voltage supply waveforms. The Tektronic 3022B has a maximum voltage range of ± 10 Volts. Upon inspection of the voltage waveforms it was decided the 3022B could not produce a stable voltage waveform with the required current output. This was evident particularly in the square waveform where the voltage decreased during the high period and increased during the low period of the waveform. The deformation of the voltage waveform is caused by the relative high current demand during the voltage

cycle. The sonic output of the transducer was barely audible between the frequencies of 1 to 15 kHz. Figure 34 shows the unstable square waveform voltage supply.

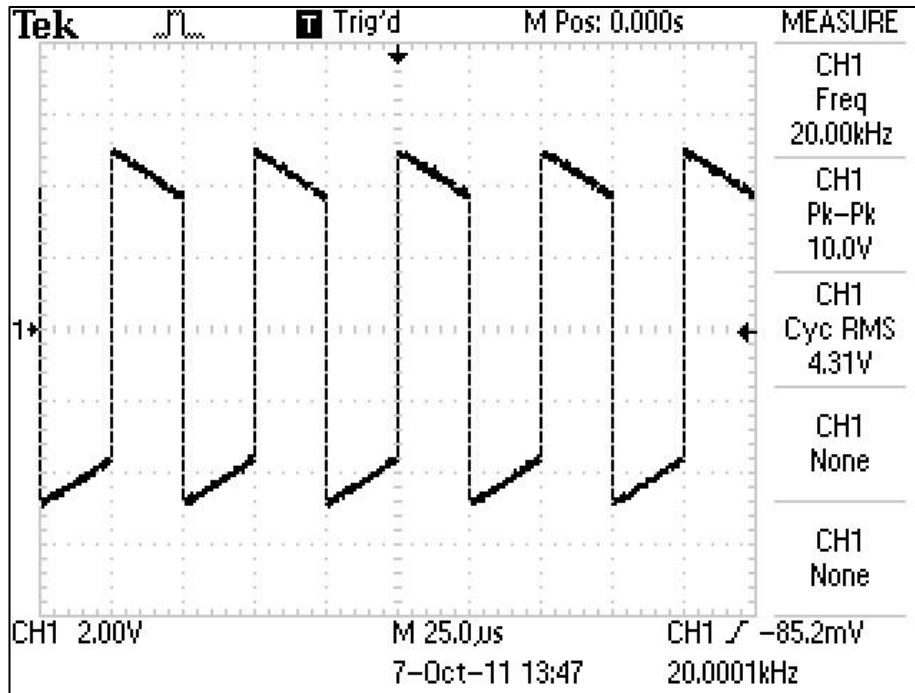


Figure 34. Unstable Square Waveform for Tektronic AFG 3022B.

8.2.2 HAMEG HM 8030–4 Function Generator

The HAMEG HM8030–4 Function Generator was able to satisfy all requirements for testing of the UMST. Table x provide a basic characteristic of the HAMEG HM 8030–4.

Table x. Characteristics of HAMEG HM 8030–4.

Property		Value
Output Voltage	Volts (peak to peak)	10V
	DC offset	±2.5V
Sinusoidal Waveform	Min	0.3 Hz

	Max	3 MHz
Square Waveform	Min	0.3 Hz
	Max	3 MHz
Triangular Waveform	Min	0.3 Hz
	Max	3 MHz

The HAMEG HM 8030-4 function generator was then used to provide the various voltage waveforms. Upon inspection of the voltage waveforms it was decided the HAMEG 8030-4 could not produce a stable voltage waveform with the required current output. This was evident particularly in the square waveform where the voltage decreased during the high period and increased during the low period of the waveform. The deformation of the voltage waveform is caused by the relative high current demand during the voltage cycle. The sonic output of the transducer was barely audible between the frequencies of 1 to 15 kHz. Figure 35 shows the unstable square waveform voltage supply.

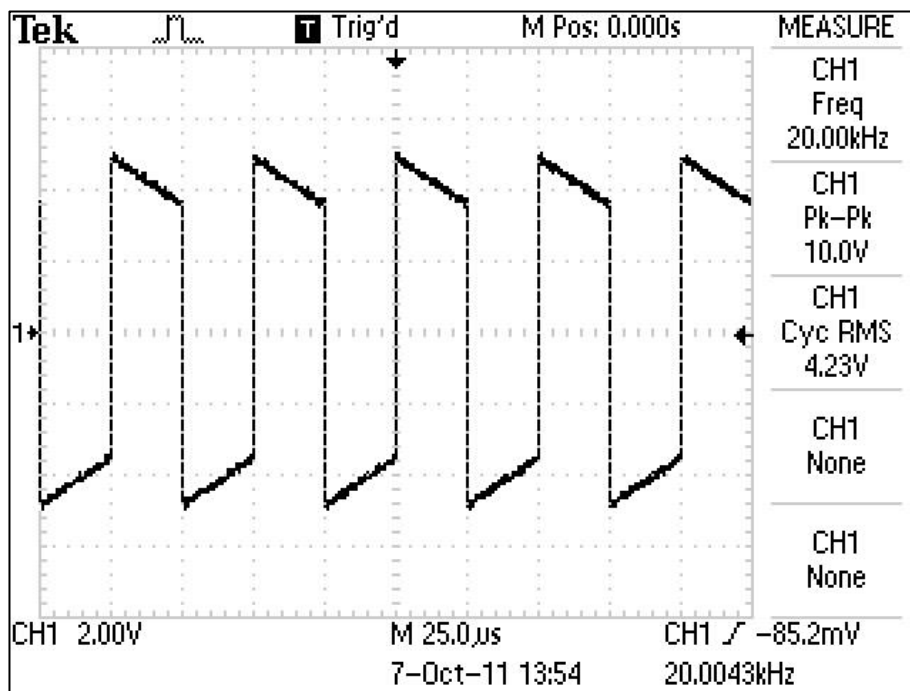


Figure 35. Unstable Square Waveform from HAMEG HM8030-4.

8.2.3 BWD 160A Function Generator

The BWD 160A Function Generator was able to satisfy all requirements for testing of the UMST. Table xi provide a basic characteristic of the BWD 160A.

Table xi. Characteristics of BWD 160A.

Property		Value
Output Voltage	Volts (peak to peak)	40 V
	DC offset	± 10 V
Sinusoidal Waveform	Min	0.02 Hz
	Max	2 MHz
Square Waveform	Min	0.02 Hz
	Max	2 MHz
Triangular Waveform	Min	0.02 Hz
	Max	2 MHz

A BWD 160A function generator was then used to provide the various voltage waveforms. Upon inspection of the voltage waveforms, the BWD 160A could not produce a stable voltage waveform with the required current output. This was evident particularly in the square waveform where the voltage decreased during the high period and increased during the low period of the waveform. The deformation of the voltage waveform is caused by the relative high current demand during the voltage cycle. The BWD 160A was able to provide enough current to produce audible tones between the frequencies of 1 to 15 kHz. Figure 36 shows the unstable square waveform voltage supply.

The BWD 160A was chosen as the preferred function generator as it had a voltage supply range of ± 20 Volts and appeared to have similar deformation as the Tektronic 3022B. The BWD 160A provided the highest audible tones.

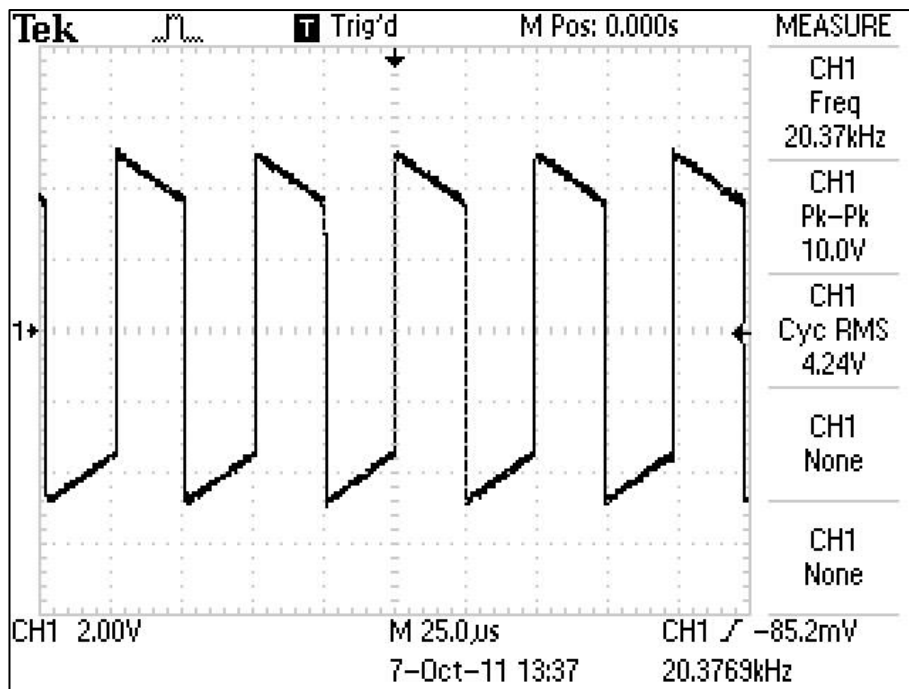


Figure 36. Unstable Square Waveform for BWD 160A.

Supply of an amplifier was investigated but due to the unique operating frequencies being between 3 and 30 kHz it was not financially viable. Audio amplifiers that operate in the sonic region are readily available but they are not able to provide the required frequency range.

8.2.4 IGBT Semikron AN-8005

The Semikron AN-8005 was connected as the power supply for the transducer to achieve cavitation. The AN-8005 was connected as a half controlled 'H' bridge. The AN-8005 was supplied by two Topward 6303A Dual Tracking DC Power Supplies connected in series which enable up to 90V DC. 60V DC was used as the preferred peak to peak voltage. This minimised the current demand placed on the two Topward 6303A DC supplies while still achieving cavitation. The square waveform produced from the AN-8005 is shown in figure 37.

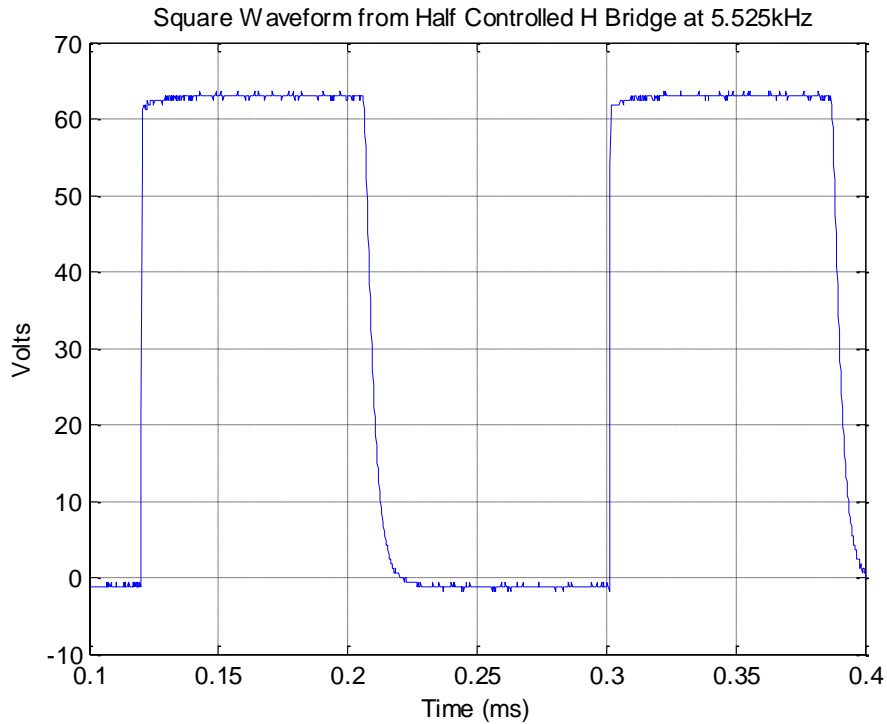


Figure 37. Square Waveform from the Semikron AN-8005.

The half controlled H bridge was triggered by either the BWD 160A or by Siemens Simatic S7-200 PLC (Programmable Logic Controller). These enabled the frequency of switching for the half controlled H bridge. After many tests the S7-200 PLC was chosen to be the primary switching source.

An example of a half controlled H bridge is provided in figure 38.

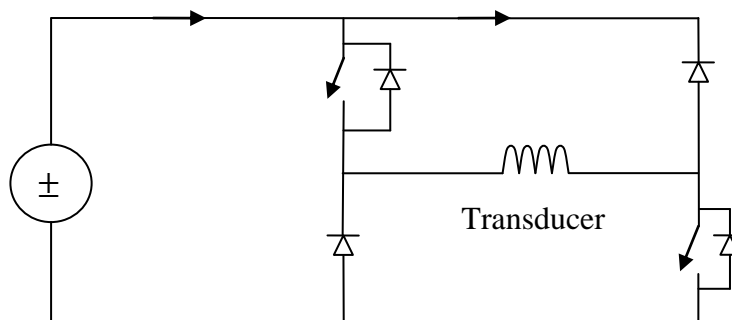


Figure 38. Circuit Diagram for Half Controlled H Bridge.

8.3 Recording equipment

Initial testing involved electrical measurements where digital oscilloscopes were required. Upon inspection of the electrical data it was decided more testing was required. Also in accordance with IEC 6072, mechanical measurements were taken with the use of a vibration meter. A LCR meter and a Gauss meter were then used to confirm the inductance and the magnetic flux density values of the transducers.

8.3.1 Digital Oscilloscope

Certified calibration was not provided on all oscilloscopes.

Two oscilloscopes were used to record the operating parameter of the transducer. They were the Tektronic TDS 1002B (1002B) and the Tektronic TDS 5034B (5034B). A current probe was connected to the 5034B. The 5034B was able to calculate the rms power value and the phase difference between the supply voltage and supply current.

8.3.2 Vibration Meter

Certified calibration was not provided on vibration equipment.

The data acquisition was performed by a LMS type SCM05 with a PCB U333A32 being the one dimension accelerometer. The accelerometer was used to measure the mechanical output power of the transducer. The SCM05 was able to record a maximum of 51 200 data points per second. When used with Fourier analysis and Nyquist theorem a maximum frequency of 25.6 kHz is extracted.

The SCM05 records a value in gravity and with an increased sensitivity of 1 000 000. When the data was extracted it is required to be converted in acceleration and have the sensitivity decreased. The sensitivity was increased to allow more significant

figures. The acceleration data was then converted to meters per second squared, then integrated by the trapezoidal method to produce velocity in meters per second.

Fast Fourier Transform (FFT) was performed on the acceleration data that enabled a frequency spectrum up to 25.6 kHz.

8.3.3 LCR Meter

A Tenma 72-8155 LCR meter was used to measure the inductance of all windings with and without the nickel lamination. The Tenma 72-8155 was calibrated as it was less than 12 months old.

8.3.4 Gauss Meter

Certified calibration was not provided on Gauss meter.

A Lakeshore 455 DSP Gauss meter was used to measure the magnetic flux density of the windings with and without the nickel lamination. All measurement were taken in Tesla's (T).

Chapter 9 – Results and Discussion

9.1 Introduction

All function generators provided unstable voltage waveforms. Section 8.3 shows the unstable waveforms from all three function generators. Due to the unstable voltage waveforms it was decided to only use the 643 turn small transducer. The 643 provided maximum impedance and therefore a minimum demand for current. The minimal load current will produce a more reliable voltage waveform. The BWD 160A was chosen as it supplied more current at lower frequencies as compared to the other two function generators. The BWD 160A also had an operating voltage range of $\pm 20\text{V}$.

After many tests the BWD 160A was discarded as the results could not be duplicated and confirmed.

The Tektronic 3022B was then selected as the preferred function generator. All experiments were repeated. The results from the testing were able to be repeated and duplicated using the Tektronic 3022B.

In all tests the function generators were able to operate the UMST in the linear region where the voltage waveform was sinusoidal.

With the combination of unstable waveforms and wide frequency measurements, all data is considered as approximate. No ‘lines of best fit’ or other forms of interpolation are incorporated in the data. The lack of interpolation is to reduce the errors and assumptions.

9.2 Input Electrical Power

The transducer consisted of the small lamination and the 643 turns winding. The 5034B was used as the impedance method outlined in Section 7.3.1. The 5034B was able to measure the supply voltage and supply current. The electrical resonance test was conducted under the unloaded and loaded condition. The unloaded condition is referred to the transducer operating in air and the loaded condition is where the transducer is operating in a medium. Tap water was the medium used in all loaded experiments.

The three different voltage waveforms are compared in figures 39 and 40 over the frequency spectrum of 3 to 35 kHz. The voltage supply is maintained to 10 Volts peak to peak.

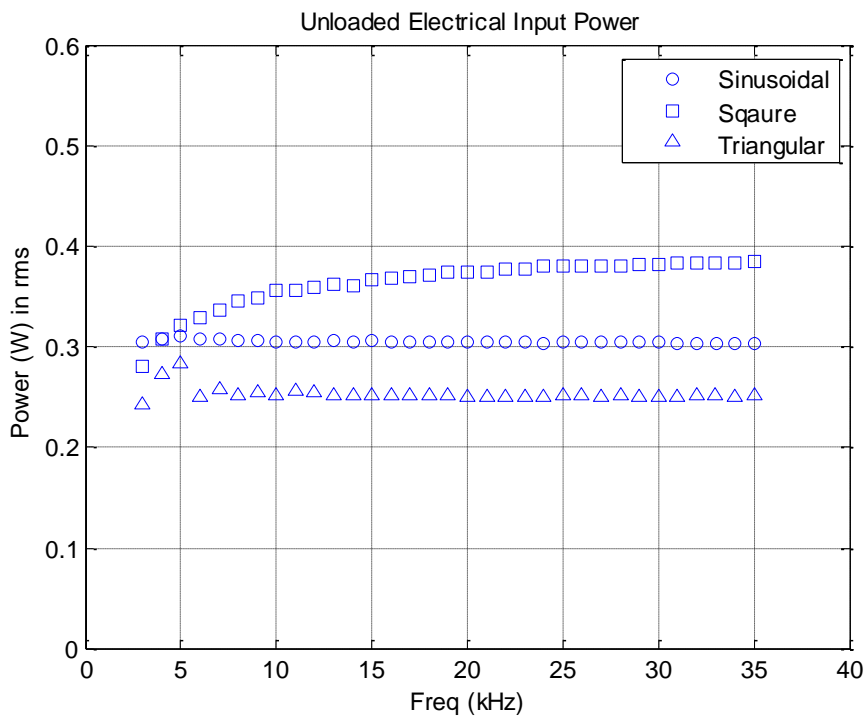


Figure 39. Unloaded Electrical Input Power.

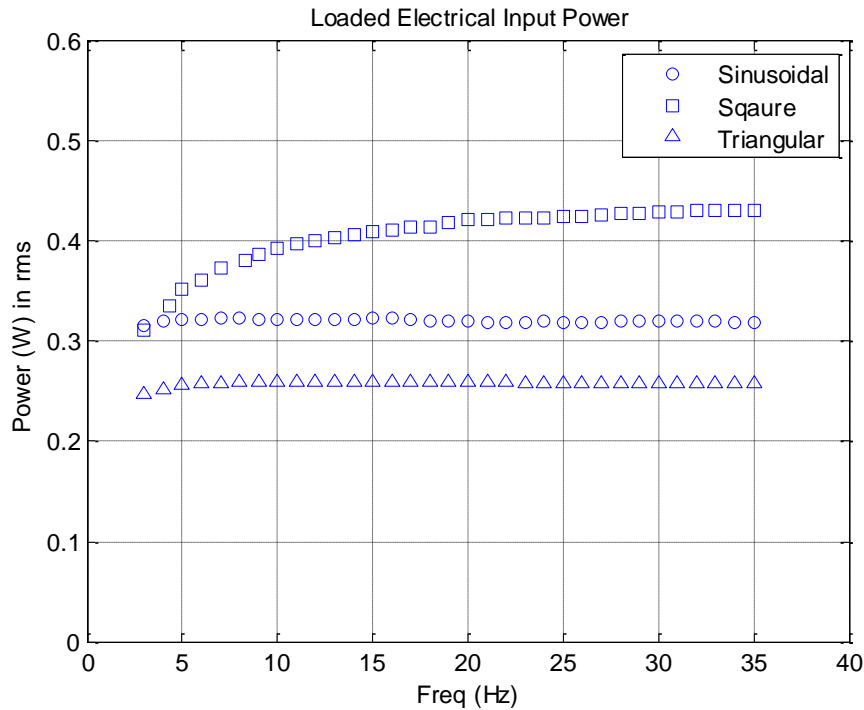


Figure 40. Loaded Electrical Input Power.

It can be seen that the square waveform provide the most power in the unloaded and loaded state. This can be easily explained as the transducer is primarily an inductor. An inductor can also be known as an integrator, where the amount of current is determined by the duration and magnitude of the voltage. The greater duration and magnitude of voltage will increase the magnitude of current, also reflected in (20).

9.3 Electrical Resonance

The transducer consisted of the small lamination and the 643 turns winding. The 5034B was used as the impedance method outlined in section 7.3.2. The 5034B was able to measure the supply voltage and supply current. The electrical resonance test was conducted under the unloaded and loaded conditions.

9.3.1 Unloaded Electrical Resonance

The small transducer was used with the 643 turn winding with the 3022B function generator as its power supply. All voltage waveforms were set to 10 Volts (peak to peak). Figure 41 shows the electrical input power as compared to the frequency.

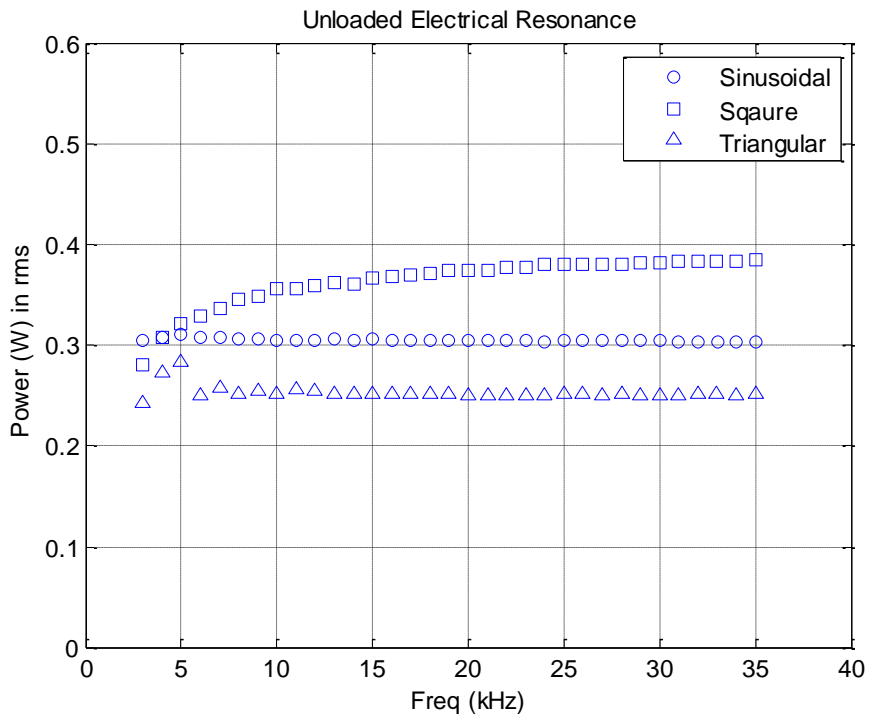


Figure 41. Unloaded Electrical Resonance.

In the unloaded state, a resonant frequency cannot be found by the wide frequency sweep conducted by the three different waveforms.

9.3.2 Loaded Electrical Resonance

The small transducer was used with the 643 turn winding with the 3022B function generator as its power supply. All voltage waveforms were set to 10 Volts (peak to peak). Figure 42 shows the electrical input power as compared to the frequency.

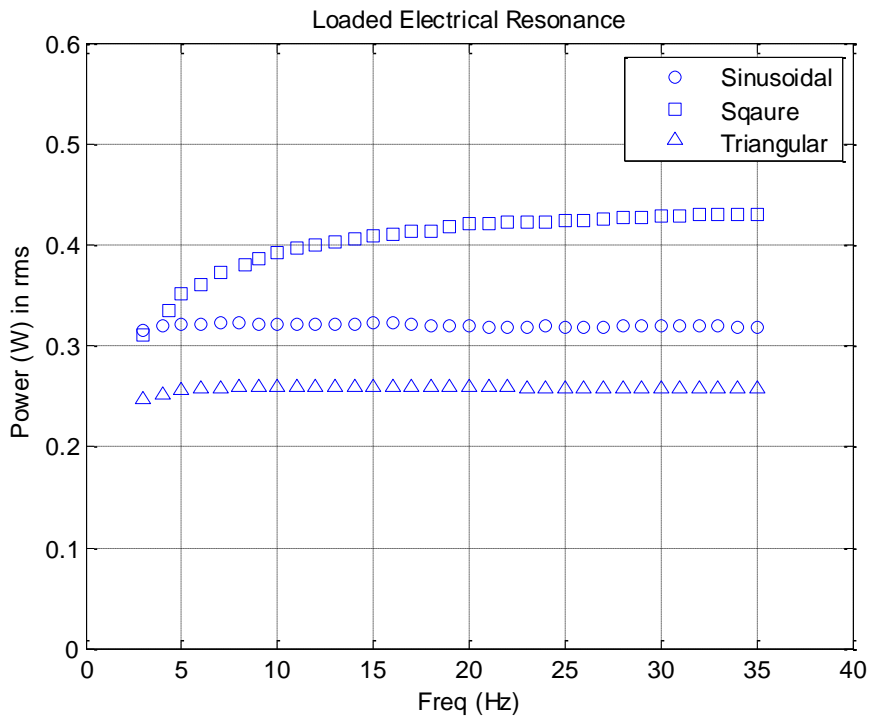


Figure 42. Loaded Electrical Resonance.

In the loaded state, a resonant frequency cannot be found in the wide frequency sweep conducted by the three different waveforms.

The square voltage waveform requires the most electrical input power in both the loaded and unloaded state of the transducer.

9.4 Mechanical Resonance

The transducer consisted of the small lamination and the 643 turns winding. Due to the unreliable power supplies and the inability to locate an electrical resonant frequency it was decided to find the resonant frequency via mechanical resonance. The UMST was again tested in the loaded and unloaded state, with the three different voltage supply waveform, at various frequencies.

9.4.1 Unloaded Mechanical Resonance

The UMST transducer was operated in an unloaded state with an accelerometer attached to the conducting face. Figure 43 show the results of a wide frequency sweep. It can be seen that all three waveforms have a greater magnitude of acceleration around the 20 kHz region. The square waveform produces the most acceleration compared to sinusoidal, with triangular producing the least. Individual graphs of the sinusoidal, square and triangular waveform are provided in appendix E.

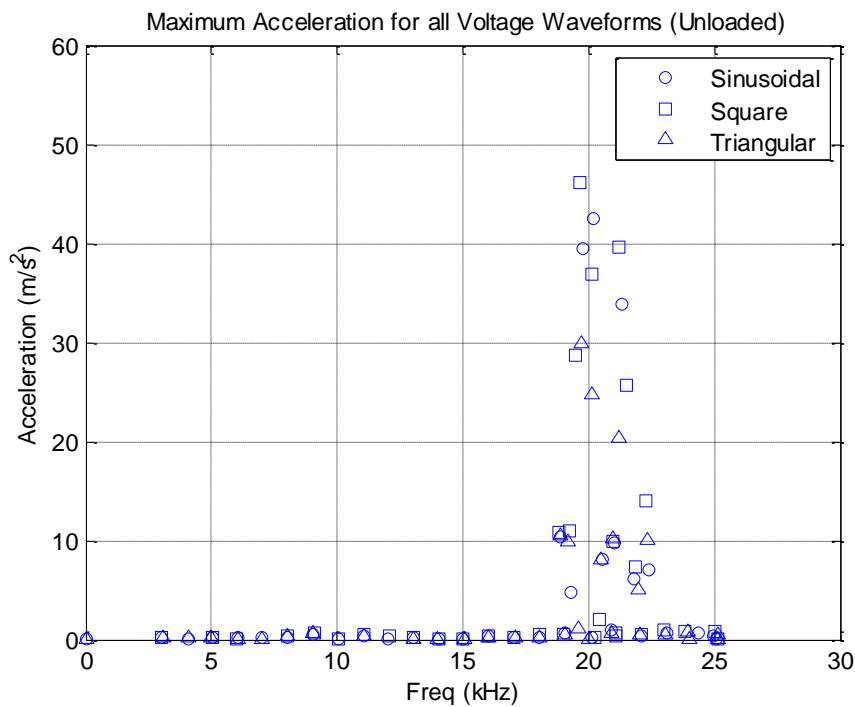


Figure 43. Unloaded Mechanical Resonance.

Due to the wide frequency sweep approximate resonant frequencies can only be deduced. Table xii shows the approximate unloaded resonant frequencies for the three voltage waveforms.

Table xii. Approximate Unloaded Resonant Frequencies.

	Resonant Frequency (kHz)
Ideal	20.000
Small Transducer (append B.1)	18.831
Sinusoidal	20.164
Square	19.668
Triangular	19.722

9.4.2 Loaded Mechanical Resonance

The UMST transducer was operated in a loaded state with an accelerometer attached to the conducting face. Figure 44 show the results of a wide frequency sweep. It can be seen that all three waveforms have a greater magnitude of acceleration around the 20 kHz region. The sinusoidal waveform produces the most acceleration compared to the square waveform, with triangular waveform producing the least. Individual graphs of the sinusoidal, square and triangular waveform are provided in appendix F.

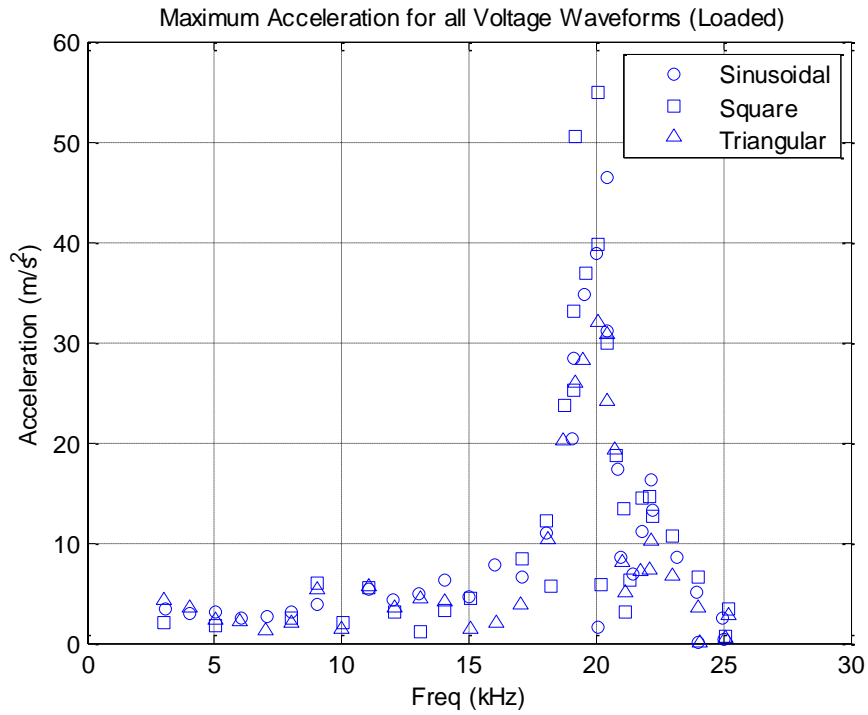


Figure 44. Loaded Mechanical Resonance.

Due to the wide frequency sweep, approximate resonant frequencies can only be deduced. Table xiii shows the approximate loaded resonant frequencies for the three voltage waveforms.

Table xiii. Approximate Loaded Resonant Frequencies.

	Resonant Frequency (kHz)
Ideal	20.000
Small Transducer (append B.1)	18.831
Sinusoidal	20.439
Square	20.087
Triangular	20.045

9.5 Bandwidth (Δf) and Mechanical Quality (Q) Factor

The transducer consisted of the small lamination and the 643 turns winding. Each of the three different voltage waveforms were individually examined. The bandwidth and quality factor of each waveform differs significantly. Due to the unstable voltage waveforms and wide frequency measurements, interpolation of data is not performed.

9.5.1 Sinusoidal Bandwidth and Mechanical Quality Factor

Figure 45 provides a magnified view of the acceleration versus frequency with a sinusoidal voltage waveform.

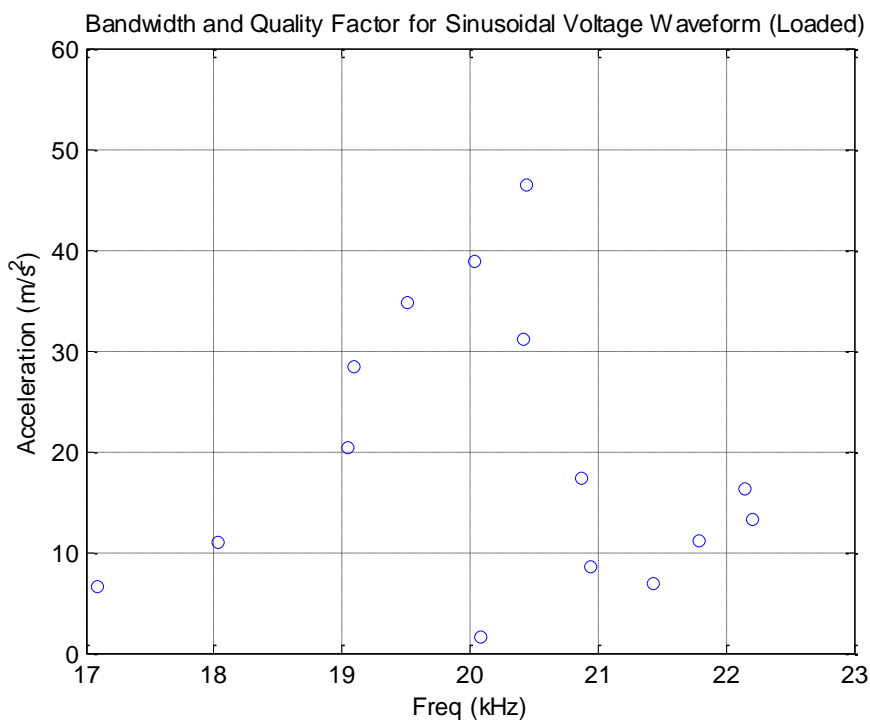


Figure 45. Bandwidth and Quality Factor for Sinusoidal Waveform (Loaded).

Using half acceleration is equivalent to half power then the following information can be approximated in table xiv.

Table xiv. Sinusoidal Bandwidth and Quality Factor (approx).

Sinusoidal Bandwidth and Quality Factor (approx)	
Resonant Frequency (kHz)	20.439
Lower Half Acceleration Limit (kHz)	19.1
Upper Half Acceleration Limit (kHz)	20.8
Bandwidth (kHz)	0.85
Quality Factor	24.0459

9.5.2 Square Bandwidth and Mechanical Quality Factor

Figure 46 provides a magnified view of the acceleration versus frequency with a square voltage waveform.

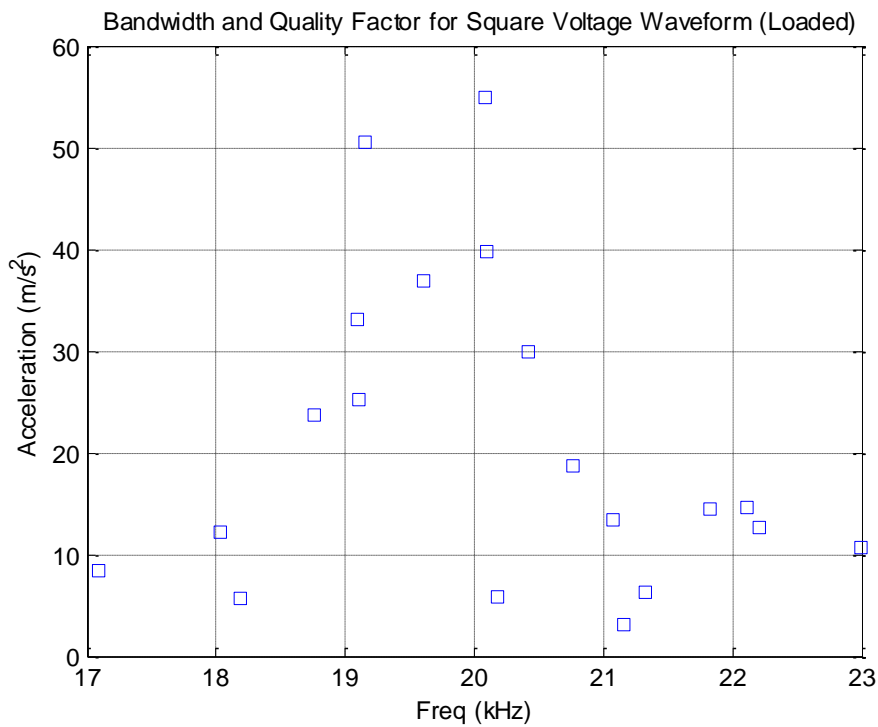


Figure 46. Bandwidth and Quality Factor for Square Voltage Waveform (Loaded).

Using half acceleration is equivalent to half power then the following information can be approximated in table xv.

Table xv. Square Bandwidth and Quality Factor (approx).

Square Bandwidth and Quality Factor (approx)	
Resonant Frequency (kHz)	20.087
Lower Half Acceleration Limit (kHz)	19.1
Upper Half Acceleration Limit (kHz)	20.5
Bandwidth (kHz)	0.7
Quality Factor	28.696

9.5.3 Triangular Bandwidth and Mechanical Quality Factor

Figure 47 provides a magnified view of the acceleration versus frequency with a triangular voltage waveform.

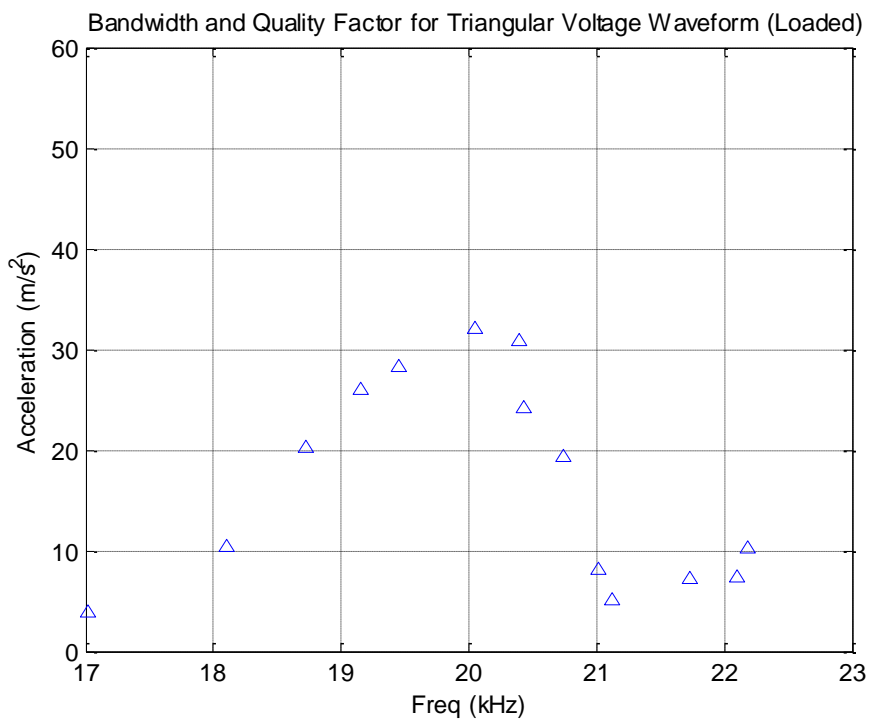


Figure 47. Bandwidth and Quality Factor for Triangular Voltage Waveform (Loaded).

Using half acceleration is equivalent to half power then the following information can be approximated in table xvi.

Table xvi. Triangular Bandwidth and Quality Factor (approx).

Triangular Bandwidth and Quality Factor (approx)	
Resonant Frequency (kHz)	20.045
Lower Half Acceleration Limit (kHz)	18.5
Upper Half Acceleration Limit (kHz)	20.8
Bandwidth (kHz)	1.15
Quality Factor	12.149

9.6 Electrical Impedance at Resonance

The transducer consisted of the small lamination and the 643 turns winding. The electrical impedance at resonance was carried out with the sinusoidal, square and triangular waveforms while the transducer was unloaded.

9.6.1 Sinusoidal Electrical Impedance at Resonance

The sinusoidal voltage waveform has a V_T of 3.511V and a I_T of 0.0868A. Using (34), the impedance (Z_T) of the transducer can be calculated at the resonant frequency of 20.439 kHz to be

$$Z_T = \frac{V_T}{I_T} = \frac{3.456}{0.0835} = 41.289\Omega.$$

The phase angle was determined by the 5034B to be 88.707°

9.6.2 Square Electrical Impedance at Resonance

The square voltage waveform has a V_T of 4.605 V and a I_T of 0.085 A. Using (34), the impedance (Z_T) of the transducer can be calculated at the resonant frequency of 20.087 kHz to be

$$Z_T = \frac{V_T}{I_T} = \frac{4.235}{0.0854} = 49.590\Omega.$$

The phase angle (ϕ) was determined by the 5034B to be 85.399°.

9.6.3 Triangular Electrical Impedance at Resonance

The triangular voltage waveform has a V_T of 2.867 V and a I_T of 0.091 A. Using (34), the impedance (Z_T) of the transducer can be calculated at the resonant frequency of 20.045 kHz to be

$$Z_T = \frac{V_T}{I_T} = \frac{2.867}{0.0875} = 32.767\Omega.$$

The phase angle (ϕ) was determined by the 5034B to be 88.740°.

9.7 Electrical Impedance Outside of Resonance

The transducer consisted of the small lamination and the 643 turns winding. The electrical impedance outside of resonance was carried out with the sinusoidal, square and triangular voltage waveforms while the transducer was unloaded. The outside of resonance frequency was set to 10.000 kHz.

9.7.1 Sinusoidal Electrical Impedance Outside of Resonance

The sinusoidal voltage waveform has a V_T of 3.456 V and a I_T of 0.080 A. Using (36), the impedance (Z_T) of the transducer can be calculated at the frequency of 10.000 kHz to be

$$Z_T = \frac{V_T}{I_T} = \frac{3.456}{0.0797} = 43.363\Omega.$$

The phase angle (ϕ) was determined by the 5034B to be 80.957°.

9.7.2 Square Electrical Impedance Outside of Resonance

The square voltage waveform has a V_T of 4.272 V and an I_T of 0.080 A. Using (36), the impedance (Z_T) of the transducer can be calculated at the frequency of 10.000 kHz to be

$$Z_T = \frac{V_T}{I_T} = \frac{3.981}{0.0776} = 51.302\Omega.$$

The phase angle (ϕ) was determined by the 5034B to be 80.199°.

9.7.3 Triangular Electrical Impedance Outside of Resonance

The triangular voltage waveform has a V_T of 2.850 V and an I_T of 0.084 A. Using (36), the impedance (Z_T) of the of the transducer can be calculated at the frequency of 10.000 kHz to be

$$Z_T = \frac{V_T}{I_T} = \frac{2.849}{0.0807} = 35.304\Omega.$$

The phase angle (ϕ) was determined by the 5034B to be 84.308°.

Table xvii is a comparison of all results from sections 9.6 and 9.7.

Table xvii. Transducer Impedance and Phase Angle.

Waveform	Frequency (kHz)	Absolute Impedance ($ Z_T $)	Phase Angle (ϕ)
Sinusoidal	20.493	41.289	88.707
	10.000	43.590	80.957

Square	20.087	49.590	85.399
	10.000	51.302	80.199
Triangular	20.045	32.766	88.470
	10.000	35.304	84.308

9.8 Mechanical Output Power (Vibration Analysis)

The transducer consisted of the small lamination and the 643 turns winding. The accelerometer was fixed to the transducer to record the acceleration. Using section 7.6 to determine the mass of the water and (64) the mechanical output power of the transducer was determined with all three waveforms.

9.8.1 Sinusoidal Voltage Mechanical Output Power

The transducer was operated with a sinusoidal voltage waveform at the resonant frequency of 20.493 kHz. The acceleration data was provided by the SCM05. MatLab scripting was used to calculate the velocity of the transducer face and the mass of medium against the transducer face was previously calculated to be 75×10^{-6} kg. This results in the output real power (P_{out}) of the transducer to be 0.065 1 Watts.

9.8.2 Square Voltage Mechanical Output Power

The transducer was operated with a square voltage waveform at the resonant frequency of 20.087 kHz. The acceleration data was provided by the SCM05. MatLab scripting was used to calculate the velocity of the transducer face and the mass of medium against the transducer face was previously calculated to be 75×10^{-6} kg. This results in the real output power (P_{out}) of the transducer to be 0.131 5 Watts.

9.8.3 Triangular Voltage Mechanical Output Power

The transducer was operated with a sinusoidal voltage waveform at the resonant frequency of 20.045 kHz. The acceleration data was provided by the SCM05. MatLab scripting was used to calculate the velocity of the transducer face and the mass of medium against the transducer face was previously calculated to be 75×10^{-6} kg. This results in the real output power (P_{out}) of the transducer to be 0.083 1 Watts.

9.8.4 Comparison of Mechanical Output Power

A comparison of the output mechanical power from the three principle waveforms is shown in table xviii.

Table xviii. Mechanical Output Power.

Voltage Waveform	Output Power (W)
Sinusoidal	0.065
Square	0.132
Triangular	0.083

9.9 Electroacoustic Efficiency

With the output power determined by section 9.8 and the input electrical power determined by section 9.2 at corresponding mechanical resonant frequency, the electroacoustic efficiency of the transducer can be determined without the detail of section 7.3.6.

9.9.1 Sinusoidal Voltage Electroacoustic Efficiency

The loaded input electrical power of the transducer operating at the resonant frequency of 20.493 kHz was 0.319 Watts with 0.065 Watts as the real output power of the transducer. Therefore the electroacoustic efficiency is

$$\frac{P_{out}}{P_{in}} = \frac{0.0651}{0.3195} = 20.38\%.$$

Figure 48 shows the electroacoustic efficiency for the sinusoidal voltage waveform.

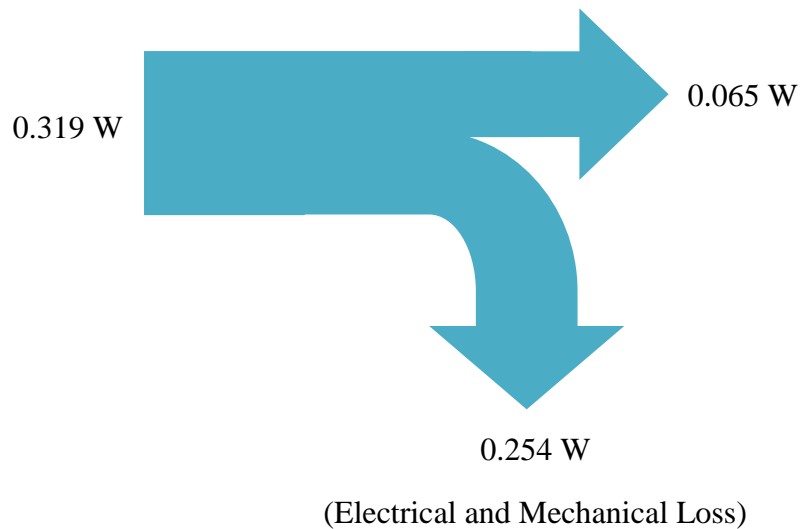


Figure 48. Electroacoustic Efficiency Diagram for Sinusoidal Voltage Waveform.

9.9.2 Square Voltage Electroacoustic Efficiency

The loaded input electrical power of the transducer operating at the resonant frequency of 20.087 kHz was 0.421 Watts with 0.132 Watts as the real output power of the transducer. Therefore the electroacoustic efficiency is

$$\frac{P_{out}}{P_{in}} = \frac{0.1315}{0.4213} = 31.21\%.$$

Figure 49 shows the electroacoustic efficiency for the square voltage waveform.

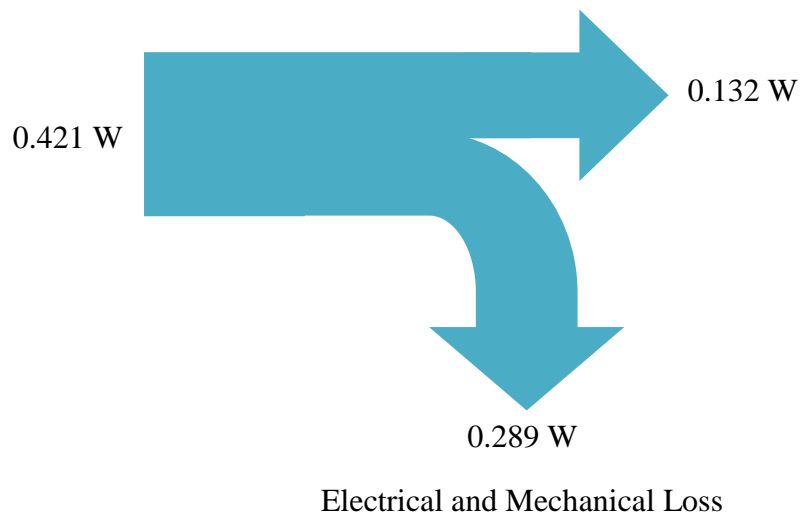


Figure 49. Electroacoustic Efficiency Diagram for Square Voltage Waveform.

9.9.3 Triangular Voltage Electroacoustic Efficiency

The loaded input electrical power of the transducer operating at the resonant frequency of 20.045 kHz was 0.260 Watts with 0.083 Watts as the real output power of the transducer. Therefore the electroacoustic efficiency is

$$\frac{P_{out}}{P_{in}} = \frac{0.0831}{0.2601} = 31.95\%.$$

Figure 50 shows the electroacoustic efficiency for the triangular voltage waveform.

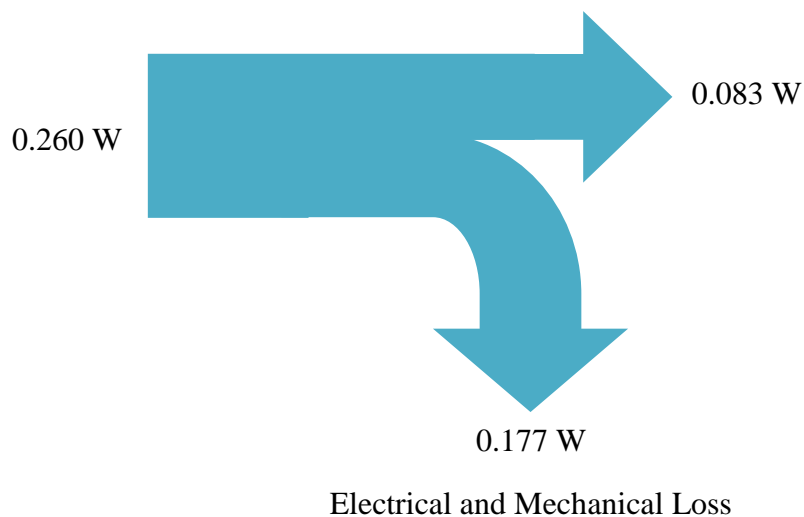


Figure 50. Electroacoustic Efficiency Diagram for Triangular Voltage Waveform.

9.9.4 Comparison of Electroacoustic Efficiency

A comparison of electroacoustic values are shown in table xix.

Table xix. Comparison of Electroacoustic Efficiency for all Three Voltage Waveforms.

Waveform	Electroacoustic Efficiency (%)
Sinusoidal	20.38
Square	31.21
Triangular	31.95

9.10 Equivalent RLC Electrical Circuit

The transducer consisted of the small lamination and the 643 turns winding. With the measurements taken from sections 9.2 to 9.8 and the procedure outlined in section 7.5 an equivalent electrical circuit can be obtained for all three principle voltage waveforms.

9.10.1 Sinusoidal Voltage Equivalent RLC Electrical Circuit

Z_T is previous calculated to be 43.363Ω with a phase angle of 80.957° when the transducer is operated outside of the resonant frequency. This results in

$$R_0 = |Z_T| \cos \varphi = 43.363 \times \cos(80.957) = 6.816\Omega$$

$$X_0 = |Z_T| \sin \varphi = 43.363 \times \sin(80.957) = 42.824\Omega$$

making

$$Z_T = 6.816\Omega + j42.824\Omega,$$

leading to

$$L_0 = \frac{X_0}{2\pi f} = \frac{42.824}{2\pi \times 10000} = 681.566 \times 10^{-6}H.$$

L_L and C_L are calculated by the using equations 7.19 and 7.24.

Solving simultaneously, L_L is approximately 22.423×10^{-6} H (22.423 μ H) and C_L is approximately 2.778×10^{-6} F (2.778 μ F).

R_L is calculate by the following,

$$R_L = \frac{V^2}{P_{out}} = \frac{3.512^2}{0.0651} = 189.465\Omega$$

allowing

$$R_{mec} \approx \frac{R_L R_0}{R_L - R_0} \approx \frac{189.465 \times 6.816}{189.465 - 6.816} \approx 7.070\Omega$$

and

$$R_{rad} \approx R_L - R_{mec} \approx 189.465 - 7.070 \approx 182.395\Omega.$$

The resultant equivalent RLC electrical circuit for the sinusoidal voltage input is shown in figure 51.

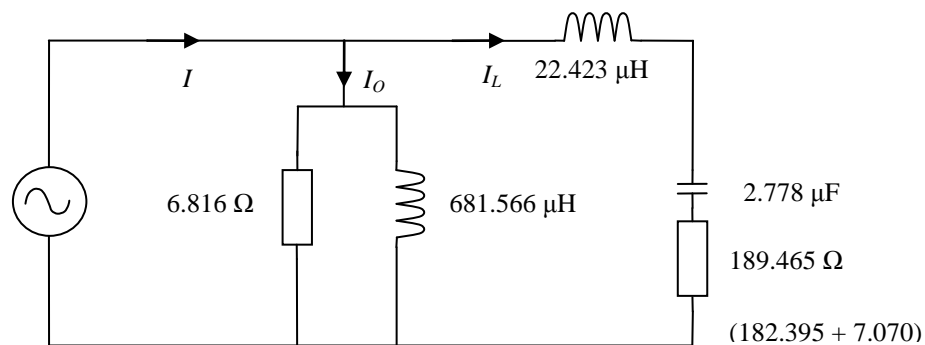


Figure 51. Sinusoidal Voltage Supply Equivalent RLC Electrical Circuit.

9.10.2 Square Voltage Equivalent RLC Electrical Circuit

Z_T is previous calculated to be 51.302Ω with a phase angle of 80.199° when the transducer is operated outside of the resonant frequency. This results in

$$R_0 = |Z_T| \cos \varphi = 51.302 \cos(80.199) = 8.733 \Omega$$

$$X_0 = |Z_T| \sin \varphi = 51.302 \sin(80.199) = 50.553 \Omega$$

making

$$Z_T = 8.733 \Omega + j50.553 \Omega$$

leading to

$$L_0 = \frac{X_0}{2\pi f} = \frac{50.553}{2\pi \times 10000} = 804.580 \times 10^{-6} H.$$

L_L and C_L are calculated by the using equations 41 and 46.

Solving simultaneously, L_L is approximately $34.646 \times 10^{-6} H$ ($34.646 \mu H$) and C_L is approximately $1.89 \times 10^{-6} F$ ($1.89 \mu F$).

R_L is calculate by the following,

$$R_L = \frac{V^2}{P_{out}} = \frac{4.605^2}{0.1315} = 161.263 \Omega$$

allowing

$$R_{mec} \approx \frac{R_L R_0}{R_L - R_0} \approx \frac{161.263 \times 8.733}{161.263 - 8.773} \approx 9.233 \Omega$$

and

$$R_{rad} \approx R_L - R_{mec} \approx 161.263 - 9.233 \approx 152.030 \Omega.$$

The resultant equivalent RLC electrical circuit for the square voltage input is shown in figure 52.

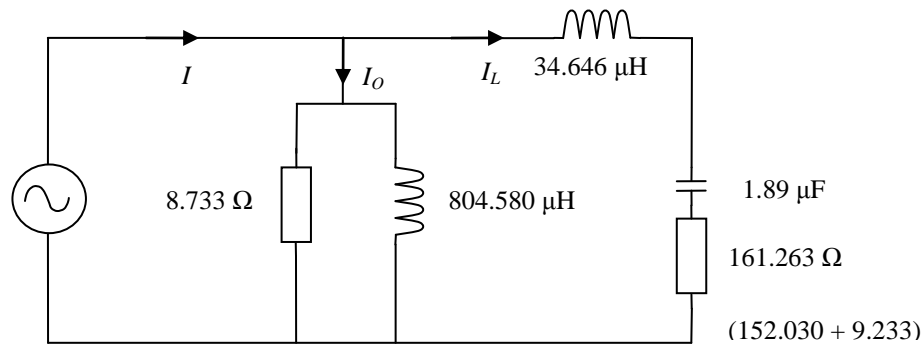


Figure 52. Square Voltage Supply Equivalent RLC Electrical Circuit.

9.10.3 Triangular Voltage Equivalent RLC Electrical Circuit

Z_T is previous calculated to be 35.304Ω with a phase angle of 84.308° when the transducer is operated outside of the resonant frequency. This results in

$$R_0 = |Z_T| \cos \varphi = 35.304 \times \cos(84.308) = 3.501 \Omega$$

$$X_0 = |Z_T| \sin \varphi = 35.304 \times \sin(84.308) = 35.130 \Omega$$

making

$$|Z_T| = 3.501 \Omega + j35.130 \Omega$$

leading to

$$L_0 = \frac{X_0}{2\pi f_{res}} = \frac{35.130}{2\pi \times 10000} = 559.111 \times 10^{-6} H.$$

L_L and C_L are calculated by the using (41) and (46).

Solving simultaneously, L_L is approximately $18.464 \times 10^{-6} H$ (18.464 μH) and C_L is approximately $3.527 \times 10^{-6} F$ (3.527 μF).

R_L is calculate by the following

$$R_L = \frac{V^2}{P_{out}} = \frac{2.867^2}{0.0831} = 98.913\Omega$$

allowing

$$R_{mec} \approx \frac{R_L R_0}{R_L - R_0} \approx \frac{98.913 \times 3.501}{98.913 - 3.501} \approx 3.629\Omega$$

and

$$R_{rad} \approx R_L - R_{mec} \approx 98.913 - 3.629 \approx 95.284 \Omega.$$

The resultant equivalent RLC electrical circuit for the triangular voltage input is shown in figure 53.

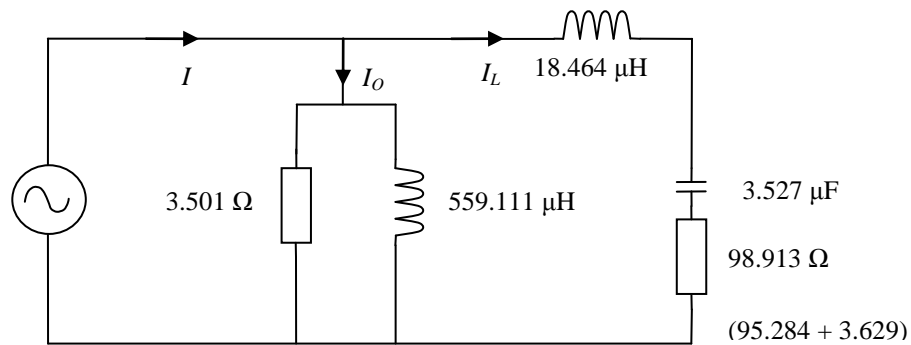


Figure 53. Triangular Voltage Supply Equivalent RLC Electrical Circuit.

9.11 Inductance Results

Three different methods were discussed in section 7 in determining the overall inductance of the transducers. The following sub sections provide the results of measured inductance.

9.11.1 Calculated Inductance

Using (20) the calculated inductance is

$$L = \frac{\mu N^2 A}{l} = \frac{4\pi \times 10^{-7} \times 643^2 \times 301.5 \times 10^{-6}}{48 \times 10^{-3}} = 3.263 \times 10^{-3} H$$

where N , A , and l are provided by the design of magnetostrictive transducer. The permeability of the core is assume to be equal to air where μ is $4\pi \times 10^{-7}$.

9.11.2 Measured Inductance via LCR Meter

All windings were measured with and without a nickel lamination for their inherent inductance values. The values are shown in table xx.

Table xx. Measured Inductance Values of all Tranducers.

Transducer Size	No. of Turns	Inductance with nickel lamination (mH)	Inductance without nickel lamination (mH)
Small	249	0.563	0.470
	643	3.71	3.05
Large	96	0.231	0.205
	115	0.476	0.410

9.11.3 Calculated Inductance via Measure Peak Current

Due to the unstable power supply the peak to peak current and the peak to peak voltage is an approximation and only the small transducer with 643 turns was tested. The peak to peak current and voltage were measured when the transducer was loaded and operating at the resonant frequency of the various voltage waveforms. Using (20) the inductance can be calculated as shown in Table xxi.

Table xxi. Calculated Inductance via Peak Current Values.

Waveform	No. of Turns	Peak Voltage	Peak Current	Resonant Frequency	Rise Time (μs)	Inductance (mH)
Sinusoidal	643	9.987	0.125	20 493	24.399	1.949
Square	643	10.007	0.121	20 087	24.892	2.059
Triangular	643	9.961	0.128	20 045	24.944	1.941

9.11.4 Calculated Inductance via RLC Equivalent Electrical Circuit

The calculated inductance values is provided by L_0 as C_L and L_L cancel each other when the circuit is operating at the resonant frequency. The values of circuit inductance are provided by section 9.10 and differ dramatically from the inductance values determined by LCR meter and peak current method and .

A comparison is provided in the following subsection.

9.11.5 Comparison of Calculated and Measured Inductance

A comparison of inductance result are shown in table xxii.

Table xxii. Comparison of Calculated Inductance.

Waveform	No. of Turns	Inductance from (20) (mH)	Inductance from LCR meter (mH)	Inductance from Peak Current (mH)	Inductance from Equivalent RLC Circuit (mH)
Sinusoidal	643	3.263	3.71	1.949	0.682
Square	643	3.263	3.71	2.059	0.805
Triangular	643	3.263	3.71	1.941	0.559

The difference between the LCR meter and the peak current method can be attributed to the function generators not suitable to the demands of the transducer. The increased errors associated with the equivalent RLC circuit are also cause by the unsuitable function generator but are compounding due to the mathematic involved in determining the values in equivalent RLC circuit.

Inductance values could also be affected due to the low power supplied to the transducer. Even though it was minimised by the selection of only the small lamination with the 643 turn winding.

9.12 Variations of the Square Voltage Waveform

All of the previous tests were performed on principle waveforms. Variation in DC offset and duty cycle of a square waveform were examined.

It can be determined that a 5 V_{PP} square waveform with a DC offset of -2.5 V and a duty cycle of 25 per cent will supply more electrical input power.

9.12.1 Variations in the DC Offset

Three different DC offsets were tested to confirm that more electrical power could be supplied to the transducer. The three different DC offset are -2.5 V , 0.0 V and $+2.5\text{ V}$. The three different DC offset produced an rms voltage of 3.535 V , 2.5 V and 3.535 V respectively. Figure 54 shows the expected result of the -2.5 V and $+2.5\text{ V}$ DC offset being similar in power rating as the rms voltage is the same, and the 0.0 V DC offset providing less power as compared to the -2.5 V and $+2.5\text{ V}$ DC offset.

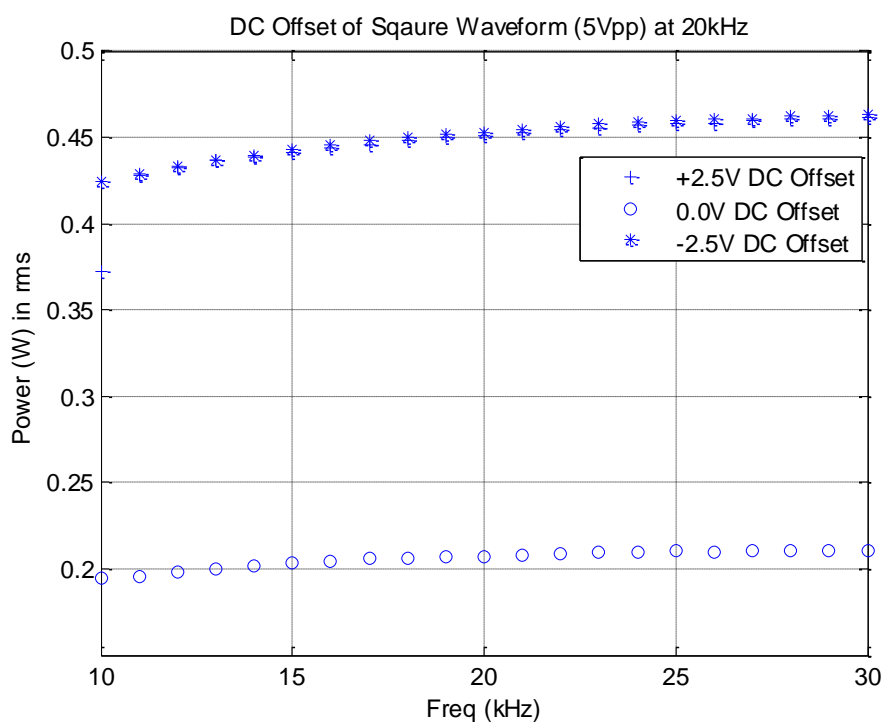


Figure 54. Variations of DC Offset for a 20kHz Square Voltage Waveform.

9.12.2 Variations in Duty Cycle

Expanding from the DC offset tests in section 9.12.1 the duty cycle of the square voltage waveform was then adjusted from 5 per cent to 95 per cent. Figure 55 shows the measured input electrical power of the transducer when the duty cycle and DC offset is changed on the square voltage waveform. The confirmation of -2.5 V and $+2.5\text{ V}$ DC offset providing similar electrical power is not supported. This

disagreement is believed to be caused by the design of the transducer lamination, where there is more nickel at one end as compared to the open end.

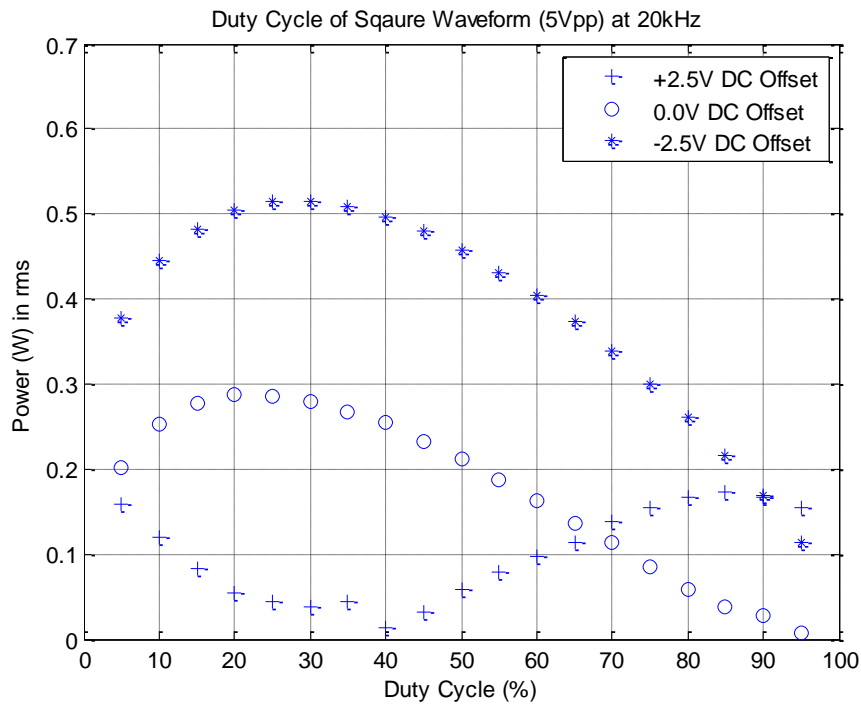


Figure 55. Variations of Duty Cycle for a 20kHz Square Voltage Waveform.

9.12.3 Variations in Polarity

The reverse connection was to confirm the correct operation of the windings and transducer and to prove or disprove the results in section 9.12.2. The North end of the winding was determined by the right hand rule where the right fingers represent the current flow in the winding and the right thumb points to the North end. Figure 56 confirms that the direction of the windings does not have any effect on the transducer due the voltage source being alternating. Leaving the results obtained in section 9.12.2 being unresolved.

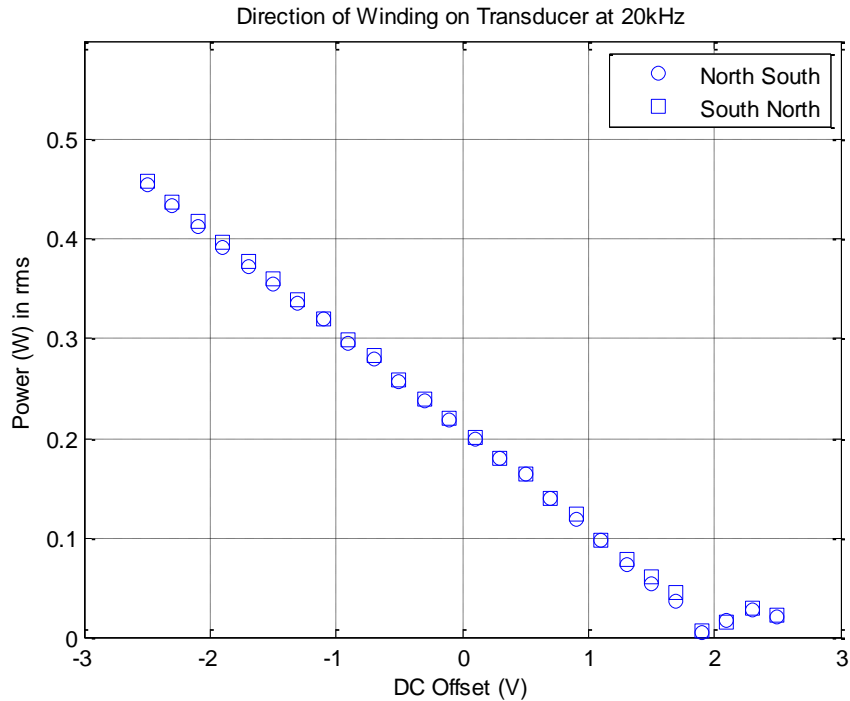


Figure 56. Variations of Polarity for a 20kHz Square Voltage Waveform (including DC offset).

9.13 Cavitation

As identified in section 9.3 and 9.4, the square voltage waveform provides the most electrical power, produces the most mechanical power and has a relative high electroacoustic efficiency. The square waveform was then examined to produce cavitation. No other voltage waveforms were investigated in the creation of cavitation. All other possible transducer combination were briefly tested for cavitation with only the small transducer and the 643 turns winding producing cavitation.

Through a frequency sweep it was visually and audibly determined that cavitation was present at 5.525 kHz. The average input electrical power was measured at 18.713 W.

Cavitation can be confirmed by the presence of a cavitation cloud. A cavitation cloud is where micro-bubble are suspended in the medium and gather in a generalised area giving the appearance of a cloud. Figure 57 shows a cavitation cloud suspended in the medium.

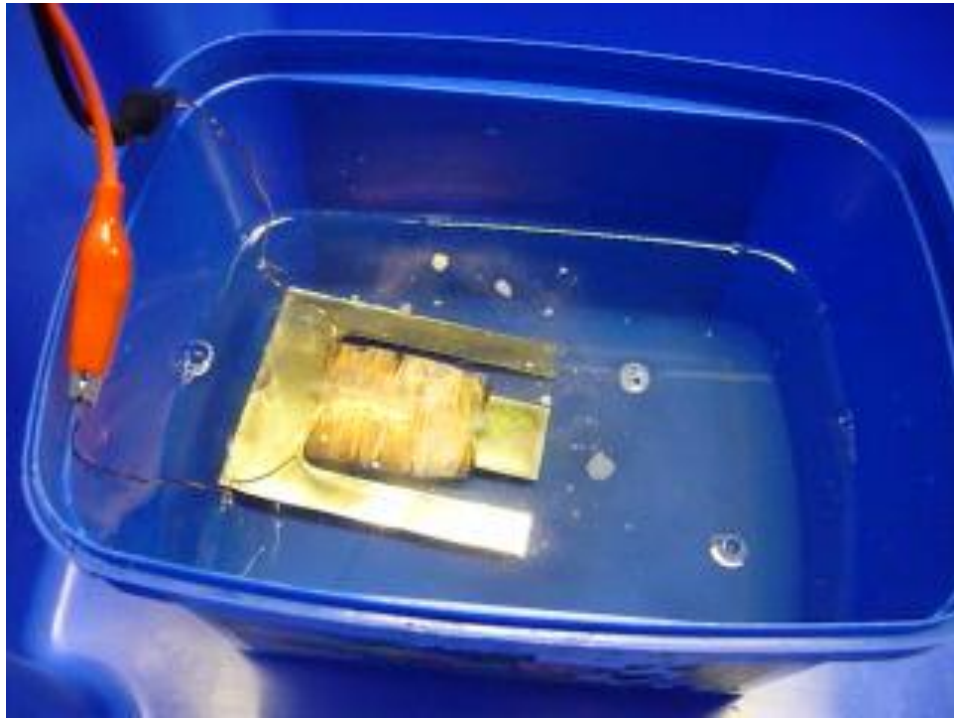


Figure 57. Creation of Cavitation Cloud..

Mechanical output power was measure by the SCM05. A FFT was performed on the acceleration data resulting in the frequencies spectrum shown in figure 58 for the 5.525 kHz transmitted frequency. The mechanical output power was calculated to be 0.108W.

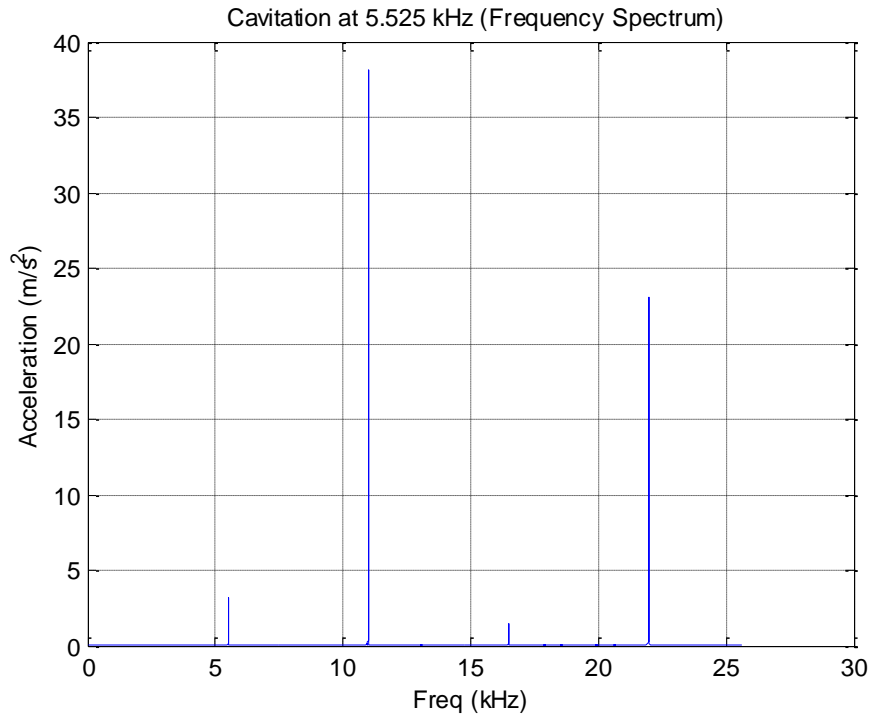


Figure 58. Frequency Spectrum of 5.255 kHz at Cavitation.

Even though the transmitted frequency was 5.525 kHz there is a major frequency component around the 11 kHz region.

With the input and output power known the electroacoustic efficiency can be calculated, as shown in table xxiii.

Table xxiii. Cavitation at 5.525 kHz Electroacoustic Efficiency.

Cavitation at 5.525kHz	
Input Electrical Power	18.713 W
Output Mechanical Power	0.108 W
Electroacoustic Efficiency	0.577%

Using (20) the value of inductance of the transducer can be calculated by

$$L = V \frac{dt}{di} = 62 \times \frac{181 \times 10^{-6}}{2.6} = 4.316 \text{ mH.}$$

This is comparable to the measured inductance of 3.71 mH and calculate inductance of 3.263 mH. It is also evident that the increase in current during the on-time of the cycle and the decrease in current during the off-time of the cycle are linear, as to be expected of an inductor.

A large magnitude of acceleration was identified around the 11 kHz region in figure 58 leading to a sweep around that frequency. Visual and audible confirmation of cavitation was identified at 11.013 kHz. Figure 59 is an image of the supply voltage waveform, current waveform and resultant power waveform.

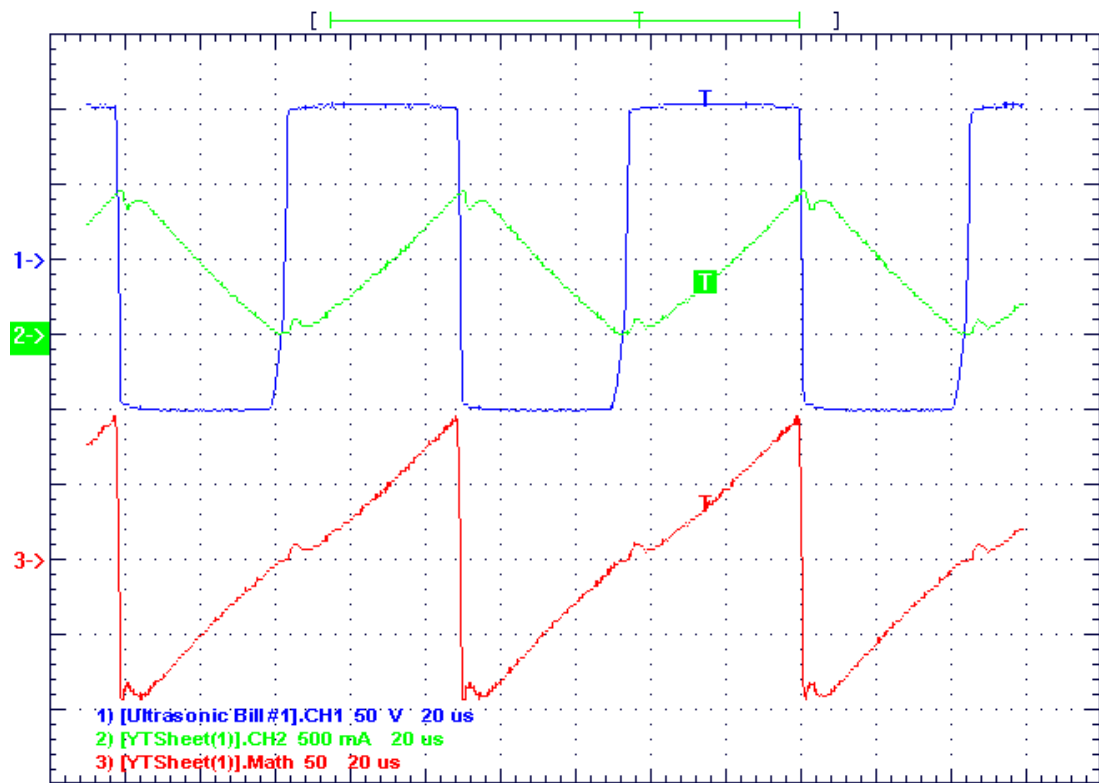


Figure 59. Input Electrical Power Waveforms at 11.013 kHz Producing Cavitation.

From figure 59 and using (65) the magnetic field intensity was $308.64\text{A}\cdot\text{m}^{-1}$ where the number of turns is 643 and the peak current is 0.480 A. This is approximately one third the of the saturated magnetic field intensity of the transducer.

A FFT was performed on the acceleration data resulting in the frequencies spectrum shown in figure 60 for the 11.013 kHz transmitted frequency.

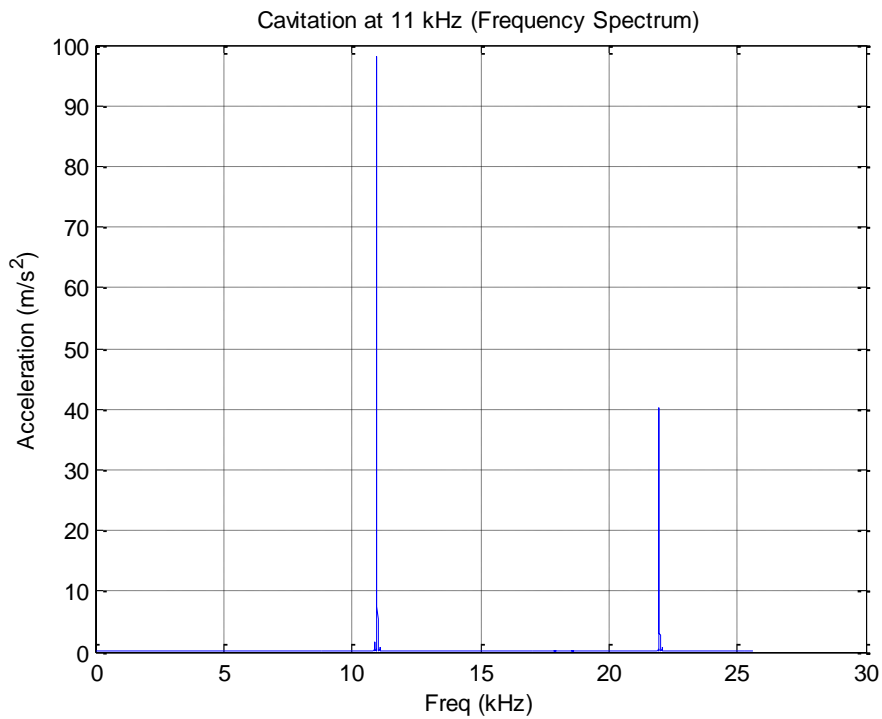


Figure 60. Frequency Spectrum of 11.013 kHz at Cavitation.

In a separate test the input power was measured to be 14.659 W and the mechanical output power was calculated to be 0.560 W. With the input and output power known the electroacoustic efficiency can be calculated, as shown in table xxiv and figure 61.

Table xxiv. Cavitation at 11.013 kHz Electroacoustic Efficiency.

Cavitation at 11.013 kHz	
Input Electrical Power	14.659 W
Output Mechanical Power	0.560 W
Electroacoustic Efficiency	3.82%

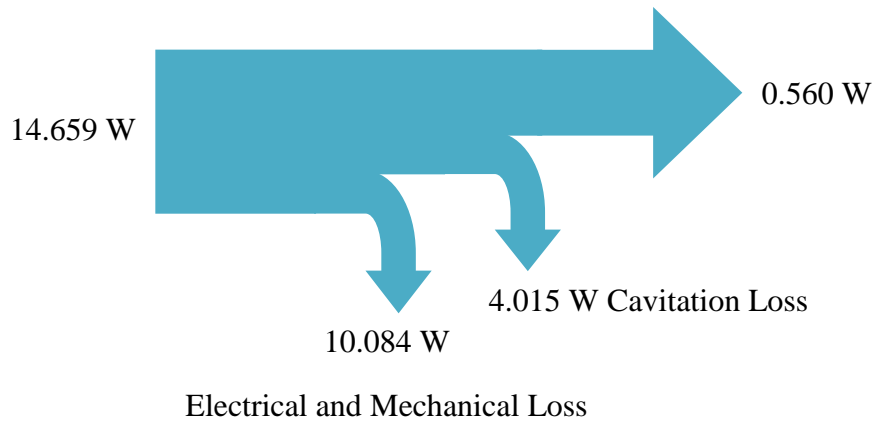


Figure 61. Electro-cavitation Efficiency Diagram at 11.013 kHz.

Using (20) the value of inductance of the transducer can be calculated

$$L = V \frac{dt}{di} = 104 \times \frac{45.4 \times 10^{-6}}{0.98} = 4.818 \text{ mH}$$

This is comparable to the measured inductance of 3.71 mH and calculate inductance of 3.263 mH. It is also evident that the increase in current during the on-time of the cycle and the decrease in current during the off-time of the cycle are linear as to be expected of an inductor.

The 16.5 kHz and 22 kHz (harmonics of 5.525 kHz and 11.013 kHz) regions were then examined but cavitation could not be confirmed, so no results are discussed.

Chapter 10 – Conclusion

10.1 Achievement of Project

Overall the project was a success although with some limitation. The ability of the function generators hampered the results but with persistence was able to provide some useable data. The procedure provided by IEC 60782 [35] and Petošić et al [23] provided a large benefit in examining the magnetostrictive transducer. Limited investigation was then performed on cavitation which provided some interesting results.

The research of magnetostriction was performed including the interaction of Magnetic Flux and mechanical action by various methods. The research involved the implementation of procedures provided by IEC60782 [35] and Petošić et al [23].

The development of a power electronic system to accurately drive the magnetostrictive effect of the transducer was mainly determined by the efficiencies associated with the principle waveforms. It was determined that a square waveform with a 25 per cent duty cycle and negative DC offset provided the most electrical input power. The electroacoustic efficiency of the square waveform is similar in values to the best performing efficiency provided by the Triangular waveform. In a power electronic system the square voltage waveform happens to be the easiest to produce as compared to the sinusoidal and triangular waveforms. But due to the nature of the magnetostrictive transducer relative high current can be required which may affect the voltage waveform.

An equivalent RLC circuit was produced for all principle waveforms. The details of the equivalent RLC circuit are not reliable due the unstable waveforms supplied by the function generators.

Determining the mechanical output from the electrical input was investigated, with results being unsatisfactory. An alternative method to determine output mechanical power was provided by mechanical vibration analysis.

Optimisation of the power electronic design to suit standard mains supply was indirectly discussed as a square voltage waveform was proven to supply more input

electrical power. A power supply providing a square voltage waveform is easier to adapt to main power as compared to the sinusoidal and triangular voltage waveforms.

The magnetostrictive effect was investigated on different transducer designs when used to create cavitation. With only the 643 turn small transducer producing cavitation. Results for the other transducer combination were not recorded as they did not produce cavitation.

Other ferromagnetic materials were not investigated.

The wave pattern produced from the transducer were not investigated.

Cavitation was additionally investigated with results confirming there are losses associated with the transfer of ultrasonic energy to cavitation. It was also witnessed that the resonant frequency associated with cavitation (11 kHz) is approximately half the resonant frequency of ultrasonic energy (20 kHz). It appeared the transducer was operating with minimal input power to achieve cavitation at the preferred frequency of 11 kHz. The current required to produce minimal cavitation was approximately one third of the maximum current for the 643 turn transducer to achieve magnetic field intensity saturation.

So to achieve conclusive cavitation with the small lamination and 643 turn winding, the winding would have to contain approximately 1800 turns or be supplied with 600 V_{PP} . This reinforces equations

$$H \approx (I \times n)$$

or

$$H \approx \left(\frac{V}{X_L} \times n \right).$$

10.2 Project Limitation

Most of the data gather was provided from test equipment that was uncalibrated, therefore the accuracy of the data cannot be classed as reliable.

The major limitation was the inability of the function generators to provide adequate relative current with the various voltage waveforms. This resulted in only one of the

four possible transducers being examined. Results improved when the supply power was increase to the transducer via the Half controlled H bridge.

The maximum detectable frequency was 25.6 kHz with the mechanical vibration analysis. While the mechanical vibration analysis frequency range was similar to the frequency range under investigation a higher detectable frequency would have been beneficial.

10.3 Further Research Recommendations

The results provided in this project are not conclusive and should be confirmed.

The results obtained by this project were determined by large discrete increments, for example the frequency sweep was recorded in 500 Hz increments. Improved accuracy will be obtained with smaller discrete increments.

The interest shown by industry suggests further research can conducted on cavitation. Confirmation of definitive cavitation where the magnetic field intensity is 818.3 A.m^{-1} with the small nickel lamination with either increased number of turns or increased voltage.

Appendices

Appendix A. Project Specification.

University of Southern Queensland

FACULTY OF ENGINEERING AND SURVEYING

ENG4111/4112 Research Project
Project Specification

FOR: **WILLIAM MCHUGH**

TOPIC: PROPERTIES OF NICKEL AS A MAGNETOSTRICTIVE MATERIAL FOR ULTRASONIC
CONDITIONS

SUPERVISORS: Mr Les Bowtell

SPONSORSHIP: New Wave Leathers Pty Ltd.

ENROLMENT: ENG4111 – S1, D, 2011;
ENG4112 – S2, D, 2011

PROJECT AIM: This project investigates the design of a Nickel laminated magnetostrictive ultrasonic transducer including an electromagnetic simulation of the transducer with the aim of optimizing operating parameters.


PROGRAMME: Issue A, 16th March 2011

1. Research Magnetostriction including the interaction of Magnetic Flux and mechanical action.
2. Develop a power electronic system to accurately drive the magnetostrictive effect of the transducer.
3. Design an electromagnetic simulation of a known transducer.
4. Investigate the electrical method of determining mechanical output.
5. Optimise the power electronic design to suit standard mains supply.


As time permits:

6. Simulate the Magnetostrictive effect of different materials.
7. Simulate the Magnetostrictive effect on different physical transducer designs.
8. Investigate the mechanical wave pattern produced by different transducer designs.

AGREED:



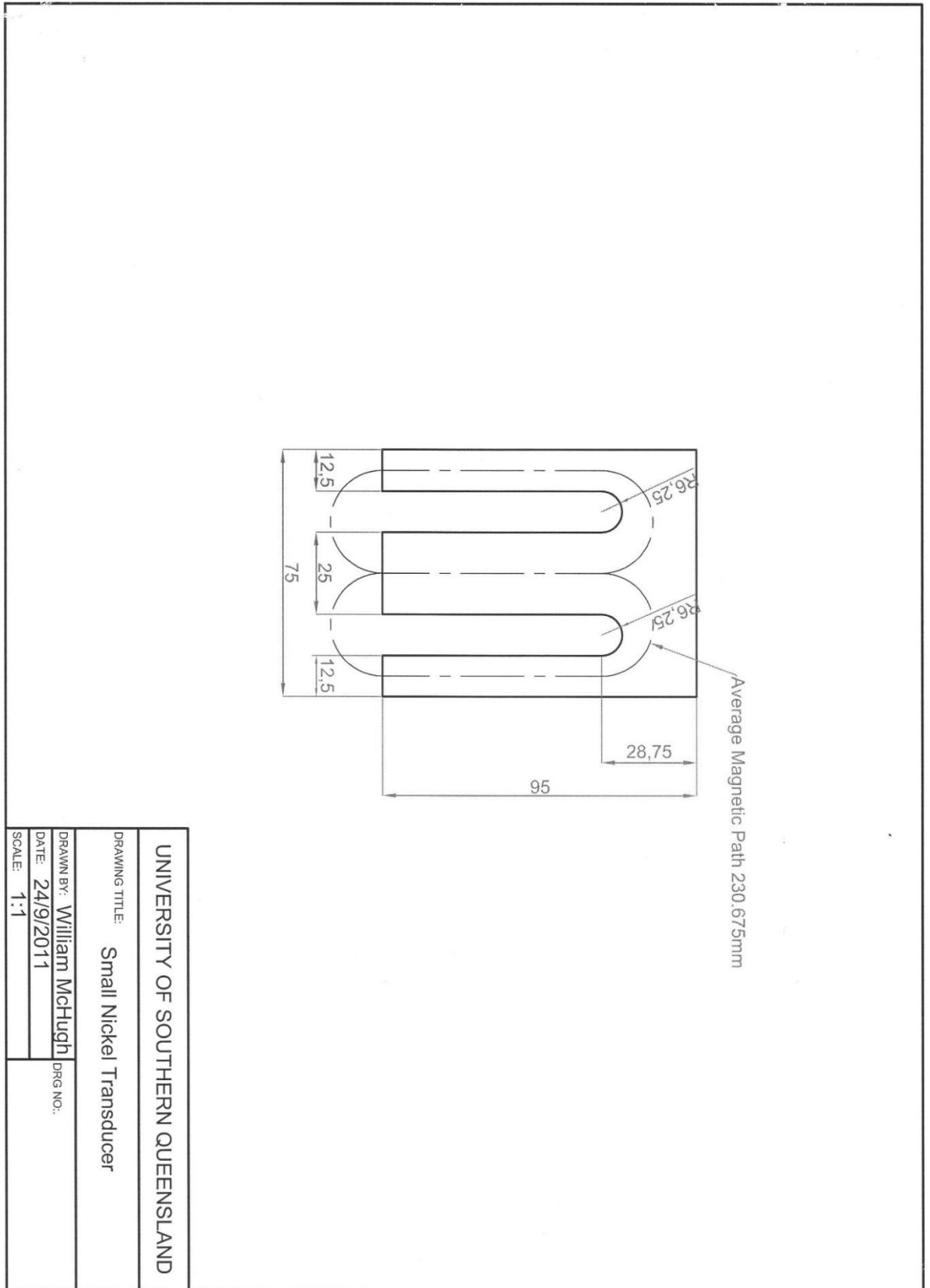
16 / 3 / 2011
(Student)



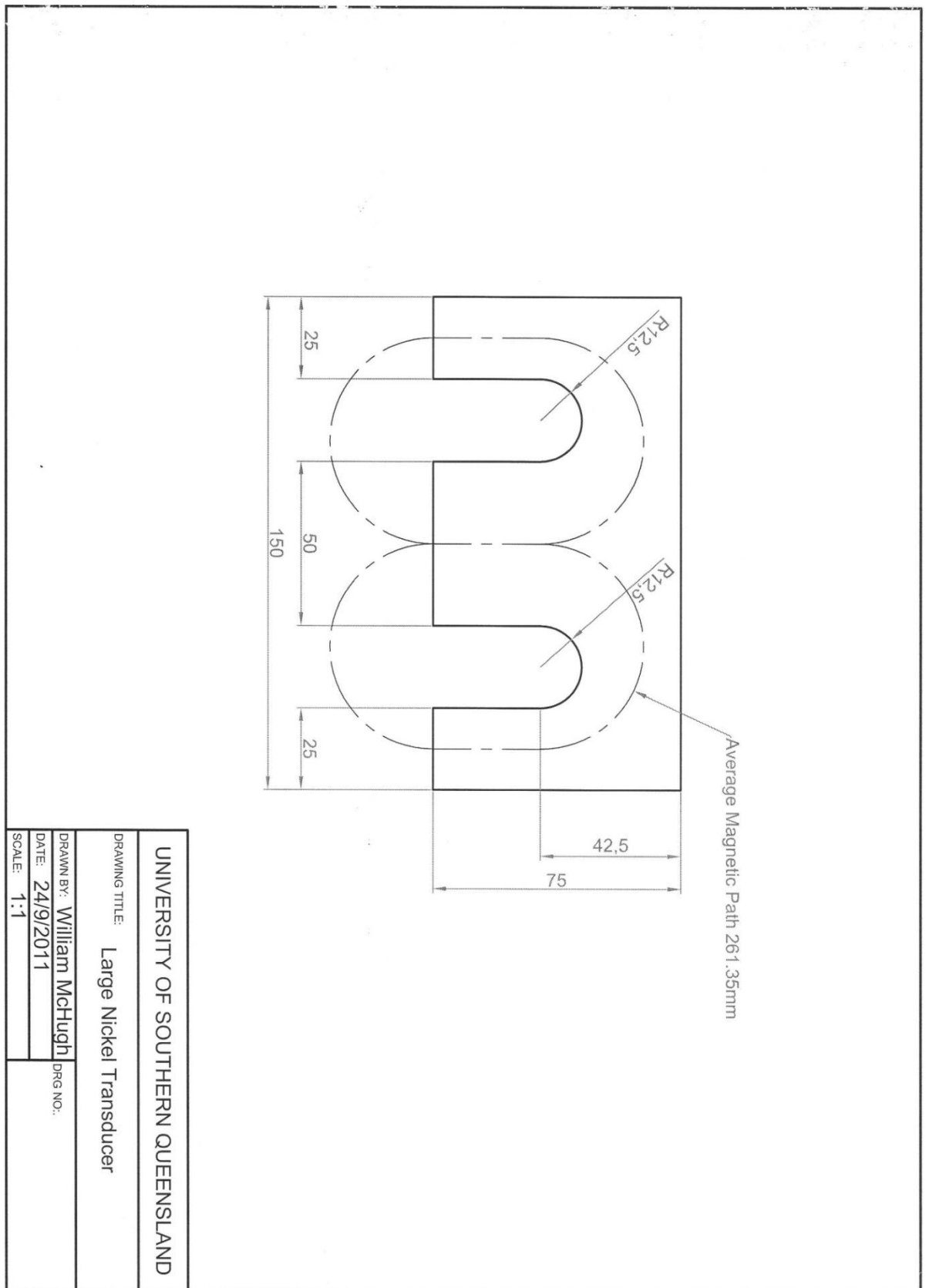
16 / 3 / 2011
(Supervisor)

Appendix B. Transducer Design.

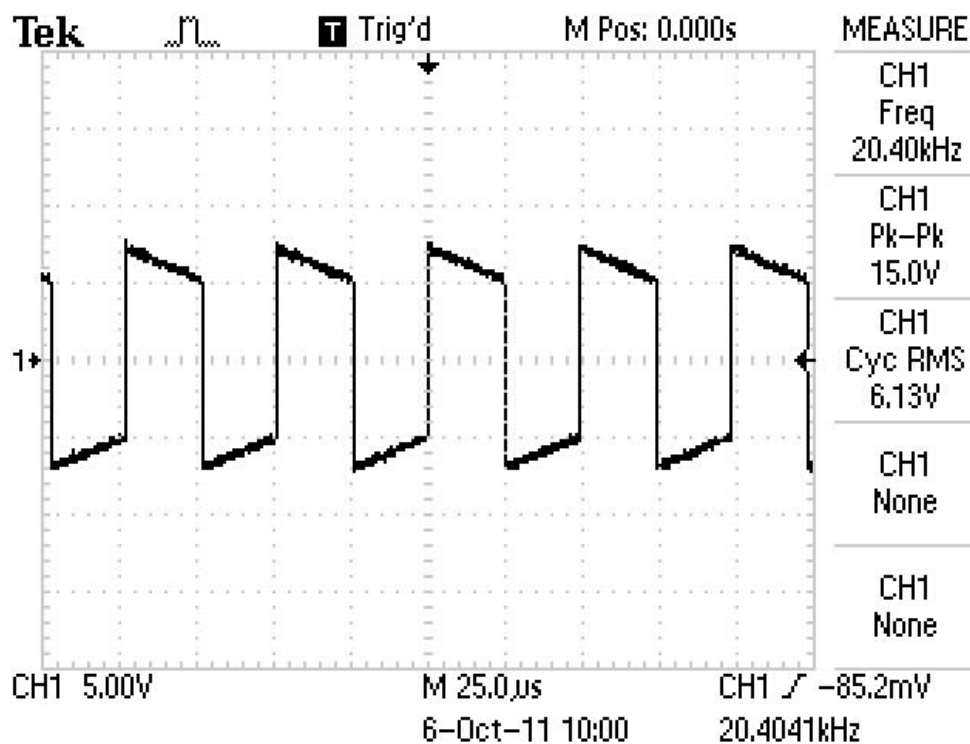
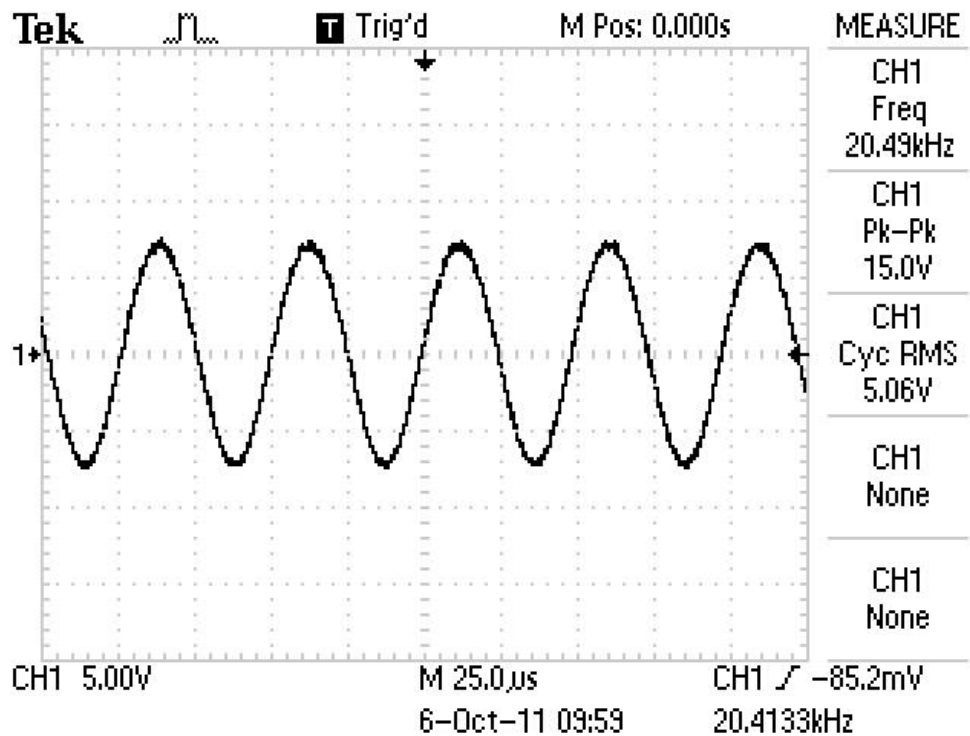
B.1. Small Transducer Design.

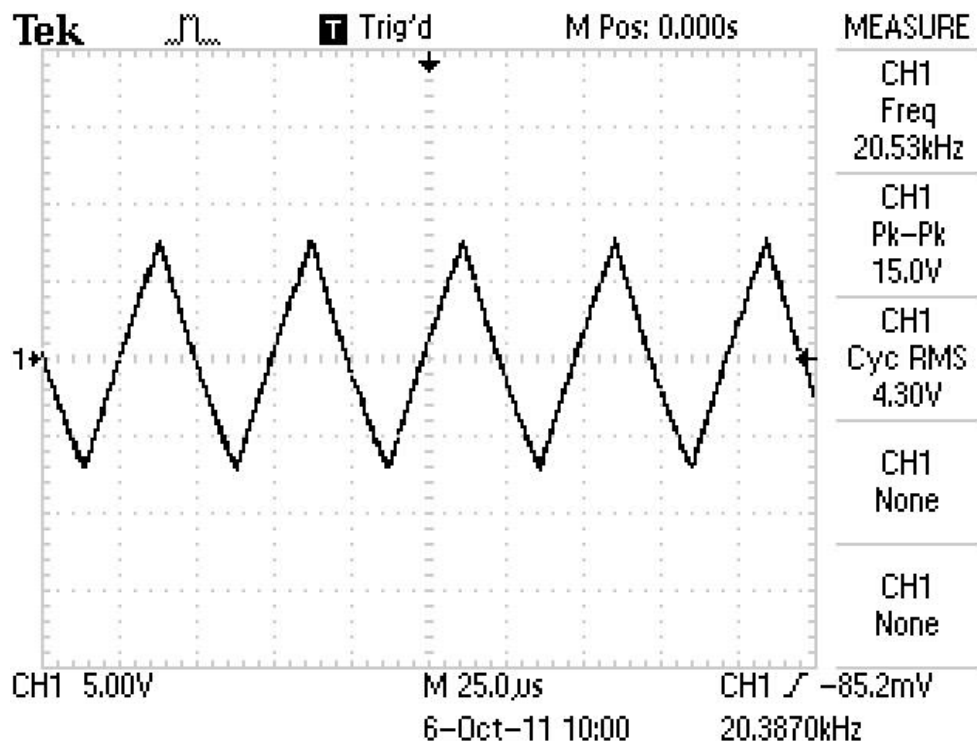


B.2. Large Transducer Design.

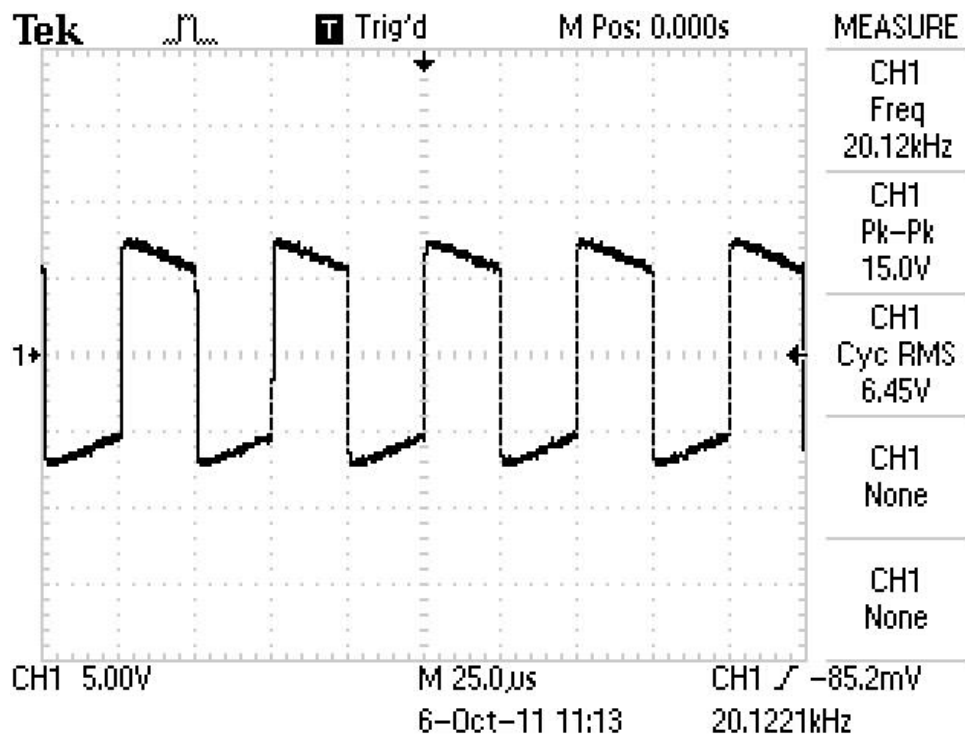
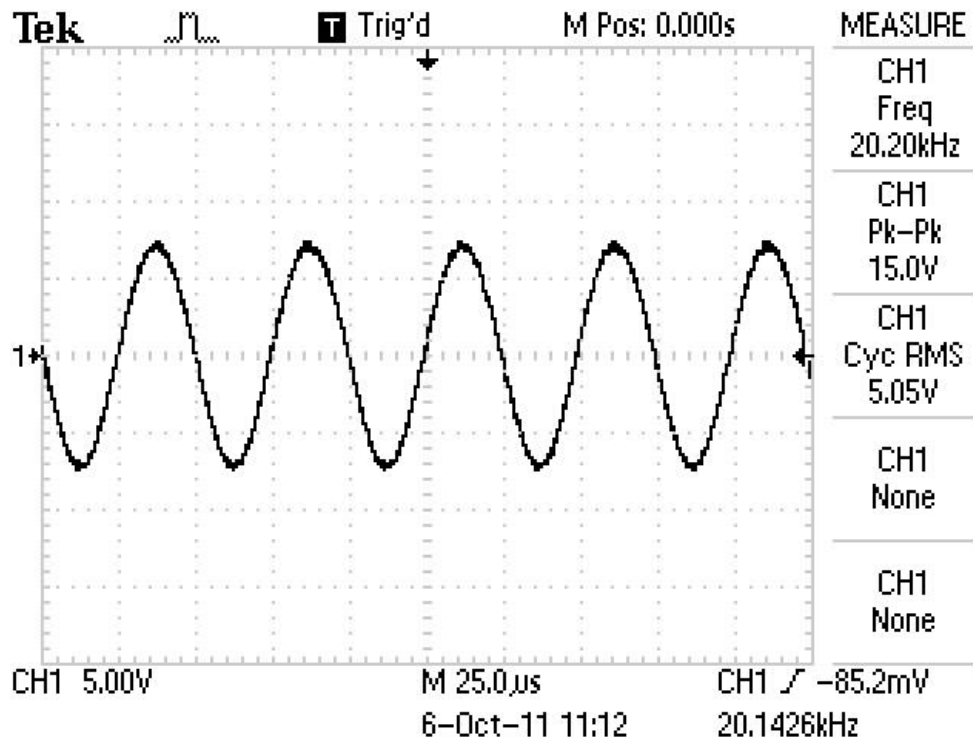


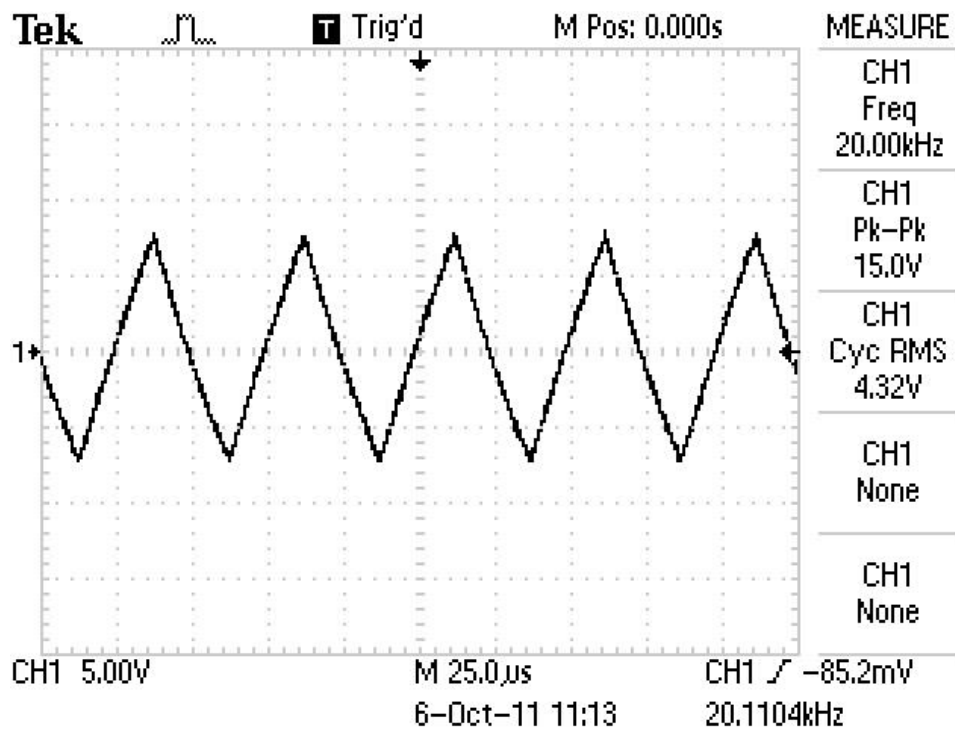
Appendix C. Unloaded UMST. Various Voltage Waveforms.



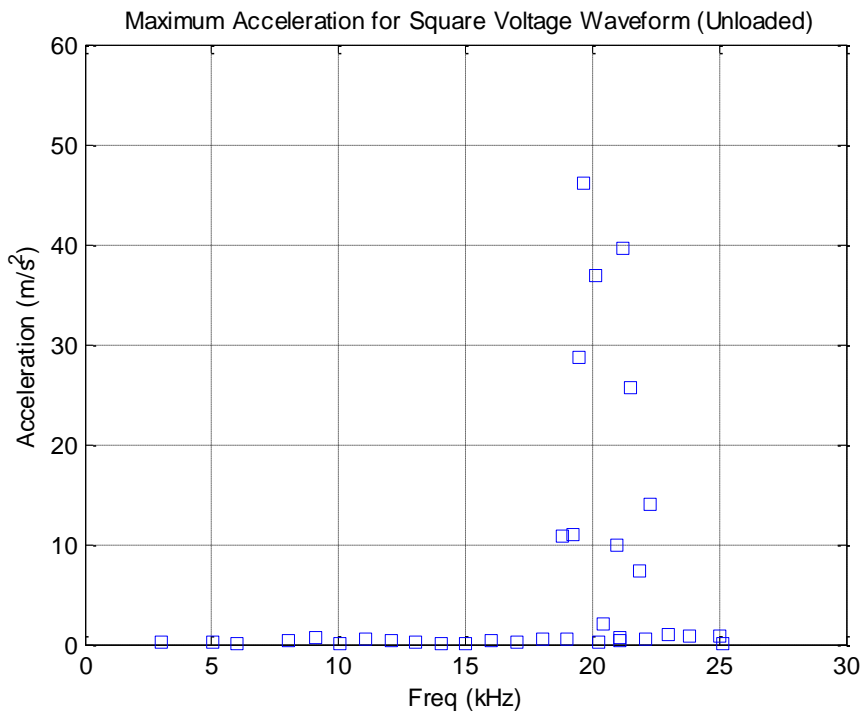
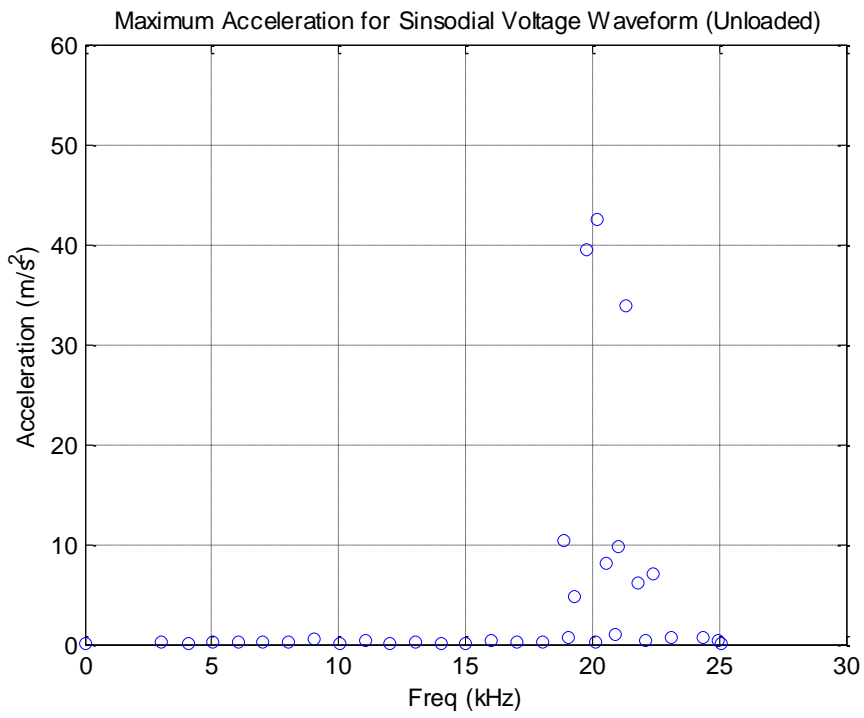


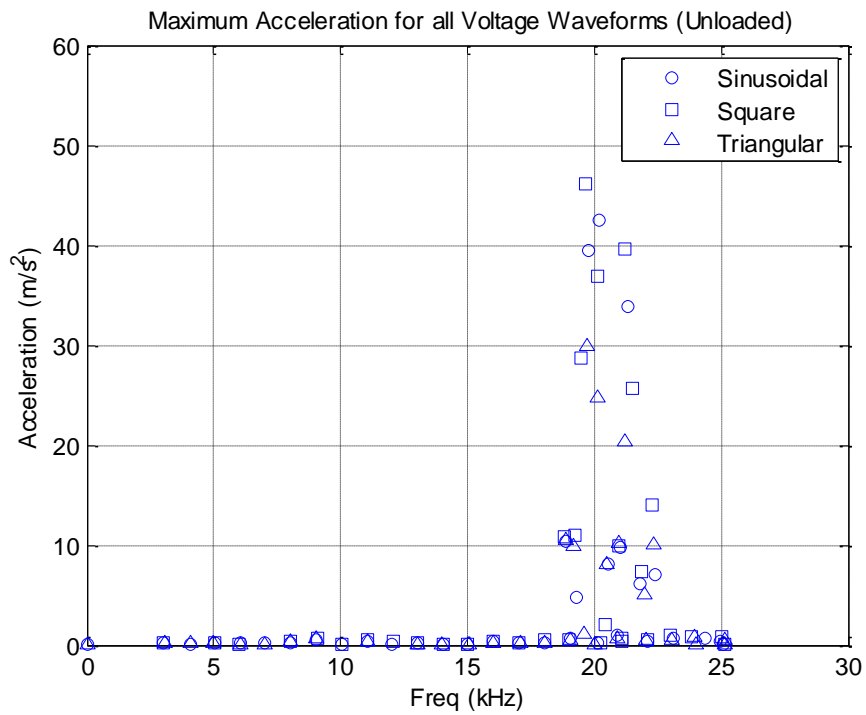
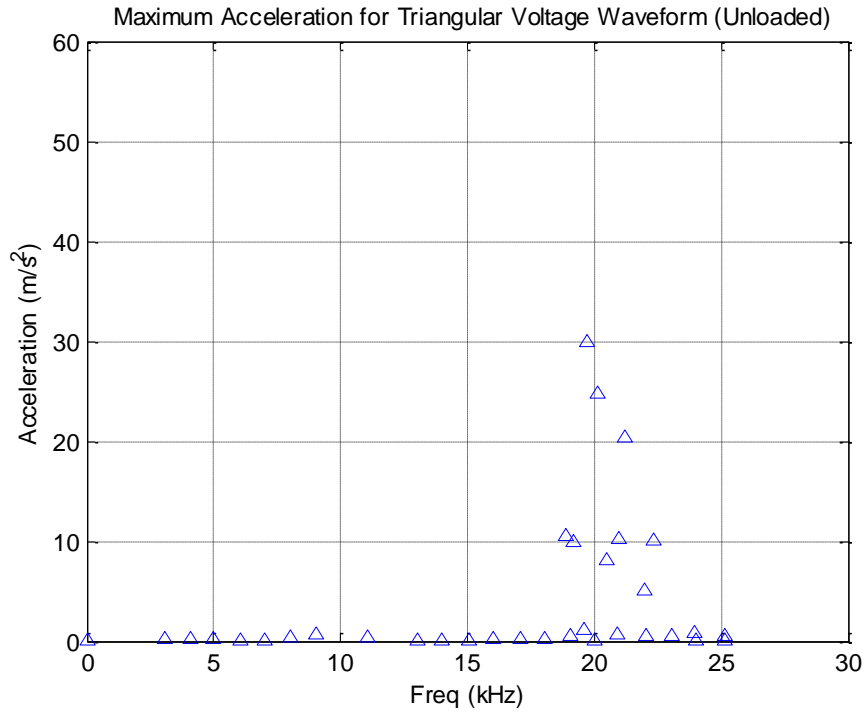
Appendix D. Loaded UMST. Various Voltage Waveforms.



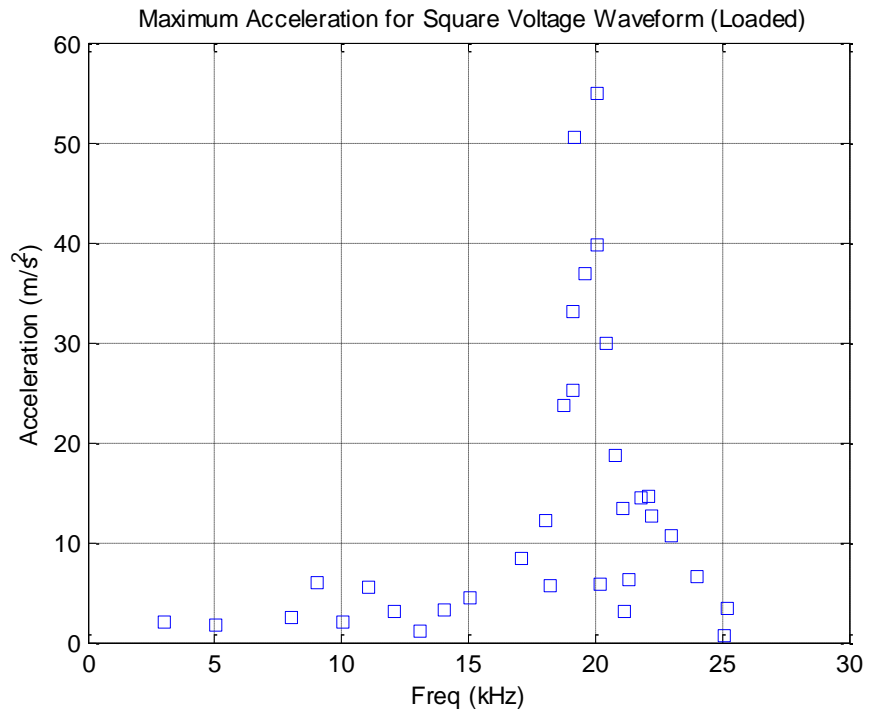
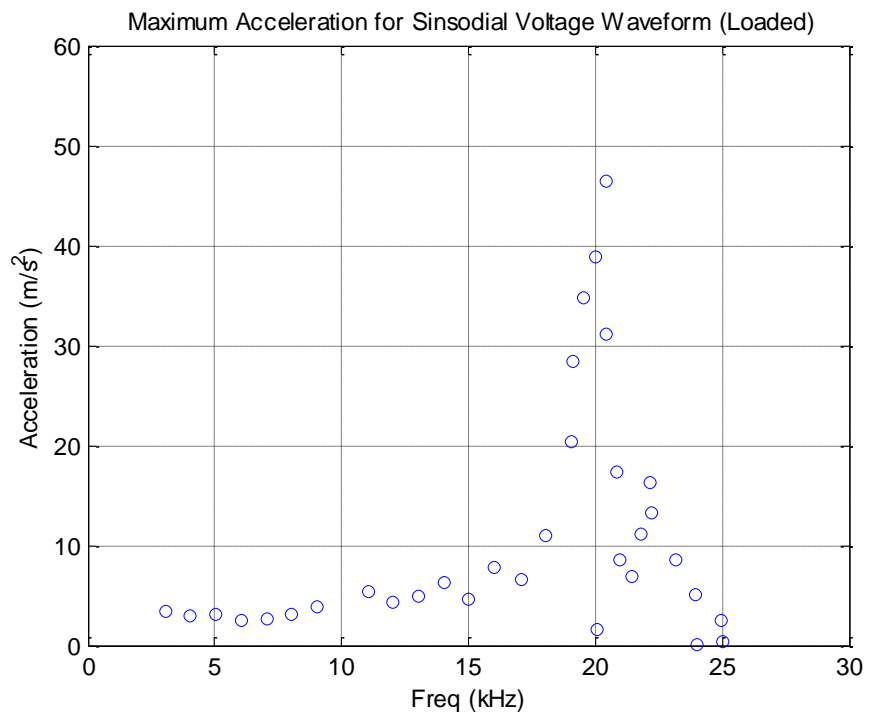


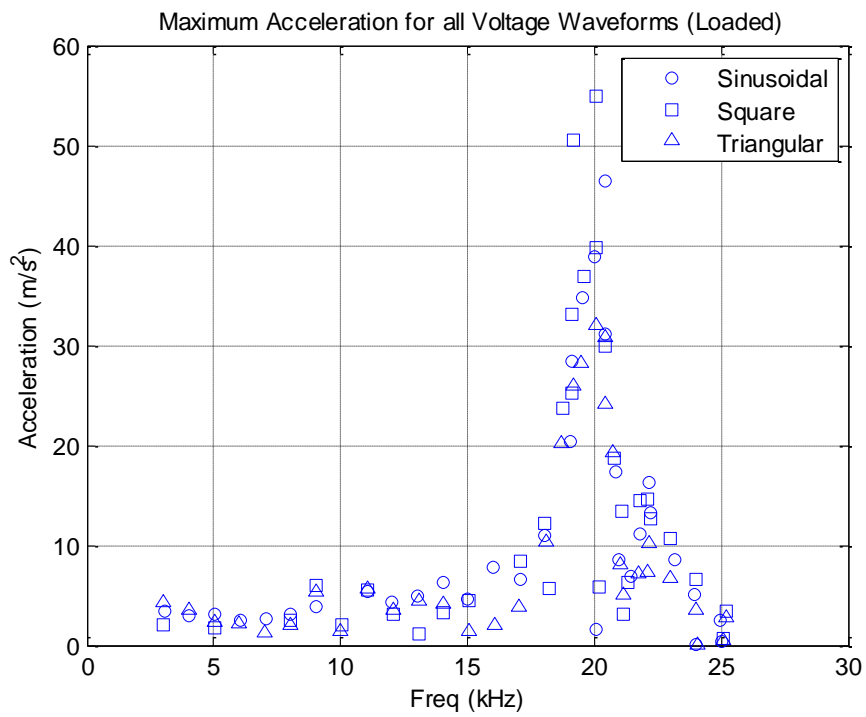
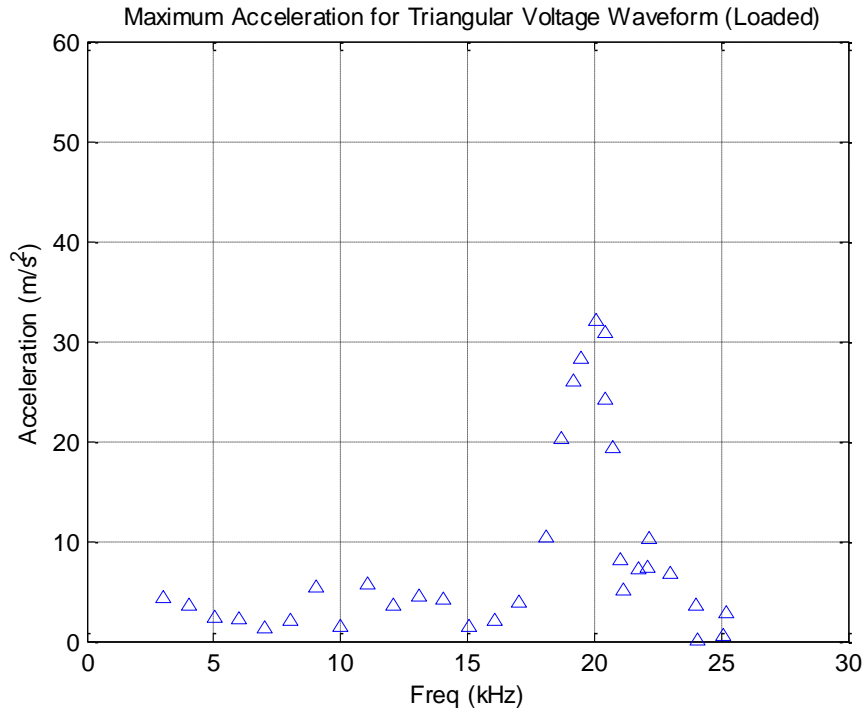
Appendix E. Vibration Analysis of Unloaded UMST. Various Voltage Waveforms.





Appendix F. Vibration Analysis of Loaded UMST. Various Voltage Waveforms.





References

- [1] J. P. Joule, "On the effects of magnetism upon the dimensions of iron and steel bars," *The London, Edinburgh and Dublin philosophical magazine and journal of science*, vol. 30, pp. 76-87, 1842.
- [2] G. L. Gooberman, *Ultrasonics: Theory and application*. London: The English Universities Press Ltd, 1968.
- [3] B. Niemczewski, "Observations of water cavitation intensity under practical ultrasonic cleaning conditions," *Ultrasonics Sonochemistry*, vol. 14, pp. 13-18, 2007.
- [4] K. H. J. Buschow, *et al.*, "Encyclopedia of Materials: Science and Technology," in *Encyclopedia of Materials: Science and Technology* vol. 1 - 11, ed: Elsevier Science Ltd, 2001.
- [5] P. S. Neelakanta, *Handbook of electromagnetic materials*: CRC Press, 1995.
- [6] J. P. Joule, *Philosophical Magazine*, vol. 30, p. 46, 1847.
- [7] K. Aoyagi, "On method for the determination of the magnetostriction constants and some notes on the motional impedances of magnetostrictive resonators," *The Journal of the Institute of Electrical Engineering of Japan*, vol. 52, pp. 654-666, 1933.
- [8] S. Butterworth and F. D. Smith, "The equivalent circuit of the magnetostrictive oscillator," *Proceedings of the Physical Society*, vol. 43, pp. 165-185, 1931.
- [9] F. D. Smith, "The magnetostrictive constant for alternating magnetic fields," *Proceedings of the Physical Society*, vol. 43, pp. 165-185, 1930.
- [10] P. S. Sanchez, "An Anomalous Magnetoelastic Effect in Nickel," *IEEE Transaction on Magnetics*, vol. Mag-15, pp. 1154-1157, 1979.
- [11] B. Carlin, *Ultrasonics*, 2nd ed. New York: McGraw-Hill, 1960.
- [12] Y. Kikuchi, "Magnetostrictive materials and applications," *IEEE Transaction on Magnetics*, vol. Mag-4, pp. 107-117, 1968.
- [13] G. L. Gooberman and J. Lamb, *Journal of Polymer Society*, vol. 42, p. 35, 1960.
- [14] P. Kapitza, "The Study of the Magnetic Properties of matter in Strong Magnetic Fields. III. Magnetostriction.," *Proceedings of the Royal Society of London* vol. 135, pp. 537-554, 1931.
- [15] K. H. J. Buschow and F. R. De Boer. (2003). *Physics of Magnetism and Magnetic Materials* [Electronic Book].
- [16] E. L. Huston, *et al.*, "Magnetic and magnetostrictive properties of cube textured nickel for magnetostrictive transducer applications," *IEEE TRANSACTIONS ON MAGNETICS*, vol. Mag-9, pp. 636-640, 1973.
- [17] V. A. M. Brabers, *et al.*, "Magnetostriction of nickel ferrous ferrites," *Journal of Magnetism and Magnetic Materials*, vol. 15-18, pp. 599-600, 1980.
- [18] V. I. Nizhankovskii, "Classical magnetostriction of nickel in high magnetic field," *The European Physical Journal B*, vol. 53, pp. 1-4, 2006.
- [19] Y. Kikuchi, "The theoretical limit of mechanical output power available from magnetostriction vibrators," *IEEE Transactions on Sonics and Ultrasonics*, vol. SU-15, pp. 1-12, 1968.
- [20] H. Kikuchi, "On the Magnetostrictivity," *Nippon Electric Communication Engineering Report*, 30th October 1942 1942.

- [21] M. Schwartz, "Encyclopedia of Smart Materials," in *Encyclopedia of Smart Materials* vol. 1&2, M. Schwartz, Ed., ed. New York: John Wiley and Sons Inc, 2002.
- [22] V. GmbH, *Soft Magnetic Materials. Fundamentals, Alloys, Properties, Products, Applications*. London: Heyden & Sons Ltd, 1979.
- [23] A. Petošić, *et al.*, "Comparison of measured acoustic power results gained by using three different methods on an ultrasonic low-frequency device," *Ultrasonics Sonochemistry*, vol. 18, pp. 567-576, 2011.
- [24] C. J. Cleveland and C. Morris, "Dictionary of Energy," in *Dictionary of Energy*, ed. Amsterdam: Elsevier 2009.
- [25] Y. Aurégan, *Sound-flow interactions*. Berlin ; New York: Springer, 2002.
- [26] M. S. Howe, *Acoustics of fluid-structure interactions*. Cambridge, UK ; New York: Cambridge University Press, 1998.
- [27] M. J. Crocker, *Encyclopedia of acoustics*. New York: John Wiley, 1997.
- [28] P. C. Etter, *Underwater acoustic modeling : principles, techniques, and applications*, 2nd ed. London: E & FN Spon, 1996.
- [29] R. Vetri Murugan and R. Nagarajan, "Pulsed ultrasonic mixing: An experimental study," *Chemical Engineering Research & Design: Transactions of the Institution of Chemical Engineers Part A*, vol. 86, pp. 454-460, 2008.
- [30] J. A. Gallego-Juarez, *et al.*, "Ultrasonic system for continuous washing of textiles in liquid layers," *Ultrasonics Sonochemistry*, vol. 17, pp. 234-238, 2010.
- [31] O. V. Abramov, *High-intensity ultrasonics : theory and industrial applications*. Amsterdam, The Netherlands: Gordon and Breach Science Publishers, 1998.
- [32] S. T. P. Ltd. (2011, 24/11/2011). *Cavitation Bubble* [Web Page]. Available: <http://www.shockwavetherapy.us/page6.html>
- [33] R. Esche, "Acustica," *Akust. Beih.*, vol. 2, p. 208, 1952.
- [34] B. Brown, *British Communications and Electronics*, vol. 9, p. 918, 1962.
- [35] I. E. Commision, "IEC 60782 - Measurements of ultrasonic magnetostrictive transducers," ed. Geneva, Switzerland: International Electrotechnical Commission, 1984.
- [36] A. Petošić, *et al.*, "Measuring derived acoustic power of an ultrasound surgical device in the linear and nonlinear operating modes," *Ultrasonics*, vol. 49, pp. 522-531, 2009.
- [37] I. E. Commission, "International Standard IEC 61847, Ultrasonics - Surgical Systems, Measurement and Declaration of the Basic Output Characteristics," 1998.
- [38] I. E. Commission, "International Standard IEC 61088, Characterization and Measurements of Ultrasonic Piezoceramic Transducers," ed. Geneva, Switzerland: International Electrotechnical Commission, 1991.
- [39] I. E. Commission, "International Standard IEC 60782, Measurements of Ultrasonic Magnetostrictive Transducers," ed. Geneva, Switzerland: International Electrotechnical Commission, 1984.
- [40] R. Ross, *Metallic Materials Specification Handbook*, Third ed. New York: E. & F. M. Spon Ltd, 1980.
- [41] S. Australia, "AS/NZS 3008.1.1:2009 Electrical Installation - Selection of Cable," in *Cables for Alternating Voltages up to and including 0.6/1kV*, ed. Sydney, Australia: Standards Australia, 2009.